NUMERICAL MODELING OF CURRENT AND WAVE INTERACTIONS OF AN INLET-BEACH SYSTEM

By

YIXIN YAN

A DISSERTATION PRESENTED TO THE GRADUATE SCHOOL
OF THE UNIVERSITY OF FLORIDA IN
PARTIAL FULFILLMENT OF THE REQUIREMENTS
FOR THE DEGREE OF DOCTOR OF PHILOSOPHY

UNIVERSITY OF FLORIDA

1987

ACKNOWLEDGEMENTS

The author would like to express his deepest appreciation to his adviser, Dr. Hsiang Wang, Professor of Coastal and Oceanographic Engineering, for his continuing advice and encouragement throughout this study, also to co-adviser Dr. James T.Kirby, Assistant Professor of Coastal and Oceanographic Engineering, for his guidance and support. Appreciation is extended to Dr. Robert G. Dean, Graduate Research Professor of Coastal and Oceanographic Engineering, Dr. D. Max Sheppard, Professor of Coastal and Oceanographic Engineering, Dr. Ulrich H. Kurzweg, Professor of Engineering Science and Dr. James E. Keesling, Professor of Mathematics, for their valuable suggestions in this research.

The author also wants to thank Dr. Y. Peter Sheng and Dr. Joseph L. Hammack for their Suggestions and help.

The author is indebted to all staff of the Coastal Engineering Laboratory at University of Florida, specially to Marc Perlin, Sidney Schofield, Vernon Sparkman, Charles Broward and Jimmy E. Joiner, for their cooperation and assistance with the experiments.

Thanks also go to Subarna B. Malakar for the helping with programming and Ms. Lillean A. Pieter for the drafting of figures.

Finally, the author would like to thank his wife Ran Liu for her support, encouragement and patience.

TABLE OF CONTENTS

ACKNOWLEDGEMENTS ii

LIST OF FIGURES vi

LIST OF TABLES x

ABSTRACT xi

CHAPTERS

1 INTRODUCTION 1

1.1 Statement of Problem 1

1.2 Past Study 2

1.3 Scope of Study 3

2 THEORETICAL EQUATIONS OF THE MODEL 5

2.1 Introduction 5

2.2 Governing Equations 5

2.2.1 Depth-Averaged Equation of Continuity 7

2.2.2 Depth-Averaged Equations of Momentum 10

2.2.3 Wave Energy Conservation Equation 14

2.2.4 Dispersion Relation 30

2.2.5 Radiation Stresses, Lateral Mixing Stresses and Bottom Stresses . . 35

2.2.6 Wave Breaking Criterion 42

2.3 Summary 44

3 NUMERICAL SCHEME 46

3.1 Grid System and Definition of Variables 46

3.2 Finite Difference Scheme for Combined Continuity- Momentum Equation . 47

3.2.1 Linearized Implicit Model 47
3.2.2 Numerical Scheme for the Full Equations 52
3.2.3 Method of Calculation and Boundary Conditions 54
3.2.4 Stability Criteria 57
3.3 Finite Difference Scheme for the Wave Equation 57
3.4 Method of Solution 59
4 PERFORMANCE OF THE MODEL 61
4.1 Wave Setup on Plane Beach 61
4.2 Open Lateral Boundary Conditions and Longshore Current Distributions on a Plane Beach 63
4.3 Nearshore Circulation 64
4.4 Combined Refraction, Diffraction and Current Interaction Case 66
4.4.1 The Circular Shoal on a Flat Bottom 66
4.4.2 Circular Symmetric Shoal on Plane Beach 70
5 EXPERIMENTAL COMPARISONS 81
5.1 Purpose of Experiments 81
5.2 Facilities and Instruments 82
5.2.1 The Laboratory Facilities 82
5.2.2 Instrumentation 86
5.3 Experimental Arrangement and Measurements 89
5.4 Experimental Results and Numerical Comparisons 90
5.4.1 Wave Shoaling on Plane Beach 91
5.4.2 Flow Field due to Inlet on Sloping Beach with no Waves 94
5.4.3 Inlet on Sloping Beach with Waves 95
6 CONCLUSIONS AND RECOMMENDATIONS 133
APPENDICES
A WAVE EQUATION DERIVED BY USING PERTURBATION METHOD . . . 136

B NON-SLIP BOTTOM BOUNDARY CONDITION APPLIED IN WAVE EQUATION 149
C NUMERICAL SCHEME FOR CONTINUITY-MOMENTUN EQUATION . . . 152
D DOUBLE-SWEEP METHOD IN SOLVING NUMERICAL MODELS 155
BIBLIOGRAPHY 159
BIOGRAPHICAL SKETCH 164

LIST OF FIGURES

2.1	Outline of Studied Area	6
2.2	Variations of Dispersion Relation with $U/c_0 = -0.1$ and ϵ, ····· Linear; –·– Hedges; - - - Whitham; —— Composite	33
2.3	Variations of Dispersion Relation with $U/c_0 = -0.1$ and ϵ, ····· Linear; –·– Hedges; - - - Whitham; —— Composite	34
2.4	Velocity Profiles for different friction models —· (2.107); - - - (2.117)	39
2.5	Longuet-Higgen's Longshore Current Profiles	41
2.6	Variations of Eddy Vicosity Coefficients. —· = 0. ; ··· =0.001; –·– =0.01; - - - Von Kàrmàn's Model with upper-limit =0.001. unit= m^2/s	43
3.1	Grid Scheme	48
3.2	Definitions of $X^n_{i,j}$ and $(Y_s)^n_{i,j}$	49
4.1	Set-up on a Plane Beach. —— Eq.(2.138); - - - Linear Wave; △ Data	62
4.2	Longshore Current Generated by Obliquely Incident Waves. –·– no mixing; —— breaking mixing coeff.=$0.01m^2/s$; - - - breaking mixing coeff. =$0.01m^2/s$ and eddy vis. coeff.=$0.005m^2/s$	65
4.3	Velocity Field of Periodic Bottom Topography	67
4.4	Wave Amplitude Variations along Centerline —— $A_0k_0 = 0.16$; - - - $A_0k_0 = 0.32$	69
4.5	Wave Amplitude Variations across Centerline —— $A_0k_0 = 0.16$; - - - $A_0k_0 = 0.32$	71
4.6	Wave Amplitude Variations across Centerline —— $A_0k_0 = 0.16$; - - - $A_0k_0 = 0.32$	72
4.7	Bottom Topography : a Circular Shoal with Parabolic Configuration on the Plane Beach	73
4.8	Description of Water Depth	74

4.9 Velocity Vector Field for Circular Shoal Located on the Plane Beach (no inlet) 76

4.10 Longshore Current Distributions at Lowest Boundary. —— No Inlet; - - - with Inlet 77

4.11 Velocity Vector field for Circular Shoal Located on the Plane Beach with Current from Inlet 78

4.12 Contour Plot of Wave Amplitudes on the Circular Shoal Located on the Plane Beach (no inlet) 79

4.13 Contour Plot of Wave Amplitudes on the Circular Shoal Located on the Plane Beach with Current from Inlet 80

5.1 Plan View of Wave Tank 83

5.2 Cross-Section Views of Wave Tank 84

5.3 Cross-Sections of Measurement 85

5.4 Velocity Distribution at I=Idry 87

5.5 Instrument Calibrations 88

5.6 Instrument Connections 89

5.7 Velocity Variations along the Beach, — $\eta(1,j) = 0$; $\diamond$ $\eta(1,j) = -a^2/(2\sinh kh)$ 92

5.8 Wave Height Variations along the Beach, — $\eta(1,j) = 0$; $\diamond$ $\eta(1,j) = -a^2/(2\sinh kh)$ 92

5.9 Comparisons between m = 43 with $\triangle x = 0.12$ m, ——; and m = 83 with $\triangle x = 0.06$ m, - - - at I1 = 15,30 for m = 43 and I2 = 29,59 for m = 83 93

5.10 Wave Height Variations along the Beach (no current), — – Wave Eq. (2.138); - - - Linear Shoaling; x Measured Data 100

5.11 Velocity profiles for $Q_0 = 0.0056m^3/sec.$ (no waves) 101

5.12 Velocity profiles for $Q_0 = 0.0076m^3/sec.$ (no waves) 102

5.13 Variation of x-Component Velocity. Case a: $Q_0 = 0.0056m^3/s$; T = 0.87 sec.; $H_0 = 0.97$ cm. —— Numerical Model; $\diamond$ Measured Data 103

5.14 Comparisons of Calculating Velocities between with and without Waves. Case a: $Q_0 = 0.0056m^3/s$, T = 0.87 sec.; $H_0 = 0.97$ cm. —— with Waves; - - - no Waves 104

5.15 Variation of x-Component Velocity. Case b: $Q_0 = 0.0056m^3/s$; T = 1.16 sec.; $H_0 = 0.88$ cm. —— Numerical Model; $\diamond$ Measured Data 105

5.16 Comparisons of Calculating Velocities between with and without Waves. Case b: $Q_0 = 0.0056m^3/s$, T = 1.16 sec.; $H_0 = 0.88$ cm. —— with Waves; - - - no Waves 106

5.17 Variation of x-Component Velocity. Case c: $Q_0 = 0.0056m^3/s$; T = 1.36 sec.; $H_0 = 0.97$ cm. —— Numerical Model; ◇ Measured Data 107

5.18 Comparisons of Calculating Velocities between with and without Waves. Case c: $Q_0 = 0.0056m^3/s$, T = 1.36 sec.; $H_0 = 0.97$ cm. —— with Waves; - - - no Waves 108

5.19 Variation of x-Component Velocity. Case d: $Q_0 = 0.0076m^3/s$; T = 0.87 sec.; $H_0 = 1.23$ cm. —— Numerical Model; ◇ Measured Data 109

5.20 Comparisons of Calculating Velocities between with and without Waves. Case d: $Q_0 = 0.0076m^3/s$, T = 0.87 sec.; $H_0 = 1.23$ cm. —— with Waves; - - - no Waves 110

5.21 Variation of x-Component Velocity. Case e: $Q_0 = 0.0076m^3/s$; T = 1.16 sec.; $H_0 = 0.95$ cm. —— Numerical Model; ◇ Measured Data 111

5.22 Comparisons of Calculating Velocities between with and without waves. Case e: $Q_0 = 0.0076m^3/s$, T = 1.16 sec.; $H_0 = 0.95$ cm. —— with Waves; - - - no Waves 112

5.23 Variation of x-Component Velocity. Case f: $Q_0 = 0.0076m^3/s$; T = 1,36 sec.; $H_0 = 0.97$ cm. —— Numerical Model; ◇ Measured Data 113

5.24 Comparisons of Calculating Velocities between with and without Waves. Case f: $Q_0 = 0.0076m^3/s$, T = 1.36 sec.; $H_0 = 0.97$ cm. —— with Waves; - - - no Waves 114

5.25 Velocity Field and Contour Lines in Flat Bottom. f = 0 115

5.26 Velocity Field and Contour Lines in Flat Bottom. f = 0.01 116

5.27 Contour Plot of Velocity. Case i: $Q_0 = 0.0056m^3/s$ (no waves) 117

5.28 Contour Plot of Velocity. Case a: $Q_0 = 0.0056m^3/s$; T = 0.87; $H_0 =$ 0.97 cm 118

5.29 Contour Plot of Velocity. Case b: $Q_0 = 0.0056m^3/s$; T = 1.16; $H_0 =$ 0.88 cm 119

5.30 Contour Plot of Velocity. Case c: $Q_0 = 0.0056m^3/s$; T = 1.36; $H_0 =$ 0.97 cm 120

5.31 Contour Plot of Velocity. Case ii: $Q_0 = 0.0076m^3/s$ (no waves) 121

5.32 Contour Plot of Velocity. Case d: $Q_0 = 0.0076m^3/s$; T = 0.87; $H_0 =$ 1.23 cm 122

5.33 Contour Plot of Velocity. Case e: $Q_0 = 0.0076m^3/s$; T = 1.16; H_0 = 0.95 cm 123

5.34 Contour Plot of Velocity. Case f: $Q_0 = 0.0076m^3/s$; T = 1.36; H_0 = 0.97 cm 124

5.35 Bottom Friction Coefficients f as Function of u_m/U_i 125

5.36 Wave Amplitude Variations. Case a: $Q_0 = 0.0056m^3/s$; T = 0.87 sec.; $H_0 = 0.97$ cm. —— Numerical Model; △ Data 126

5.37 Wave Amplitude Variations. Case b: $Q_0 = 0.0056m^3/s$; T = 1.16 sec.; $H_0 = 0.88$ cm. —— Numerical Model; △ Data 127

5.38 Wave Amplitude Variations. Case c: $Q_0 = 0.0056m^3/s$; T = 1.36 sec.; $H_0 = 0.97$ cm. —— Numerical Model; △ Data 128

5.39 Wave Amplitude Variations. Case d: $Q_0 = 0.0076m^3/s$; T = 0.87 sec.; $H_0 = 1.23$ cm. —— Numerical Model; △ Data 129

5.40 Wave Amplitude Variations. Case e: $Q_0 = 0.0076m^3/s$; T = 1.16 sec.; $H_0 = 0.95$ cm. —— Numerical Model; △ Data 130

5.41 Wave Amplitude Variations. Case f: $Q_0 = 0.0076m^3/s$; T = 1.36 sec.; $H_0 = 0.97$ cm. —— Numerical Model; △ Data 131

5.42 Wave Amplitude Variations along Centerline 132

LIST OF TABLES

5.1	Test Condition	90
5.2	The values of ϵ_c and f in the Tests	96
5.3	Bottom Friction Coefficients Used in the Model	98
5.4	Incident Wave Height	99

Abstract of Dissertation Presented to the Graduate School
of the University of Florida in Partial Fulfillment of the
Requirements for the Degree of Doctor of Philosophy

NUMERICAL MODELING OF CURRENT AND WAVE INTERACTIONS OF AN INLET-BEACH SYSTEM

By

YIXIN YAN

August 1987

Chairman: Dr. Hsiang Wang
Major Department: Engineering Sciences

A numerical model for the prediction of nearshore hydrodynamics of an inlet-beach system is developed in this study. The theoretical formulation is based on the time- and depth-averaged equations of continuity and momentum, and a 3rd-order wave energy equation that retains the important nearshore effects of refraction, diffraction, current-wave interaction and energy dissipation. Variational principle as well as a parallel method by using perturbation technique is applied to arrive at the same wave equation. The application of 3rd-order wave equation is restricted to small incident wave angle and slowly varying topography.

A numerical scheme is developed to solve the above governing equations. The double-sweep Crank-Nicolson finite difference scheme is adopted for the model. In each spatial sweeping, a recently developed two time-level implicit method by Sheng is applied. The numerical model is tested against existing numerical models of simpler cases and is found to yield reasonable comparisons for all cases.

Laboratory experiments are conducted to verify the numerical model and it is found that the model performs well in predicting current field but grossly underpredicts the wave amplitude in shallow water, particular, in the center region of the inlet jet.

CHAPTER 1
INTRODUCTION

1.1 Statement of Problem

Tidal and river inlets are prominent coastal features. They play a vital role in the evolution process of coastlines. Along the east coast and gulf coast of the United States, inlets are numerous because of the extensive barrier island system. In these regions, the rules of inlets are particularly significant owing to the heavy development pressure and the competing interests of various human activities. To maintain navigation and water commerce, for instance, often requires inlets to be stabilized with man-made structures. The disruption of littoral processes owing to the presence of inlet structures, on the other hand, poses a major threat to down drift beaches, thus diminishing the value of recreational beaches and endangering waterfront structures. Many coastal communities spent millions of dollars installing coastal protective structures or simply transporting sand from one place to another. However, these measures do not always render satisfactory results owing partly to our poor understanding on complicated interactions of an inlet-beach system.

The hydrographic and shoreline changes of an inlet-beach system are the consequence of sediment movement which, in turn, is caused by the hydrodynamic forces exerted on the system. Therefore, to better predict the behavior of inlet-beach interaction one must first be able to predict the hydrodynamics.

Physically, the problem in hand is a complicated one. Both wave and current field are modified by the nearshore topography and the inlet geometry. In addition, the spatially non-uniform current will interact with the unsteady flow field induced by waves.

Mathematically, there is no unified wave theory in the first place capable of describing waves traveling through large areas of varied depth. Furthermore, the current field that we

are dealing with has a different scale of variation from that of the local wave field. The nonlinear interaction between the two systems is expected to be important as well as the non-linear behavior of the wave field.

1.2 Past Study

In the absence of an inlet, the water motion in the nearshore zone is primarily induced by waves from offshore as modified by the bottom topography and/or shore structure. The influence of bottom topography on wave direction, height and length has long been recognized and as early as in the 1940s analytical methods were already being developed to solved the so called wave refraction problem (Johnson et al. 1948; Arther et al. 1952) by tracing wave rays based on the principle of geometrical optics. Since then, significant progress has been made in treating the shallow water wave transformation phenomenon. Arthur (1950) included the effect of current into the ray method. Dobson (1967) developed one of the first computer codes to trace wave ray over an irregular bottom. Skovgaard et al. (1975) extended the ray method to include the effects of wave energy dissipation due to bottom friction. Noda et al. (1974) developed a finite difference scheme based on the conservations of wave number and wave energy, that compute spatial distributions of wave number and wave energy in shallow water. His method was extended by Wang and Yang (1981) and Chen and Wang (1983) to wave spectral transformation and the inclusion of non-stationarity, thus enabling the computation of spatial and temporal distributions of random waves. Birkemier and Dalrymple (1976) and Ebersole and Dalrymple (1979), on the other hand, expanded Noda's method by including the depth averaged continuity and momentum equations to computer wave induced nearshore circulations. In the presence of an inlet, the nearshore wave field is further modified due to the interactions with a spatially non-uniform current and the diffraction effect of inlet jetty structures.

Traditionally, the problems of wave refraction and diffraction were treated separately. Penny and Price (1944,1952) were among the first to apply Sommerfeld's (1896) solution to wave diffraction around a sharp obstacle such as a semi-infinite thin breakwater. Other

solutions of similar nature were obtained for different geometries (Wiegel,1962; Memos,1976; Monfetusco,1968; Goda et al.,1971).

Only recently, Berkhoff (1972) developed what is now referred to as the mild slope equation that governs the combined refraction- diffraction phenomenon. Various solutions became available on wave field modified by different beach-structure configurations such as waves in the vicinity of a thin groin (Liu and Lozano,1979; Liu,1982), edge waves by barred-beach topography (Kirby et al.,1981), and waves over circular shoal (Radder, 1979), etc. Booij (1981) further introduced the ambient current element into the basic wave transformation equation and derived the governing equation on variational principle. The resulting equation is a hyperbolic type and is, in general, difficult to solve. Booij's equation reduces to a parabolic type similar to Berkhoff's if the mild slope assumption is invoked. A number of simple examples were given by him. Kirby (1983) systematically studied the current-wave interaction problem and proposed a weekly non-linear model appropriate to thr Stokes wave expansion.

The present study extends the Booij's and the Kirby's model to the problem of interaction between water waves and inlet flows.

1.3 Scope of Study

The primary purpose of this study is to develop a numerical model for the prediction of wave characteristics and current field of an inlet beach system. Specifically, the mathematical formulation of the problem was performed first. This task entailed the establishment of the governing equations sufficient to solve the variables of interest. Out of necessity, simplified assumption are made such that the problem is amenable to the present computational capability.

First of all, the fluid is treated as incompressible. Second, the surface shear stress as well as part of the turbulent shear stress (normal component) is also neglected. Third, also one of the most major ones is that the irrotationality is assumed in the wave equation allowing the existence of a wave velocity potential and a current velocity potential, although

such an assumption is in contradiction to both physical reality and mathematical results of the combined velocity field. The equations governing the mean flow including both continuity and momentum equations are depth averaged. The equation governing the wave motion with due considerations of refraction, diffraction and current interaction is quasi-three dimensional owing to the velocity potential assumption. Two parallel methods were used to derived the wave energy equation: one based on variational principle and the other on perturbation method. By introducing proper scaling factors, the wave energy equation is further simplified by containing terms of only the same order of magnitude. Other relationships including dispersion relation, radiation stresses, bottom shears and lateral mixing compatible to the system under consideration are also formulated.

A numerical scheme is developed to solve the governing equations by double sweep marching method. The scheme is implicit which allows for a large time step, especially the two time level fully alternating direction implicit scheme utilized by Sheng (1981).

Attempts to verify the numerical model are made by comparing the present model with known analytical and numerical solutions of simple geometries and with laboratory experiments carried out in the Coastal and Oceanographic Engineering Laboratory. Due to wave basin limitations, the experiments were carried out only for plane beach with an inlet normal to the contours.

CHAPTER 2
THEORETICAL EQUATIONS OF THE MODEL

2.1 Introduction

In order to solve the flow field in a specified region, the governing equations with proper initial and boundary conditions must be provided. Furthermore whether a unique solution exists in the domain of interest or whether mathematical singularities will appear that will cause the equations failing to give sensible solutions should also be examined.

In this chapter, the theoretical development of the governing equations for both the mean flow field and the wave field is given in detail.

There are five basic equations employed in the computation including four flow equations: one continuity equation, two horizontal momentum equations and one wave equation, and one equation relating wave number and wave period.

2.2 Governing Equations

The basic equations, as mentioned before, are based upon the principle of conservation of mass, conservation of momentum, and conservation of wave energy and upon the gravitational wave dispersion characteristics. The wave equation under consideration includes the effects of wave refraction, diffraction and shoaling during transformation from deep water to shallow water regions. These equations, together with initial and boundary conditions, give a mathematical representation of the physical problem of interest.

Since the problem of interest entails waves propagating towards shore over a complex bathymetry, wave refraction, diffraction and breaking are expected to occur as well as current-wave interaction due to inlet discharge. Figure 2.1 depicts the physical system being studied. The problem has two apparent time scales: a short time scale associated with the

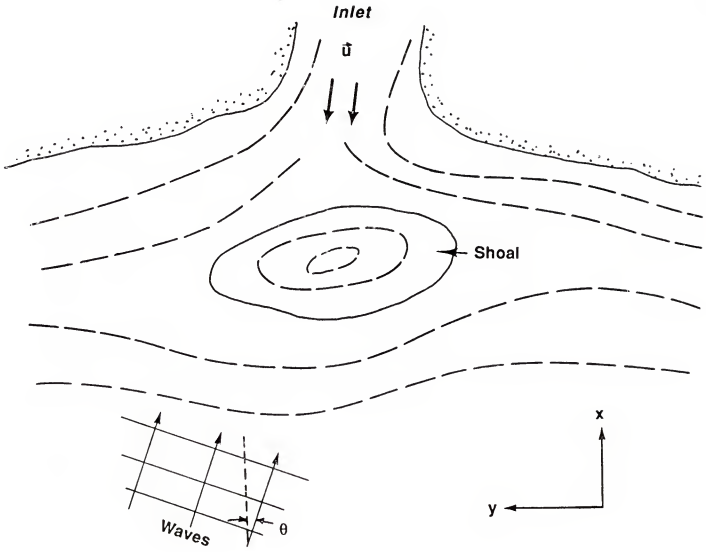

Figure 2.1: Outline of Studied Area

oscillation of the incident waves, and a larger time scale over which the characteristics of the incident wave and mean flow, such as wave height, incident wave angle and current are perceptibly modified. The larger time scale may also include the effect of changes in wind, tides and topography. Since our attention here is towards mean quantities, many of them may be averaged over a wave period to remove the direct effect of oscillation. In addition, since we are mainly interested in the net transport quantities the knowledge in the detailed structure of the velocity distribution over depth is not needed and the equations may be averaged over depth, reducing the entire problem to two dimensional in the horizontal plane.

In the derivation of wave energy conservation equation, due to the extreme complexity in mathematics, some restrictions have to be imposed on the orders of magnitude of wave height, bottom slope and current strength.

In the model, the quantities to be determined are as follows: the horizontal components of the mean current including wave-induced current and divergent current from the inlet; the local wave amplitude under the influence of refraction, diffraction and breaking ; the local wave angle and wave number and the mean water surface level.

2.2.1 Depth-Averaged Equation of Continuity

A Cartesian coordinate system is defined with x in the onshore direction, normal to the coastal line, y in the longshore direction and z vertically upward, as shown in Fig.2.1.

The summation convention adopted here states that in Cartesian coordinates whenever the same letter subscript occurs twice in a term,that subscript is to be given all possible values and the results in horizontal space add together.

The continuity equation reads

$$\frac{\partial \rho}{\partial t} + \frac{\partial \rho u_i}{\partial x_i} + \frac{\partial \rho w}{\partial z} = 0 \tag{2.1}$$

where $i = 1, 2$ represents x,y direction, respectively. ρ is the water density and $u_i = \{u, v\}$ represents the $\{x, y\}$ components of velocity,respectively, w is the velocity component in the z direction.

In application, water density which only varies slightly is considered as constant. The continuity equation reduces to

$$\frac{\partial u_i}{\partial x_i} + \frac{\partial w}{\partial z} = 0 \tag{2.2}$$

Integrating Eq.(2.2) over depth, we obtain

$$\int_{-h}^{\eta} (\frac{\partial u_i}{\partial x_i} + \frac{\partial w}{\partial z}) dz = 0 \tag{2.3}$$

where η is free surface elevation, and h is water depth. Using Leibniz's rule which states that

$$\frac{\partial}{\partial x} \int_{\beta(x)}^{\alpha(x)} f(x,z) dz = \int_{\beta(x)}^{\alpha(x)} \frac{\partial f}{\partial z} dz + \frac{\partial \alpha}{\partial x} f(x,\alpha) - \frac{\partial \beta}{\partial x} f(x,\beta)$$

Eq.(2.3) can be written as

$$\frac{\partial}{\partial x_i} \int_{-h}^{\eta} u_i dz - u_i \mid_{\eta} \frac{\partial \eta}{\partial x_i} - u_i \mid_{-h} \frac{\partial h}{\partial x_i} + w \mid_{\eta} - w \mid_{-h} = 0 \tag{2.4}$$

in which the subscripts after vertical stroke are at which the value being calculated. The bottom boundary condition (BBC) and the kinematic free surface boundary condition (KFSBC) are given as

$$u_i \frac{\partial h}{\partial x_i} + w = 0 \quad \text{(BBC)} \quad \text{at } z = -h(x,y) \tag{2.5}$$

$$\frac{\partial \eta}{\partial t} = w - u_i \frac{\partial \eta}{\partial x_i} \quad \text{(KFSBC)} \quad \text{at } z = \eta(x,y,t) \tag{2.6}$$

Substituting (2.5) and (2.6) into (2.4) results in

$$\frac{\partial \eta}{\partial t} + \frac{\partial}{\partial x_i} \int_{-h}^{\eta} u_i dz = 0 \tag{2.7}$$

We now introduce

$$u_i = \overline{U_i} + u_i'$$

$$\eta = \overline{\eta} + \eta' \tag{2.8}$$

where $\overline{U_i}$ are time and depth independent uniform current velocities, $\overline{\eta}$ is the mean surface elevation, u'_i and η' are the fluctuating components. u'_i can be separated further into two parts:

$$u'_i = u_i^w + u_i^t \tag{2.9}$$

where u_i^w and u_i^t are the slowly varying wave motion and the fast varying turbulent fluctuations, respectively. The properties of these quantities, after taking average over wave period, are expressed as

$$\overline{\overline{U_i}} = \overline{U_i}, \qquad \overline{\overline{\eta}} = \overline{\eta}$$

$$\overline{u_i^t} = 0, \qquad \overline{\eta^t} = 0$$

where the upper bar represents the time average over one wave period

$$\overline{f} = \frac{1}{T}\int_0^T f\,dt$$

Therefore, (2.7) becomes, after taking time average

$$\frac{\partial \overline{\eta}}{\partial t} + \overline{\frac{\partial}{\partial x_i}\int_{-h}^{\eta} \overline{U}\,dz} + \overline{\frac{\partial}{\partial x_i}\int_{-h}^{\eta} u'\,dz} = 0 \tag{2.10}$$

Defining

$$\hat{u}_i = \frac{\overline{\int_{-h}^{\eta} u_i^t dz}}{(h+\overline{\eta})} = \frac{\overline{\int_{-h}^{\eta} u_i^w dz}}{(h+\overline{\eta})}$$

the final form of the mean continuity equation is arrived at

$$\frac{\partial \overline{\eta}}{\partial t} + \frac{\partial}{\partial x_i}(U_i D) = 0 \tag{2.11}$$

where $D = h + \overline{\eta}$ is total depth and $U_i = \overline{U_i} + \hat{u}_i$ is total mean current velocity averaged over one wave period with $U_i = \{U, V\}$. Equation (2.11) represents conservation of mass per unit surface area under the assumption of water density being constant in space and time, and the bottom unchanged with time.

2.2.2 Depth-Averaged Equations of Momentum

The horizontal depth-averaged momentum equations used here were originally derived by Ebersole and Dalrymple(1979). A brief summary was given here. The Navier-Stokes equation in the horizontal (x,y) directions takes the following form:

$$\frac{\partial u_i}{\partial t} + u_j \frac{\partial u_i}{\partial x_j} + w \frac{\partial u_i}{\partial z} = -\frac{1}{\rho}\frac{\partial p}{\partial x_i} + \frac{1}{\rho}\frac{\partial \tau_{ji}}{\partial x_j} + \frac{1}{\rho}\frac{\partial \tau_{zi}}{\partial z} \tag{2.12}$$

and in vertical (z) direction it is

$$\frac{\partial w}{\partial t} + u_j \frac{\partial w}{\partial x_j} + w \frac{\partial w}{\partial z} = -\frac{1}{\rho}\frac{\partial p}{\partial z} + \frac{1}{\rho}\frac{\partial \tau_{jz}}{\partial x_j} + \frac{1}{\rho}\frac{\partial \tau_{zz}}{\partial z} \tag{2.13}$$

$$i = 1, 2,\ j = 1, 2$$

where p is the total pressure including dynamic and static pressures and τ_{ij} is the shear stress, where the first subscript is the surface that the stress acts on and the second subscript is the direction of shear stress. Introducing the continuity equation (2.2) into (2.12) and (2.13) we have

$$\frac{\partial u_i}{\partial t} + \frac{\partial u_i u_j}{\partial x_j} + \frac{\partial u_i w}{\partial z} = -\frac{1}{\rho}\frac{\partial p}{\partial x_i} + \frac{1}{\rho}\frac{\partial \tau_{ji}}{\partial x_j} + \frac{1}{\rho}\frac{\partial \tau_{zi}}{\partial z} \tag{2.14}$$

and

$$\frac{\partial w}{\partial t} + \frac{\partial w u_j}{\partial x_j} + \frac{\partial w w}{\partial z} = -\frac{1}{\rho}\frac{\partial p}{\partial z} + \frac{1}{\rho}\frac{\partial \tau_{zj}}{\partial x_j} + \frac{1}{\rho}\frac{\partial \tau_{zz}}{\partial z} \tag{2.15}$$

Integrating over depth and utilizing the Leibeniz's rule, the following term by term results are obtained:

i) $$\int_{-h}^{\eta} \frac{\partial u_i}{\partial t} = \frac{\partial}{\partial t}\int_{-h}^{\eta} u_i dz - u_i \mid_{\eta} \frac{\partial \eta}{\partial t}$$

ii) $$\int_{-h}^{\eta} \frac{\partial u_i u_j}{\partial x_j} dz = \frac{\partial}{\partial x_j}\int_{-h}^{\eta} u_i u_j dz - u_i u_j \mid_{\eta} \frac{\partial \eta}{\partial x_j} - u_i u_j \mid_{-h} \frac{\partial h}{\partial x_j}$$

iii) $$\int_{-h}^{\eta} \frac{\partial u_i w}{\partial z} dz = u_i w \mid_{\eta} - u_i w \mid_{-h}$$

Thus the left hand side of Eq.(2.14) becomes

$$LHS = \frac{\partial}{\partial t}\int_{-h}^{\eta} u_i dz + \frac{\partial}{\partial x_j}\int_{-h}^{\eta} u_i u_j dz - u_i \mid_{\eta} \left(\frac{\partial \eta}{\partial t} + u_j \mid_{\eta} \frac{\partial \eta}{\partial x_j} - w \mid_{\eta}\right)$$

$$-u_i\,|_{-h}\,(u_j\,|_{-h}\,\frac{\partial h}{\partial x_j}+w\,|_{-h})$$

Recognizing the last two brackets of LHS are the KFSBC and BBC, respectively, we have

$$\text{LHS}=\frac{\partial}{\partial t}\int_{-h}^{\eta}u_i dz+\frac{\partial}{\partial x_j}\int_{-h}^{\eta}u_i u_j dz$$

Again introducing the definition of

$$u_i=\overline{U}_i+u_i^w+u_i^t$$

into the above equation and time averaging over a wave period yields term by term

i) $$\overline{\frac{\partial}{\partial t}\int_{-h}^{\eta}u_i dz}=\overline{\frac{\partial}{\partial t}\int_{-h}^{\eta}(\overline{U}_i+u_i^w+u_i^t)dz}=\frac{\partial}{\partial t}(U_i D)$$

where U_i and D are total current velocity and total water depth respectively as defined earlier, and

ii) $$\overline{\frac{\partial}{\partial x_j}\int_{-h}^{\eta}u_i u_j dz}=\overline{\frac{\partial}{\partial x_j}\int_{-h}^{\eta}(\overline{U}_i+u_i^w+u_i^t)(\overline{U}_j+u_j^w+u_j^t)dt}$$

Noting that there is no interaction between wave orbital velocity and turbulent velocity, Phillips (1977), the above term can be expanded as follows

$$\overline{\frac{\partial}{\partial x_j}\int_{-h}^{\eta}\overline{U}_i\overline{U}_j dz}+\overline{\frac{\partial}{\partial x_j}\int_{-h}^{\eta}(\overline{U}_i u_j^w+\overline{U}_j u_i^w)dz}+\overline{\frac{\partial}{\partial x_j}\int_{-h}^{\eta}u_i^w u_j^w dz}+$$

$$\overline{\frac{\partial}{\partial x_j}\int_{-h}^{\eta}u_i^t u_j^t dz}$$

$$=\frac{\partial}{\partial x_j}(\overline{U}_i\overline{U}_j D)+\frac{\partial}{\partial x_j}(\overline{U}_i\hat{u}_j D)+\frac{\partial}{\partial x_j}(\overline{U}_j\hat{u}_i D)+\overline{\frac{\partial}{\partial x_j}\int_{-h}^{\eta}u_i^w u_j^w dz}+$$

$$\overline{\frac{\partial}{\partial x_j}\int_{-h}^{\eta}u_i^t u_j^t dz}$$

Introducing $U_i=\overline{U}_i+\hat{u}_i$ into the above expression, the LHS of Eq.(2.14) becomes

$$\frac{\partial}{\partial t}(U_i D)+\frac{\partial}{\partial x_j}(U_i U_j D)-\frac{\partial}{\partial x_j}(\hat{u}_i\hat{u}_j D)+\overline{\frac{\partial}{\partial x_j}\int_{-h}^{\eta}u_i^w u_j^w dz}+$$

$$\overline{\frac{\partial}{\partial x_j}\int_{-h}^{\eta} u_i^t u_j^t dz} \tag{2.16}$$

The right hand side of (2.14) is, after integrating over depth and averaging over time,

$$\text{RHS} = -\overline{\frac{1}{\rho}\int_{-h}^{\eta}\frac{\partial p}{\partial x_i}dz} + \overline{\frac{1}{\rho}\int_{-h}^{\eta}\frac{\partial \tau_{ji}}{\partial x_j}dz} + \overline{\frac{1}{\rho}\int_{-h}^{\eta}\frac{\partial \tau_{zi}}{\partial z}dz}$$

here water density is considered as constant. After neglecting the second term which is the lateral shear stress due to viscosity, we obtain

$$\text{RHS} = -\overline{\frac{1}{\rho}\frac{\partial}{\partial x_i}\int_{-h}^{\eta} p dz} + \overline{\frac{1}{\rho}p\mid_{\eta}\frac{\partial \eta}{\partial x_i}} + \overline{\frac{1}{\rho}p\mid_{-h}\frac{\partial h}{\partial x_i}} + \overline{\frac{1}{\rho}\tau_{zi}\mid_{\eta}} - \overline{\frac{1}{\rho}\tau_{zi}\mid_{-h}}$$

The datum of pressure is chosen as the atmosphere pressure, so that at free surface, $p\mid_{\eta}$ is zero. The mean pressure at the bottom $p\mid_{-h}$ consists of two parts: hydrostatic pressure and wave induced dynamic pressure, viz.

$$\begin{aligned}\overline{p\mid_{-h}} &= -\rho g(h+\overline{\eta}) + \overline{p_d\mid_{-h}} \\ &= -\rho g D + \overline{p_d\mid_{-h}}\end{aligned}$$

where p_d is the dynamic pressure. Multiplying the above equation by $\frac{1}{\rho}\frac{\partial h}{\partial x_i}$ we have

$$\overline{\frac{1}{\rho}p\mid_{-h}\frac{\partial h}{\partial x_i}} = \frac{1}{2}\frac{\partial}{\partial x_i}(gD^2) - gD\frac{\partial \overline{\eta}}{\partial x_i} + \overline{\frac{1}{\rho}p_d\mid_{-h}\frac{\partial h}{\partial x_i}}$$

The RHS can now be written as

$$-\overline{\frac{1}{\rho}\frac{\partial}{\partial x_i}\int_{-h}^{\eta} p dz} + \frac{1}{2}\frac{\partial}{\partial x_i}(gD^2) - gD\frac{\partial \overline{\eta}}{\partial x_i} + \overline{\frac{1}{\rho}p_d\mid_{-h}\frac{\partial h}{\partial x_i}} + \frac{1}{\rho}\overline{\tau}_{si}$$

$$-\frac{1}{\rho}\overline{\tau}_{bi} \tag{2.17}$$

where

$\overline{\tau}_{si} = \overline{\tau_{zi}\mid_{\eta}}$ is time averaged surface shear stress

and

$\overline{\tau}_{bi} = \overline{\tau_{zi}\mid_{-h}}$ is time averaged bottom shear stress.

Finally, combining (2.16) with (2.17), the time averaged and depth integrated horizontal momentum equation is given by

$$\frac{\partial}{\partial t}(U_i D) + \frac{\partial}{\partial x_j}(U_i U_j D) - \frac{\partial}{\partial x_j}(\hat{u}_i \hat{u}_j D) + \overline{\frac{\partial}{\partial x_j}\int_{-h}^{\eta} u_i^w u_j^w dz} + \overline{\frac{\partial}{\partial x_j}\int_{-h}^{\eta} u_i^t u_j^t dz}$$

$$= -\overline{\frac{1}{\rho}\frac{\partial}{\partial x_i}\int_{-h}^{\eta} p dz} + \frac{1}{2}\frac{\partial}{\partial x_i}(gD^2) - gD\frac{\partial \overline{\eta}}{\partial x_i} + \frac{1}{\rho}\overline{p_d|_{-h}\frac{\partial h}{\partial x_i}} + \frac{1}{\rho}\overline{\tau}_{si} - \frac{1}{\rho}\overline{\tau}_{bi}$$

or rearranged as

$$\frac{\partial}{\partial t}(U_i D) + \frac{\partial}{\partial x_j}(U_i U_j D) = -gD\frac{\partial \overline{\eta}}{\partial x_i} - \frac{1}{\rho}\frac{\partial}{\partial x_j}[\overline{\int_{-h}^{\eta} p\delta_{ij} dz} + \rho\overline{\int_{-h}^{\eta} u_i^w u_j^w dz}$$

$$-\frac{1}{2}\rho g D^2 \delta_{ij} - \rho \hat{u}_i \hat{u}_j D] + \frac{1}{\rho}\overline{p_d|_{-h}\frac{\partial h}{\partial x_i}} + \frac{1}{\rho}\overline{\tau}_{si} + \frac{1}{\rho}\overline{\tau}_{bi} - \overline{\frac{\partial}{\partial x_j}\int_{-h}^{\eta} u_i^t u_j^t dz} \qquad (2.18)$$

Collectively, the second to the fifth terms on the RHS are known as the radiation stress or the excess momentum flux due to the presence of waves, i.e.,

$$S_{ij} = \overline{\int_{-h}^{\eta} p\delta_{ij} dz} + \rho\overline{\int_{-h}^{\eta} u_i^w u_j^w dz} - \frac{1}{2}\rho g D^2 \delta_{ij} - \rho \hat{u}_i \hat{u}_j D \qquad (2.19)$$

where

$$\delta_{ij} = \begin{cases} 1 & i = j \\ 0 & i \neq j \end{cases}$$

Considering that the product of bottom slope and the mean dynamic pressure at the bottom is negligible, we obtain

$$\frac{\partial}{\partial t}(U_i D) + \frac{\partial}{\partial x_j}(U_i U_j D) = -gD\frac{\partial \overline{\eta}}{\partial x_i} - \frac{1}{\rho}\frac{\partial S_{ij}}{\partial x_j} - \frac{D}{\rho}\frac{\partial}{\partial x_j}(\rho\overline{u_i^t u_j^t}) +$$

$$\frac{1}{\rho}\overline{\tau}_{si} - \frac{1}{\rho}\overline{\tau}_{bi} \qquad (2.20)$$

after assuming $u_i^t u_j^t$ is independent of depth. The term $-\rho\overline{u_i^t u_j^t}$ is Reynolds stresses and their normal component (when $i = j$) can usually be neglected.

Writing in component form yields

X-Direction

$$\frac{\partial}{\partial t}(UD)+\frac{\partial}{\partial x}(U^2D)+\frac{\partial}{\partial y}(UVD)=-gD\frac{\partial\overline{\eta}}{\partial x}-\frac{1}{\rho}\frac{\partial S_{xx}}{\partial x}-\frac{1}{\rho}\frac{\partial S_{xy}}{\partial y}+$$

$$\frac{D}{\rho}\frac{\partial\overline{\tau}_{\ell}}{\partial y}+\frac{1}{\rho}\overline{\tau}_{sx}-\frac{1}{\rho}\overline{\tau}_{bx} \tag{2.21}$$

Y-Direction

$$\frac{\partial}{\partial t}(VD)+\frac{\partial}{\partial x}(UVD)+\frac{\partial}{\partial y}(V^2D)=-gD\frac{\partial\overline{\eta}}{\partial y}-\frac{1}{\rho}\frac{\partial S_{xy}}{\partial x}-\frac{1}{\rho}\frac{\partial S_{yy}}{\partial y}+$$

$$\frac{D}{\rho}\frac{\partial\overline{\tau}_{\ell}}{\partial x}+\frac{1}{\rho}\overline{\tau}_{sy}-\frac{1}{\rho}\overline{\tau}_{by} \tag{2.22}$$

where $\overline{\tau}_{\ell}=-\rho\overline{u_i^{\ell}u_j^{\ell}}$ is the lateral friction due to Reynolds stress. In the model, $\overline{\tau}_{si}$ will not be considered. The possible formations of $\overline{\tau}_{bi}$ and $\overline{\tau}_{\ell}$ will discuss later in this chapter. They are flow related variables.

The average continuity and momentum equations can be linearized. Noda et al.(1974) gave a simple form of those equations after neglecting the nonlinear and time dependent terms in (2.11) and (2.20). They are

$$\frac{\partial}{\partial x_i}(U_iD)=0 \tag{2.23}$$

$$0=-gD\frac{\partial\overline{\eta}}{\partial x_i}-\frac{1}{\rho}\frac{\partial S_{ij}}{\partial x_j}-\frac{1}{\rho}\overline{\tau}_{bi} \tag{2.24}$$

The surface shear stresses and lateral shear stresses are also neglected.

2.2.3 Wave Energy Conservation Equation

The equation considering both refraction and diffraction with current has been developed by Boiij (1981) and corrections were made later by Kirby (1984). Both used variational principle. In this study, a method that modified Kirby's derivation is developed. In

parallel, the perturbation technique is also applied. Same results are obtained and are given in Appendix 1. Here only the derivation from variational principle is presented.

The variational principle, first applied in the irrotational flow motion by Luke (1967), states that the variation of a certain conservative quantity, often an integral, vanishes if the function that describes the evolution of the physical process is subjected to small variations. It is represented as

$$\delta[\int_t \int_{\mathbf{x}} L d\mathbf{x} dt] = 0 \tag{2.25}$$

where $\mathbf{x} = x\hat{i} + y\hat{j}$ is in horizontal space. For irrotational flow, the energy is conserved and L can be chosen as the Bernoulli sum:

$$L = \int_{-h}^{\eta} [\phi_t + \frac{1}{2}(\nabla\phi)^2 + gz] dz \tag{2.26}$$

where

$\phi_t = \frac{\partial \phi}{\partial t}$,

∇ is the three dimensional gradient operator,

$\nabla = \frac{\partial}{\partial x}\hat{i} + \frac{\partial}{\partial y}\hat{j} + \frac{\partial}{\partial z}\hat{k}$,

$\hat{i}$, $\hat{j}$ and $\hat{k}$ are unit vectors in x, y and z directions, respectively.

The potential function ϕ consists of two parts

$$\phi = \phi_w + \phi_c \tag{2.27}$$

where ϕ_w and ϕ_c are wave potential and current potential functions,respectively. A weak point about the expression of ϕ_c is that the mean current field may be rotational, since we do not know a priori whether the mean flow field derived from momentum equations satisfies the condition of irrotationality everywhere, i.e.,

$$curl \quad \mathbf{U} = 0$$

However, the irrotational assumption will be used here.

For a slowly varying bottom topography ϕ can be expressed as (Kirby, 1983):

$$\phi(x,y,z,t) = \delta\phi_c(\mu x,\mu y) + \epsilon\phi_{w1}(x,\mu^{1/2}y,\mu y,\mu x,z,t) + \epsilon^2\phi_{w2}(x,\mu^{1/2}y,\mu y,\mu x,z,t) \tag{2.28}$$

where μ is a scale parameter with an order of magnitude $0(\nabla_h h/kh)$ representing the spatial change over the space of wave length in which ∇_h is horizontal spatial gradient and $k = 2\pi/L$ is wave number where L is wave length. δ is the strength parameter of current defined as $\nabla_h\phi_c/\sqrt{gh}$. ϵ is the Stokes wave steepness parameter $\epsilon = 0(ak)$, a is the wave amplitude.

The spatial scale parameter μ is introduced to differentiate two different spatial scales in the model: one is related to the fast wave-like functions, and the other one is connected to the slow spatial modulations, such as bottom topography, the changes of current speed, wave length etc. Therefore, we have

$$x = x + \mu x = X + X_2 \tag{2.29}$$

$$y = \mu^{1/2}y + \mu y = Y_1 + Y_2 \tag{2.30}$$

and their derivatives are replaced by

$$\frac{\partial}{\partial x} = \frac{\partial}{\partial X} + \mu\frac{\partial}{\partial X_2} \tag{2.31}$$

$$\frac{\partial}{\partial y} = \mu^{1/2}\frac{\partial}{\partial Y_1} + \mu\frac{\partial}{\partial Y_2} \tag{2.32}$$

The scales as selected imply that spatial derivative with respect to phase function occurs only in the x-direction which is true when the angle of wave propagating is small with respect to the x-axis, i.e., it is assumed that no fast wave-like variations occur in the y-direction. It is consistent with the forward scattering approach that the complex amplitude A is allowed to vary as $0(\mu^{1/2})$ in the y-direction. The problem is further considered to be quasi-steady; time derivatives only appear in wave term.

There are three magnitude parameters δ, μ and ϵ in the formulation. Different ratios among those parameters will yield different forms of the energy equation. In the present

study, we adopt Kirby's (1983) model given the relationship as follows

$$\frac{\delta}{\epsilon^{-2}} = 1, \quad \frac{\mu}{\epsilon^2} = 1 \tag{2.33}$$

which represent slow varying topography, strong mean current, and small incident wave angles.

In equation (2.28) ϕ_{w1} and ϕ_{w2} are first and second order potential function, respectively. ϕ_{w1} and ϕ_{w2} are expressed as follows:

$$\phi_{w1} = A_1^m(x, \mu^{1/2}y, \mu x, \mu y, t) f_1^m(\mu x, \mu y, z) \tag{2.34}$$

$$\phi_{w2} = A_2^m(x, \mu^{1/2}y, \mu x, \mu y, t) f_2^m(\mu x, \mu y, z) \tag{2.35}$$

The A_j^m can be split into two parts: a modulated amplitude function and a phase function:

$$A_j^m(x, \mu^{1/2}y, \mu x, \mu y, t) = A'^m_j(\mu^{1/2}y, \mu x, \mu y) e^{im\psi} + c.c \tag{2.36}$$

where A'^m_j is the complex amplitude, ψ is the phase function and c.c is the complex conjugate. The phase function is defined as

$$\psi = \int^x k_1 dx - \omega t \tag{2.37}$$

where k_1 is the wave number in main (or x) direction and $\omega = 2\pi/T$ is the angular wave frequency in which T is the wave period. The real wave direction which is different from the main direction is absorbed in the amplitude function. The subscripts and superscripts in the equations represent the order and harmonics, respectively. However the absolute superscript values should be no bigger than the subscript values. Substituting (2.34) and (2.35) into (2.28), yields

$$\begin{aligned} \phi \;=\; & \epsilon^{-2}\phi_c(\epsilon^2 x, \epsilon^2 y) + \epsilon A_1^m(x, \epsilon y, \epsilon^2 x, \epsilon^2 y, t) f_1^m(\epsilon^2 x, \epsilon^2 y, z) + \\ & \epsilon^2 A_2^m(x, \epsilon y, \epsilon^2 x, \epsilon^2 y, t) f_2^m(\epsilon^2 x, \epsilon^2 y, z) \end{aligned} \tag{2.38}$$

where δ and μ have been replaced by ϵ^{-2} and ϵ^2, respectively, by virtue of Eq.(2.33).

Substituting (2.38) into (2.26), we obtain with (2.37), term by term

$$\phi_t = \epsilon A_{1t}^m f_1^m + \epsilon^2 A_{2t}^m f_2^m \tag{2.39}$$

$$\begin{aligned}\nabla\phi &= \nabla_h\phi_c + \epsilon f_1^m A_{1X}^m \hat{i} + \epsilon^2 f_1^m A_{1Y_1}^m \hat{j} + \epsilon^3 f_1^m \nabla_h A_1^m + \epsilon^3 A_1^m \nabla_h f_1^m \\ &\quad + \epsilon^2 f_2^m A_{2X}^m \hat{i} + \epsilon^3 f_2^m A_{2Y_1}^m \hat{j} + \epsilon^4 f_2^m \nabla_h A_2^m + \epsilon^4 A_2^m \nabla_h f_2^m \\ &\quad + (\epsilon A_1^m f_{1z}^m + \epsilon^2 A_2^m f_{2z}^m)\hat{k} \end{aligned} \tag{2.40}$$

where

∇_h is the horizontal gradient operator,

$$\nabla_h = \frac{\partial}{\partial x}\hat{i} + \frac{\partial}{\partial y}\hat{j}.$$

Therefore, by definition we have

$$\nabla_h\phi_c = U\,\hat{i} + V\,\hat{j} \tag{2.41}$$

where velocities include wave induced mean current.

The first two terms in Eq.(2.40) represents linear wave superimposed upon uniform current over flat bottom. In Eq.(2.26), the $(\nabla\phi)^2$ term when computed to fourth order becomes

$$\begin{aligned}(\nabla\phi)^2 &= (\nabla_h\phi_c)^2 + \epsilon^2 f_1^m f_1^n A_{1X}^m A_{1X}^n + \epsilon^4 f_1^m f_1^n A_{1Y_1}^m A_{1Y_1}^n + \epsilon^4 f_2^m f_2^n A_{2X}^m A_{2X}^n \\ &\quad + \epsilon^2 f_{1z}^m f_{1z}^n A_1^m A_1^n + \epsilon^4 f_{2z}^m f_{2z}^n A_2^m A_2^n + \epsilon 2U f_1^m A_{1X}^m + \epsilon^2 2V f_1^m A_{1Y_1}^m \\ &\quad + \epsilon^3 2 f_1^m \nabla_h\phi_c \cdot \nabla_h A_1^m + \epsilon^3 2 A_1^m \nabla_h\phi_c \cdot \nabla_h f_1^m + \epsilon^2 2U f_2^m A_{2X}^m + \epsilon^3 2V f_2^m A_{2Y_1}^m \\ &\quad + \epsilon^4 2 f_2^m \nabla_h\phi_c \cdot \nabla_h A_2^m + \epsilon^4 2 A_2^m \nabla_h\phi_c \cdot \nabla_h f_2^m + \epsilon^4 2 f_1^m f_1^n A_{1X}^m A_{1X_2}^n \\ &\quad + \epsilon^4 2 f_1^m f_{1X_2}^n A_1^m A_{1X}^n + \epsilon^3 2 f_1^m f_2^n A_{1X}^m A_{2X}^n + \epsilon^3 2 A_1^m A_2^n f_{1z}^m f_{2z}^n \end{aligned} \tag{2.42}$$

The subscripts X, Y and z are partial derivatives. The superscripts m and n represent interaction between two harmonics.

Free surface envelope can be considered as two parts: one is related to mean current as η_0 and another one is driven by waves as η'. Later we will see η_0 has the same order as $|\,U\,|$.

$$\eta(x,y,t) = \eta_0(x,y) + \eta'(x,y,t) \tag{2.43}$$

or in the stretched coordinates

$$\eta(x,\epsilon y,\epsilon^2 x,\epsilon^2 y,t)=\eta_0(\epsilon^2 x,\epsilon^2 y)+\eta'(x,\epsilon y,\epsilon^2 x,\epsilon^2 y,t) \tag{2.44}$$

where η' has the order $0(\epsilon)$ at most and it can be expressed as

$$\eta'=\epsilon\eta_1^m+\epsilon^2\eta_2^m+0(\epsilon^3) \tag{2.45}$$

where η_1 and η_2 are first and second order surface elevations, respectively. By virtue of (2.45), (2.43) can be rewritten as

$$\eta=\eta_0+\epsilon\eta_1^m+\epsilon^2\eta_2^m \tag{2.46}$$

Expanding (2.26) in Taylor series about $z=\eta_0$, results in

$$\begin{aligned} L &= \int_{-h}^{\eta}[\phi_t+\frac{1}{2}(\nabla\phi)^2]dz+\frac{1}{2}g\eta^2-\frac{1}{2}gh^2 \\ &= \int_{-h}^{\eta}[\phi_t+\frac{1}{2}(\nabla\phi)^2]dz+\eta'[\phi_t+\frac{1}{2}(\nabla\phi)^2]_{z=\eta_0}+\frac{1}{2}\eta'^2\frac{\partial}{\partial z}[\phi_t+\frac{1}{2}(\nabla\phi)^2]_{z=\eta_0} \\ &\quad +\frac{1}{6}\eta'^3\frac{\partial}{\partial z^2}[\phi_t+\frac{1}{2}(\nabla\phi)^2]_{z=\eta_0}+\frac{1}{2}g\eta^2-\frac{1}{2}gh+\cdots \end{aligned} \tag{2.47}$$

Introducing a shifting coordinate defined as

$$z'=z-\eta_0,\quad h'=h+\eta_0$$

and substituting into (2.47), we get, after dropping the primes on h' and z' for convenience,

$$\begin{aligned} L &= \int_{-h}^{0}[\phi_t+\frac{1}{2}(\nabla\phi)^2]dz+\eta'[\phi_t+\frac{1}{2}(\nabla\phi)^2]_{z=0}+\frac{1}{2}\eta'^2\frac{\partial}{\partial z}[\phi_t+\frac{1}{2}(\nabla\phi)^2]_{z=0} \\ &\quad +\frac{1}{6}\eta'^3\frac{\partial}{\partial z^2}[\phi_t+\frac{1}{2}(\nabla\phi)^2]_{z=0}+\frac{1}{2}g\eta^2-\frac{1}{2}gh_0 \end{aligned} \tag{2.48}$$

where we denote h_0 as still water depth. The expansion is carried out to fourth term only as the higher order terms will not affect the third order wave equation.

Certain integrations in (2.48) that involve f_i^m of Eqs.(2.34) and (2.35) are defined as follows for future use:

$$\int_{-h}^{0} f_i^m dz = Q_1^m \tag{2.49}$$

$$\int_{-h}^{0} f_i^m f_j^n dz = P_{ij}^{mn} \tag{2.50}$$

$$\int_{-h}^{0} f_{iz}^m f_{jz}^n dz = R_{ij}^{mn} \tag{2.51}$$

where i, j, m and n are free indexes and subscript z represents partial derivatives. From Stokes wave theory, the well-known expressions for the f_1^m and f_2^n are

$$f_1^1 = f_1^{-1} = \frac{\cosh k(h+z)}{\cosh kh} \tag{2.52}$$

$$f_2^2 = f_2^{-2} = \frac{\cosh 2k(h+z)}{\cosh 2kh} \tag{2.53}$$

The typical results in (2.49)-(2.51) that will be used later are given as follows:

$$Q_1^1 = \frac{c^2}{g}$$

$$P_{11}^{11} = \frac{\cosh kh}{k \sinh^3 h}$$

$$P_{12}^{12} = \frac{1 + 2\cosh^2 kh}{3k \cosh kh \sinh^3 kh}$$

$$P_{22}^{22} = \frac{1}{\sinh^3 kh}\left(\frac{h}{2} + \frac{\sinh 4kh}{8k}\right)$$

$$R_{11}^{11} = \frac{1}{g}(\sigma^2 - k^2 c c_g)$$

$$R_{12}^{12} = \frac{4k}{3 \cosh kh \sinh kh}$$

$$R_{22}^{22} = \frac{k^2}{2\sinh^8 kh}\left(\frac{\sinh 4kh}{k} - h\right)$$

where c is the wave celerity, $c = \frac{L}{T}$;

c_g is the group velocity, $c_g = c \cdot n$ with

$n = \frac{1}{2}(1 + \frac{2kh}{\sinh 2kh})$;

$\sigma = \sqrt{gk\tanh kh}$ is the local angular wave frequency, it will be discussed in section (2.2.4).

Substituting (2.39) and (2.42) into (2.48),with the definition (2.49)-(2.51), we have

$$\begin{aligned}
L = \; & \epsilon Q_1^m A_{1t}^n + \frac{1}{2}\epsilon^2 P_{11}^{mn} A_{1X}^m A_{1X}^n + \frac{1}{2}\epsilon^4 P_{11}^{mn} A_{1Y_1}^m A_{1Y_1}^n + \frac{1}{2}\epsilon^2 R_{11}^{mn} A_1^m A_1^n \\
& + \epsilon Q_1^m U A_{1X}^n + \epsilon^2 Q_1^m V A_{1Y_1}^n + \epsilon^3 Q_1^m \nabla_h \phi_c \cdot \nabla_h A_1^m + \epsilon^4 P_{11}^{mn} A_{1X}^m A_{1X_2}^n \\
& + \epsilon^3 P_{12}^{mn} A_{1X}^m A_{2X}^n + \epsilon^3 R_{12}^{mn} A_1^m A_2^n + \frac{1}{2} g(\epsilon 2\eta_0 \eta_1^m + \epsilon^2 \varsigma_2^m + \epsilon^3 2\eta_1^m \eta_2^n) + \epsilon^2 \eta_1^m f_1^n A_{1t}^n \\
& + \epsilon^3 \eta_1^m f_2^n A_{2t}^n + \epsilon^3 \eta_2^m f_1^n A_{1t}^n + \frac{1}{2}\epsilon \eta_1^m (\nabla_h \phi_c)^2 + \frac{1}{2}\epsilon^3 \eta_1^k f_1^m f_1^n A_{1X}^m A_{1X}^n \\
& + \frac{1}{2}\epsilon^3 \eta_1^k f_{1z}^m f_{1z}^n A_1^m A_1^n + \epsilon^2 \eta_1^m U f_1^n A_{1X}^n + \epsilon^3 \eta_1^m V f_1^n A_{1Y_1}^n + \epsilon^4 \eta_1^m f_1^n \nabla_h \phi_c \cdot \nabla_h A_1^n \\
& + \epsilon^3 \eta_1^m U f_2^n A_{2X}^n + \epsilon^4 \eta_1^m V f_2^n A_{2Y_1}^n + \epsilon^4 \eta_1^k f_1^m f_2^n A_{1X}^m A_{2X}^n + \epsilon^4 \eta_1^k f_{1z}^m f_{2z}^n A_1^m A_2^n \\
& + \frac{1}{2}\epsilon^4 \eta_2^k f_1^m f_1^n A_{1X}^m A_{1X}^n + \frac{1}{2}\epsilon^4 \eta_2^k f_{1z}^m f_{1z}^n A_1^m A_1^n + \epsilon^3 \eta_2^m U f_1^n A_{1X}^n + \epsilon^4 \eta_2^m V f_1^n A_{1Y_1}^n \\
& + \frac{1}{2}\epsilon^3 \varsigma_2^m f_{1z}^n A_{1t}^n + \frac{1}{2}\epsilon^4 \varsigma_2^m f_{2z}^n A_{2t}^n + \epsilon^4 \eta_1^k \eta_2^m f_{1z}^n A_{1t}^n + \frac{1}{2}\epsilon^4 \varsigma_2^k f_1^m f_{1z}^n A_{1X}^m A_{1X}^n \\
& + \frac{1}{2}\epsilon^4 \varsigma_2^k f_{1z}^m f_{1zz}^n A_1^m A_1^n + \frac{1}{2}\epsilon^3 \varsigma_2^m U f_{1z}^n A_{1X}^n + \frac{1}{2}\epsilon^4 \varsigma_2^m V f_{1z}^n A_{1Y_1}^n + \frac{1}{2}\epsilon^4 \varsigma_2^m U f_{2z}^n A_{2X}^n \\
& + \epsilon^4 \eta_1^k \eta_2^m U f_{1z}^n A_{1X}^n + \frac{1}{6}\epsilon^4 \varsigma_3^m f_{1zz}^n A_{1t}^n + \epsilon^4 \frac{1}{6} \varsigma_3^m U f_{1zz}^n A_{1X}^n
\end{aligned} \tag{2.54}$$

where the condition of $\nabla_h f_1^n = 0$ has been involved. All terms are evaluated at $z = 0$. For simplicity, we only keep terms containing η_1 and A_1, since as will be shown L varies with respect to η_1 and A_1 only. In (2.54), the superscripts are free indexes (nonrepeating) which may not assume the same value for different terms, but they give same value in one term. The terms of ς_m^n are defined as

$$\varsigma_2^k = \delta_{mn} \eta_1^m \eta_1^n \qquad m + n = k \tag{2.55}$$

$$\varsigma_3^j = \delta_{kmn} \eta_1^k \eta_1^m \eta_1^n \qquad k + m + n = j \tag{2.56}$$

where

when $m = n$ or $k = m = n$, δ_{mn} and δ_{kmn} equal to unit, otherwise they assume the values of 2 and 3, respectively. Those give

$$\begin{aligned}
\varsigma_2^0 &= \eta_1^0\eta_1^0 + 2\eta_1^1\eta_1^{-1} \\
\varsigma_2^1 &= 2\eta_1^0\eta_1^1 \\
\varsigma_2^{-1} &= 2\eta_1^0\eta_1^{-1} \\
\varsigma_2^2 &= \eta_1^1\eta_1^1 \\
\varsigma_3^1 &= 3\eta_1^1\eta_1^1\eta_1^{-1} + 3\eta_1^0\eta_1^0\eta_1^1 \\
\varsigma_3^{-1} &= 3\eta_1^1\eta_1^{-1}\eta_1^{-1} + 3\eta_1^0\eta_1^0\eta_1^{-1}
\end{aligned}$$

After introducing the following

$$L = L_0 + \epsilon L_1 + \epsilon^2 L_2 + \epsilon^3 L_3 + \epsilon^4 L_4 + \cdots \tag{2.57}$$

Equation (2.54) can be separated by grouping the terms of the same order:

$O(\epsilon)$

$$L_1 = \frac{1}{2}Q_1^m A_{1t}^m + Q_1^m U A_{1X}^m + g\eta_0\eta_1^m + \frac{1}{2}\eta_1^m(\nabla_h\phi_c)^2 \tag{2.58}$$

$O(\epsilon^2)$

$$\begin{aligned}
L_2 = &\frac{1}{2}P_{11}^{mn}A_{1X}^m A_{1X}^n + \frac{1}{2}R_{11}^{mn}A_1^m A_1^n + Q_1^m V A_{1Y_1}^m + \frac{1}{2}g\varsigma_2^m + \eta_1^m f_1^n A_{1t}^n \\
&+\eta_1^m U f_1^n A_{1X}^n
\end{aligned} \tag{2.59}$$

$O(\epsilon^3)$

$$\begin{aligned}
L_3 = &Q_1^m\nabla_h\phi_c\cdot\nabla_h A_1^m + P_{12}^{mn}A_{1X}^m A_{2X}^n + R_{12}^{mn}A_1^m A_2^n + g\eta_1^m\eta_2^n + \eta_1^m f_2^n A_{2t}^n \\
&+\eta_2^m f_1^n A_{1t}^n + \frac{1}{2}\eta_1^k f_1^m f_1^n A_{1X}^m A_{1X}^n + \frac{1}{2}\eta_1^k f_{1z}^m f_{1z}^n A_1^m A_1^n + \eta_1^m V f_1^n A_{1Y_1}^n \\
&+\eta_1^m U f_2^n A_{2X}^n + \eta_2^m U f_1^n A_{1X}^n + \frac{1}{2}\varsigma_2^m f_{1z}^n A_{1t}^n + \frac{1}{2}\varsigma_2^m U f_{1z}^n A_{1X}^n
\end{aligned} \tag{2.60}$$

$O(\epsilon^4)$

$$
\begin{aligned}
L_4 = & \frac{1}{2}P_{11}^{mn}A_{1Y_1}^{m}A_{1Y_1}^{n} + P_{11}^{mn}A_{1X}^{m}A_{1X_2}^{n} + \eta_1^m f_1^n \nabla_h\phi_c\cdot\nabla_h A_1^n + \eta_1^m V f_2^n A_{2Y_1}^n \\
& + \eta_1^k f_{1z}^m f_{2z}^n A_1^m A_2^n + \eta_1^k f_1^m f_2^n A_{1X}^m A_{2X}^n + \frac{1}{2}\eta_2^k f_{1z}^m f_{1z}^n A_1^m A_1^n + \eta_2^m V f_1^n A_{1Y_1}^n \\
& + \frac{1}{2}\eta_2^k f_1^m f_1^n A_{1X}^m A_{1X}^n + \frac{1}{2}\varsigma_2^m f_{2z}^n A_{2t}^n + \eta_1^k \eta_2^m f_{1z}^n A_{1t}^n + \frac{1}{2}\varsigma_2^k f_1^m f_{1z}^n A_{1X}^m A_{1X}^n \\
& + \frac{1}{2}\varsigma_2^k f_{1zz}^m f_{1z}^n A_1^m A_1^n + \frac{1}{2}\varsigma_2^m V f_{1z}^n A_{1Y_1}^n + \frac{1}{2}\varsigma_2^m U f_{2z}^n A_{2X}^n + \eta_1^k \eta_2^m U f_{1z}^n A_{1X}^n \\
& + \frac{1}{6}\varsigma_3^m f_{1zz}^n A_{1t}^n + \frac{1}{6}\varsigma_3^m U f_{1zz}^n A_{1X}^n
\end{aligned}
\tag{2.61}
$$

There is no L_0 term, as it contains neither η_1 nor A_1 term. For each order, varying with respect to η_1 and A_1, we will obtain a series of equations. The variational principle gives

$$
\frac{\partial L_i}{\partial B} - \frac{\partial}{\partial t}\left(\frac{\partial L_i}{\partial B_t}\right) - \nabla_h\left[\frac{\partial L_i}{\partial(\nabla_h B)}\right] = D_e \tag{2.62}
$$

where B represents either η_1 or A_1, D_e is the dissipation term that is caused by bottom friction and turbulence that eventually are converted into internal energy, which is irreversible. (One possible formation of D_e is given in Appendix A by using perturbation method.) Equation (2.62) can be written in detail as

$$
\left[\frac{\partial}{\partial B} - \frac{\partial}{\partial X_2}\left(\frac{\partial}{\partial B_{X_2}}\right) - \frac{\partial}{\partial Y_1}\left(\frac{\partial}{\partial B_{Y_1}}\right) - \frac{\partial}{\partial Y_2}\left(\frac{\partial}{\partial B_{Y_2}}\right) - \frac{\partial}{\partial t}\left(\frac{\partial}{\partial B_t}\right)\right] L_i = D_e \tag{2.63}
$$

The following discussions are based on the orders of L.

1) $0(\epsilon)$

Varying (2.58) with respect to η_1^m yields

$$
\eta_0 = -\frac{1}{2g}(\nabla_h\phi_c)^2 \tag{2.64}
$$

which states that the surface elevation by mean current is simply balanced by kinetic pressure. The same result is obtained if one uses Bernoulli equation at order $0(1)$.

2) $0(\epsilon^2)$

Equation (2.59) varied with respect to η_1^m, results in

$$
\eta_1^n = -\frac{1}{g}f_1^n(A_{1t}^n + UA_{1X}^n)
$$

$$= -\frac{1}{g} f_1^n \frac{DA_1^n}{Dt} \tag{2.65}$$

$\frac{D}{Dt}$ is the total derivative related to the x- direction

$$\frac{D}{Dt} = \frac{\partial}{\partial t} + U\frac{\partial}{\partial X}$$

For $n = 0$ or the zeroth harmonic, A_1^0 is independent of X and t, which results in

$$\eta_1^n = 0 \qquad \text{for} \quad n = 0 \tag{2.66}$$

From Stokes linear waves, we know that

$$A_1^1 = -ig\frac{a}{2\sigma_1}e^{i\psi} \tag{2.67}$$

$$A_1^{-1} = ig\frac{a}{2\sigma_1}e^{-i\psi} \tag{2.68}$$

where a is a complex amplitude and σ_1 is defined as

$$\sigma_1 = \omega - Uk_1 \tag{2.69}$$

which is the apparent local angular frequency that represents the waves riding on unidirectional flow. According to linear wave theory, the dispersion relationship is

$$\sigma = \omega - Uk_1 - Vk_2 \tag{2.70}$$

where $k_1 = k\cos\theta$ and $k_2 = k\sin\theta$ are the wave numbers in x and y direction, respectively and θ is the incident wave angle as shown in Fig.2.1. From (2.69) and (2.70), we find

$$\sigma_1 = \sigma + Vk_2 = \sigma + 0(\epsilon)$$

since for small incident wave angle, $\sin\theta \sim \theta = 0(\epsilon)$. Hence for $n = 1$ and $n = -1, f_1^{-1} = f_1^1 = 1$ at $z = 0$, we have

$$\eta_1^1 = -\frac{1}{g}\frac{DA_1^1}{Dt} = \frac{a}{2}e^{i\psi} \tag{2.71}$$

$$\eta_1^{-1} = -\frac{1}{g}\frac{DA_1^{-1}}{Dt} = \frac{a}{2}e^{-i\psi} \tag{2.72}$$

both are the first harmonic solutions and the same as given by linear wave theory. η_1^1 and η_1^{-1} have the same amplitudes, but traveling in opposite directions. As mentioned before, the complex amplitude "a" absorbs the difference between real wave direction and its main direction, since phase function ψ is only defined in x the direction. Next, varying L_2 with respect to A_i^j, ($j = m$ or n), we have

$$R_{11}^{mn}A_1^m - f_1^n\eta_{1t}^m - P_{11}^{mn}A_{1XX}^m - Uf_1^n\eta_{1X}^m = 0 \tag{2.73}$$

a) let $m = 0$ (the zeroth harmonic), it gives

$$R_{11}^{n0}A_1^0 = 0$$

Therefore,

$$A_1^0 = 0 \quad \text{or} \quad f_{1x}^0 = 0 \quad \text{from (2.51)} \tag{2.74}$$

Later we can prove that if $f_{1x} = 0$, then $f_1^0 = 0$.

b) Considering the first harmonic, we obtain

$$[cc_g(k_1^2 - k^2)]\frac{A_1^1}{g} = 0 \tag{2.75}$$

It is important to note that (2.75) is of the order of $0(\epsilon^3)$, since $k^2 - k_1^2 = k_2^2 = k^2\sin^2\theta = 0(\epsilon^2)$. This term later will be combined with other third order terms to form the wave equation which is of the order of $0(\epsilon^3)$

3) $0(\epsilon^3)$

Varying L_3 with respect to η_1^j and A_1^j ($j = n$, m or k) respectively, we obtain

$$g\eta_2^n + f_2^nA_{1t}^n + \frac{1}{2}f_1^mf_1^nA_{1X}^mA_{1X}^n + \frac{1}{2}f_{1x}^mf_{1x}^nA_1^mA_1^n + Vf_1^nA_{1Y_1}^n + \eta_1^mf_{1x}^nA_{1t}^n$$
$$+Uf_2^nA_{2x}^n + \eta_1^mUf_{1x}^nA_{1X}^n = 0 \tag{2.76}$$

$$R_{11}^{mn}A_2^n + \eta_1^kf_{1x}^mf_{1x}^nA_1^n - \nabla_h\cdot(Q_1^m\nabla_h\phi_c) - P_{12}^{mn}A_{2XX}^n - f_1^n\eta_{2t}^m - f_1^mf_1^n(A_{1X}^n\eta_1^k)_X$$
$$-Vf_1^n\eta_{1Y_1}^m - Uf_1^n\eta_{2X}^m - f_{1x}^n\eta_1^k\eta_{1t}^m - f_{1x}^n\eta_1^k\eta_{1X}^m = 0 \tag{2.77}$$

we emphasize again that the superscripts only take the same values in one term; there is no relationship among different terms. There are only two unknowns, η_2^n and A_2^n, in the above two equations and so that they can be solved.

a) Collecting all the terms with zeroth harmonics in (2.76), we get

$$\eta_2^0 = -\frac{1}{g}\{f_1^{1^2}A_{1X}^1 A_{1X}^{-1} + f_{1x}^{1^2}A_1^1 A_1^{-1} + f_{1x}^1[\eta_1^1 A_{1t}^{-1} + \eta_1^{-1}A_{1t}^1] + f_{1x}^1[\eta_1^1 A_{1X}^{-1} + \eta_1^{-1}A_{1X}^1]\}$$

Here the condition of $f_1^1 = f_1^{-1}$ has been applied.

The values on the right hand side of above equation are known, so that

$$\eta_2^0 = -\mid a \mid^2[\frac{gk_1^2}{4\sigma^2} + \frac{gk^2\tanh^2 kh}{4\sigma^2} - \frac{k\tanh kh}{2}] \tag{2.78}$$

Since we only consider up to $0(\epsilon^3)$, $k_1$and σ_1 can be replaced by k and σ, and vice versa. Equation (2.78) becomes

$$\eta_2^0 = -\mid a \mid^2 \frac{k}{2\sinh 2kh} + 0(\epsilon^4) \tag{2.79}$$

This is the set-down of mean free surface with reference to the shifted coordinates. From (2.77), we obtain

$$A_2^0 = \frac{1}{R_{12}^{m0}}\nabla_h \cdot (Q_1^m \nabla_h \phi_c) \tag{2.80}$$

where m can assume any arbitary value. Hence, A_2^0 can not be determined as f_{2x}^0 remains unknown. However we will show later that $A_2^0 f_{2x}^0$ is non-zero. From (2.80), the previous statement in case 2 is confirmed, that is, let $m = 0$, we must have $f_1^0 = 0$ for $f_{1x}^0 = 0$. Otherwise, A_2^0 will approach infinity.

b) The first order harmonics in (2.76) yield the following solution

$$\eta_2^1 = -\frac{1}{g}[VA_{1Y_1}^1 - if_2^1\sigma_1 A_2^1] \tag{2.81}$$

From (2.77), together with (2.81), we have

$$A_2^1(R_{12}^{m1} + k_1^2 P_{12}^{m1} - \frac{1}{g}\sigma_1^2 f_2^1 f_1^m) = 0 \tag{2.82}$$

For $m = 1$, if we assume that f_2^1 has the same form as f_1^1, the terms in the bracket are identically equal zero. But, if m is any value less than or equal to 1, i.e., $m \leq |1|$, we may select $A_2^1 = 0$ such that

$$\eta_2^1 = -VA_{1Y_1}^1 = i\frac{V}{\sigma_1}a_{Y_1}e^{i\psi} \tag{2.83}$$

which states that the surface elevation of the first harmonic of the second order of the wave is balanced by the variation of wave amplitude modulation in longshore direction.

c) For the first negative harmonic, (2.76) and (2.77) give

$$A_2^{-1} = 0 \tag{2.84}$$

$$\eta_2^{-1} = -i\frac{V}{\sigma_1}a_{Y_1}e^{-i\psi} \tag{2.85}$$

d) Considering the second harmonic, after lower harmonic terms have been dropped, we obtain from (2.76) and (2.77), respectively

$$g\eta_2^2 + f_2^2A_{2t}^2 + \frac{1}{2}A_{1X}^{1^2} + \frac{1}{2}f_{1z}^{1^2}A_1^{1^2} + f_2^2UA_{2X}^2 + f_{1z}^1\eta_1^1A_{1t}^1 + f_{1z}^1U\eta_1^1A_{1X}^1 = 0$$

and

$$R_{12}^{12}A_2^2 + f_{1z}^{1^2}\eta_1^1A_1^1 - P_{12}^{12}A_{2XX}^2 - \eta_{2t}^2 - (A_{1X}^1\eta_1^1)_X - U\eta_{2X}^2 - f_{1z}^1\eta_1^1\eta_{1t}^1$$
$$-f_{1z}^1\eta_1^1\eta_{1X}^1 = 0$$

Solving two equations for two unknowns A_2^2 and η_2^2 yield

$$A_2^2 = -i\frac{3\sigma|a|^2}{16}e^{i2\psi} + 0(\epsilon^3) \tag{2.86}$$

$$\eta_2^2 = \frac{|a|^2k\cosh kh}{8\sinh^3 kh}(2 + \cosh 2kh)e^{i2\psi} + 0(\epsilon^3) \tag{2.87}$$

They are the same as the second order Stokes waves.

4) $0(\epsilon^4)$

Varying L_4 with respect to η_1^i, gives

$$f_1^n\nabla_h\phi_c\cdot\nabla_h A_1^n + f_{1z}^m f_{2z}^n A_1^m A_2^n + f_1^m f_2^n A_{1X}^m A_{2X}^n + \eta_1^m f_{2z}^n A_{2t}^n + \eta_2^m f_{1z}^n A_{1t}^n$$
$$+\eta_1^k f_1^m f_{1z}^n A_{1X}^m A_{1X}^n + \eta_1^k f_{1z}^m f_{1zz}^n A_1^m A_1^n + \eta_1^m U f_{2z}^n A_{2X}^n + \eta_2^m U f_{1z}^n A_{1X}^n + \frac{1}{2}\zeta_2^m f_{1zz}^n A_{1t}^n$$
$$+\frac{1}{2}\zeta_2^m f_{1zz}^n A_{1X}^n + V f_2^n A_{2Y_1}^n + \eta_1^m V f_{1z}^n A_{1Y_1}^n + V f_2^n A_{2Y_1}^n = 0$$

For the first harmonic, we have

$$\nabla_h\phi_c\cdot\nabla_h A_1^1 + f_{1z}^1 f_{2z}^1 A_1^{-1} A_2^2 + f_{1z}^1 f_{2z}^0 A_1^1 A_2^0 + f_1^1 f_2^2 A_{1X}^{-1} A_{2X}^2 + f_{2z}^2 \eta_1^{-1}\frac{DA_2^2}{Dt}$$
$$+f_{1z}^1\eta_2^0\frac{DA_1^1}{Dt} + f_{1z}^1\eta_2^2\frac{DA_1^{-1}}{Dt} + f_1^1 f_{1z}^1(2A_{1X}^1 A_{1X}^{-1}\eta_1^1 + A_{1X}^{1^2}\eta_1^{-1}) + f_{1z}^1 f_{1zz}^1$$
$$(2A_1^1 A_1^{-1}\eta_1^1 + A_1^{1^2}\eta_1^{-1}) + \frac{1}{2}f_{1zz}^1\zeta_2^0\frac{DA_1^1}{Dt} + \frac{1}{2}f_{1zz}^1\zeta_2^2\frac{DA_1^{-1}}{Dt} = 0$$

where

$$\frac{DA_1^1}{Dt} = -\frac{g}{2}ae^{i\psi};$$

$$\frac{DA_1^{-1}}{Dt} = -\frac{g}{2}ae^{-i\psi};$$

$$\frac{DA_2^2}{Dt} = -\frac{3}{8}\sigma^2|\,a\,|^2 e^{i2\psi}$$

The only unknown in the equation is $f_{2z}^0 A_2^0$, so that

$$f_{2z}^0 A_2^0 = -[\frac{g}{\sigma}\nabla_h\phi_c\cdot\nabla_h(\frac{1}{\sigma_1}) + \frac{g}{a\sigma\sigma_1}\nabla_h\phi_c\cdot\nabla_h a + i\frac{2F}{\sigma}|\,a\,|^2] \tag{2.88}$$

in which

$$F = \frac{gk^2}{16\sinh^4 kh}(3 - 2\tanh^2 kh + 4\sinh^2 kh - \sinh^2 kh\cosh^2 kh)$$

Next, varying L_4 with respect to A_1^i, also considering first harmonic, we get

$$f_{1z}^1 f_{2z}^2\eta_1^{-1}A_2^2 + f_{1z}^1 f_{2z}^0\eta_1^1 A_2^0 + f_{1z}^2(\eta_2^0 A_1^1 + \eta_2^2\eta_1^{-1}) + f_{1z}^1 f_{1z}^1(\zeta_2^0 A_1^1$$

$$+\varsigma_2^2 A_1^{-1}) + f_{1x}^1\sigma_1(\eta_1^{-1}\eta_2^2 + \eta_1^1\eta_2^0) - \frac{1}{2}\sigma_1 f_{1xx}^1(-\varsigma_2^0\eta_1^1 + \varsigma_2^2\eta_1^{-1}) - P_{11}^{11}A_{1Y_1Y_1}^1$$
$$-(P_{11}^{11}A_{1X}^1)_{X_2} - P_{11}^{11}A_{1X_2X}^1 - \nabla_h\cdot(\eta_1^1\nabla_h\phi_c) - f_2^2(\eta_1^{-1}A_{2X}^2)_X - (\eta_2^0 A_{1X}^1$$
$$-\eta_2^2 A_{1X}^{-1})_X - f_{1x}^1(\varsigma_2^2 A_{1X}^{-1} + \varsigma_2^0 A_{1X}^1) - V\eta_{2Y_1}^1 = 0$$

where again $f_1^1 = f_1^{-1} = 1$ is applied. Each term in the above equation has been calculated before. After some tedious algebraic manipulation, we obtain

$$2(cc_g k_1 + \sigma_1 U)a_{X_2} + 2\sigma_1 V a_{Y_2} - i(cc_g - V^2)a_{Y_1Y_1} + \sigma_1^2[(\frac{cc_g k_1 + U\sigma_1}{\sigma_1^2})_{X_2}$$
$$+(\frac{V}{\sigma_1})_{Y_2}]a + ikcc_g k'|\ a\ |^2 a = 0 \tag{2.89}$$

where $k' = k^3\dfrac{c}{c_g}\dfrac{\cosh 4kh + 8 - 2\tanh^2 kh}{8sinh^4 kh}$

k_1 and σ_1 in (2.89) can be replaced by k and σ without introducing errors larger than $0(\epsilon^4)$. Equation (2.89) contains information of wave refraction and diffraction, as well as wave amplitude dispersion and wave-current interaction. Finally, as we have noted before the first harmonic for L_1 varying with respect to A_1 as expressed by (2.75) is third order and, therefore, should be combined with (2.89) to reach the wave euqation. Hence, we obtain in the (x, y) coordinates

$$2(cc_g k_1 + \sigma_1 U)a_x + 2\sigma_1 V a_y - i(cc_g - V^2)a_{yy} + \sigma_1^2[(\frac{cc_g k_1 + U\sigma_1}{\sigma_1^2})_x + (\frac{V}{\sigma_1})_y$$
$$+icc_g(k_1^2 - k^2)]a + ikcc_g k'|\ a\ |^2 a = 0 \tag{2.90}$$

This is the final form of the wave equation without dissipation. If dissipation is to be considered, then a dissipation term D_e could be included in the left hand side. One possible formation of D_e is given in Appendix 1. Following Kirby and Dalrymple (1983), a phase-shifted wave amplitude is introduced to simplify the wave number computation

$$a = A'' e^{i(k_0 - \int^x k_1 dx)} \tag{2.91}$$

where k_0 is the reference wave number. Equation (2.91) implies that

$$A'' = a'' e^{i(\mathbf{k}\cdot\mathbf{x} - k_0 x)} \tag{2.92}$$

where a'' is the real wave amplitude. The final wave equation, after dropping the double primes, takes the following form:

$$
\begin{aligned}
&2(cc_g k_1 + \sigma_1 U)A_x + 2\sigma_1 V A_y - i(cc_g - V^2)A_{yy} + \sigma_1^2[(\frac{cc_g k_1 + U\sigma_1}{\sigma_1^2})_x \\
&+(\frac{V}{\sigma_1})_y + icc_g(k_1^2 - k^2) + 2i(cc_g k_1 + \sigma_1 U)(k_0 - k_1)]A + i(\sigma_0^2 - \sigma^2)A \\
&-\frac{(i-1)gk^2}{\cosh^2 kh}\sqrt{(\frac{\nu}{2\omega})}A + 2(cc_g k_1 + \sigma_1 U)WA = 0
\end{aligned}
\tag{2.93}
$$

where the cubic amplitude term in Eq.(2.90) has been replaced by $i(\sigma_0^2 - \sigma^2)A$ (Kirby and Dalrymple,(1986)), in which

$$\sigma_0^2 = gk(1 + f_1\epsilon^2 D_k)\tanh(kh + f_2\epsilon)$$

it will be discussed in next section. The last term on the left hand side is the decay of energy due to wave breaking and the details of which will be discussed in section 2.2.6, and W is defined as

$$
\begin{cases}
W = 0 & \text{before wave breaking} \\
W = \frac{q}{2D}(1 - \frac{\gamma^2 h^2}{4|A|^2}) & \text{after wave breaking, } \gamma = 0.39 \text{ and } q = 0.4
\end{cases}
$$

The dissipation term D_ϵ is given in appendix A. Equation (2.93) is the final form of the wave equation. It is similar to the wave equation given by Kirby (1984) except the additional imaginary term in the second last term. (see Liu 1986). For plane beach and in the absence of current, linearized (2.90) reduces to the conventional one-dimensional wave energy conservation equation. It reads

$$a = a_0(c_{g_0}/c_g)(b_0/b)$$

where quantities with subscripts 0 refer to known condition and b is the width between adjacent wave orthogonals.

2.2.4 Dispersion Relation

When waves travel over a varying topography or, are embraced by current, the wave number vector will change its value. The four equations established in the previous section

enable us to solve the four unknowns: $\overline{\eta}$, U, V and H, provided the wave number vector is known. Since wave number is a horizontal vector, in general two equations are required to solve its magnitude and direction. The wave number irrotationality and the wave dispersion relationship derived from dynamic free surface condition are commonly used. In the presence of a current field the mathematics could become complicated if the nonlinear behavior is fully accounted for. In the present study, a semi-nonlinear dispersion relationship is considered and is incorporated directly in the wave equation; thus the linear dispersion relationship is used in the model. Also, by assuming small incident wave angle, the directional information on wave number is incorporated into the complex wave amplitude as presented in the previous section, thus, avoiding the inclusion of the wave number irrotational equation explicitly. The linear dispersion relation with current is given as (Dean and Dalrymple, 1984)

$$\omega = \sigma + Uk_1 + Vk_2 \tag{2.94}$$

where

$$\sigma = \sqrt{gk \tanh kh}$$

$$k_1 = k\cos\theta$$

$$k_2 = k\sin\theta$$

In shallow water, $\tanh kh \rightarrow kh$ approximately, Eq.(2.94) becomes

$$\omega = k\sqrt{gh} + Uk_1 + Vk_2 \tag{2.95}$$

Several modifications have been proposed. Whitham(1967) gave a Stokes nonlinear dispersion relation for intermediate depth region in the absence of current:

$$\sigma_0 = \sigma\sqrt{1 + \epsilon^2 D_k} \tag{2.96}$$

where

$$\epsilon = ak$$

$$D_k = \frac{\cosh 4kh + 8 - 2\tanh^2 kh}{8\sinh^4 kh}$$

As waves enter shallow water, (2.96) becomes invalid as D_k approaches $(kh)^{-4}$

In the shallow water region. Hedges (1976) proposed a different formula

$$\sigma'_0 = \sqrt{gk \tanh k(h+a)} \tag{2.97}$$

for the case of no current in which a is wave amplitude. For the same wave frequency, it yields longer wave length than that given by the linear dispersion relation.

More recently, by combining both cases discussed above, Kirby and Dalrymple (1986) constructed a composite model which satisfies both intermediate water depth, Eq.(2.96), and shallow water depth, Eq.(2.97),

$$\sigma''_0 = [gk(1 + f_1\epsilon^2 D_k)\tanh(kh + f_2\epsilon)]^{1/2} \tag{2.98}$$

where

$$f_1 = \tanh^5 kh$$

$$f_2 = (kh/\sinh kh)^4$$

In deep water region, (2.98) approaches (2.96) as $f_2 \to 0$; conversely, in shallow water region, it becomes (2.97) as $f_1 \to 0$. Now assuming there is no nonlinear current effect on wave dispersion, the presence of current causes a Doppler shift and Eq.(2.98) becomes

$$\omega = \sigma''_0 + Uk_1 + Vk_2 \tag{2.99}$$

Figures 2.2 and 2.3 shows the results of ω for a constant non-dimensional velocity $U/c_0 = -0.1$ and varying of ϵ from 0.01 to 0.4, where $c_0 = \sqrt{g/k}$ is the deep water wave celerity. The dispersion equations given by (2.94), (2.96) and (2.97) are also plotted in Figs.2.2 and 2.3 for comparison.

The emprical nonlinear dispersion (2.98) can be used to modify the wave equation as we did in Eq.(2.93), in which the Eq. (2.98) is incorporated directly in the governing equation in the form of a term which directly produces the required amplitude dispersion (Kirby and Dalrymple, 1986). Consequently, the linear dispersion relation (2.94) will be used in this model.

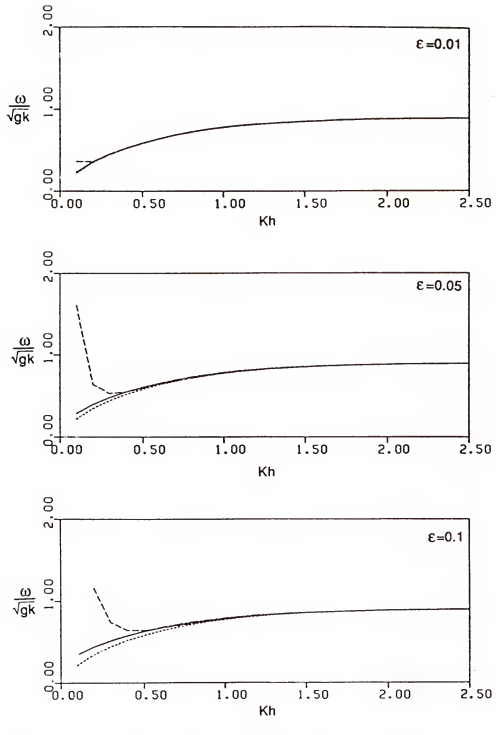

Figure 2.2: Variations of Dispersion Relation with $U/c_0 = -0.1$ and ϵ, ····· Linear; —· Hedges; - - - Witham; —— Composite

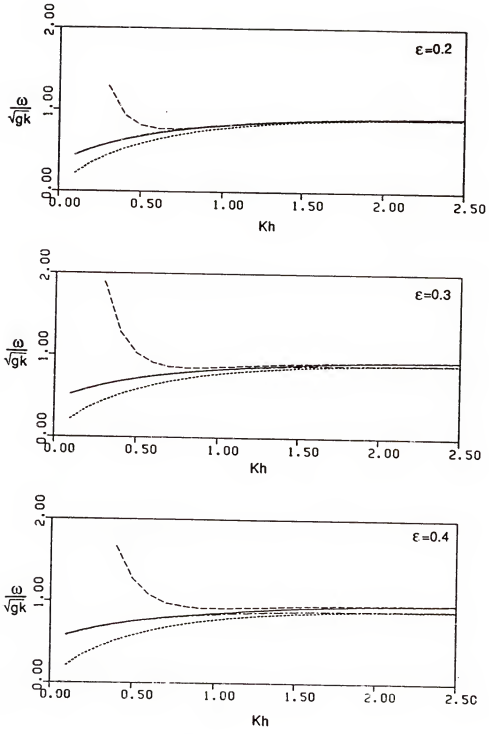

Figure 2.3: Variations of Dispersion Relation with $U/c_0 = -0.1$ and ϵ, ····· Linear; –– Hedges; - - - Whitham; —— Composite

Once the dispersion equation (2.99) is brought into the model, the cubic amplitude term in Eq.(2.90) should be dropped, since the amplitude dispersion has already been includeed in the nonlinear dispersion equation (2.98).

A wave number vector which is irrotational can be defined as:

$$\mathbf{k} = \nabla\omega \tag{2.100}$$

where $\mathbf{k}$ is a wave number vector, $\mathbf{k} = \{k_1, k_2\}$ and ω corresponds to the scaler phase function. Using the mathematical property that the curl of a gradient is identically zero, it is shown that

$$\nabla \times \nabla\omega = 0 \tag{2.101}$$

or

$$\nabla \times \mathbf{k} = 0 \tag{2.102}$$

In general, Eq.(2.102) together with Eq.(2.99) is necessary to solve the wave number field of a domain.

However, in the present study the wave angle information has already been included in the complex wave amplitude given by Eq.(2.92). Therefore equation (2.102) does not need to be included explicitly. However, the assumption that wave approaching angle is small must be observed.

2.2.5 Radiation Stresses, Lateral Mixing Stresses and Bottom Stresses

In the wave momentum equations (2.21) and (2.22), there are some undetermined terms: radiation stresses, lateral mixing stresses and bottom shear stresses. They are not independent variables and are calculated by the following equations.

Radiation Stresses

The radiation stresses are given in (2.19):

$$S_{ij} = \overline{\int_{-h}^{\eta} p\delta_{ij}dz} + \overline{\int_{-h}^{\eta} u_i^w u_j^w dz} - \frac{1}{2}\rho g D^2\delta_{ij} - \rho\hat{u}_i\hat{u}_j D$$

The form was simplified by Longuet-Higgins and Stewart (1962) to second order for a linear progressive wave system. For normal incident waves, it can be approximately by

$$[\, S_{ij}^0 \,] = \begin{bmatrix} S_{xx}^0 & S_{xy}^0 \\ S_{xy}^0 & S_{yy}^0 \end{bmatrix} = \begin{bmatrix} E(2n-0.5) & 0 \\ 0 & E(n-0.5) \end{bmatrix} \tag{2.103}$$

where E is local wave energy $E = \frac{1}{2}\rho g |\, a \,|^2$, a is complex wave amplitude and n is the ratio of wave group velocity to the wave celerity.

In general, when waves enter beach with an angle, S_{ij} can be obtained by

$$[\, S_{ij} \,] = [\, A \,][\, S_{ij}^0 \,][\, A \,]^T \tag{2.104}$$

where $[\, A \,]$ is directional matrix,

$$[\, A \,] = \begin{bmatrix} \cos\theta & -\sin\theta \\ \sin\theta & \cos\theta \end{bmatrix} \tag{2.105}$$

hence

$$[\, S_{ij} \,] = \begin{bmatrix} S_{xx} & S_{xy} \\ S_{xy} & S_{yy} \end{bmatrix} = \begin{bmatrix} E[n(\cos^2\theta + 1) - \frac{1}{2}] & \frac{1}{2}En\sin 2\theta \\ \frac{1}{2}En\sin 2\theta & E[n(\sin^2\theta + 1) - \frac{1}{2}] \end{bmatrix} \tag{2.106}$$

where θ is local wave angle.

Bottom Shear Stresses

The bottom shear stresses are customarily expressed as

$$\overline{\tau_{bi}} = \overline{\rho f u_{ti} \mid u_t \mid} \tag{2.107}$$

where u_t is total velocity composing of both wave orbital and mean current velocities, and u_{ti} is its component form. The quantity f is the friction factor. The magnitude of total velocity $\mid u_t \mid$ is equal to $\sqrt{u^2 + v^2}$. The u and v velocity components can be expressed as

$$u = U + u_x^w = U + u^w \cos\theta \tag{2.108}$$

$$v = V + u_x^y = U + u^w \sin\theta \tag{2.109}$$

where U and V are mean current components as defined before. u_x^w and u_y^w are wave orbital velocities in the x and y direction, respectively and $u^w = [(u_x^w)^2 + (u_y^w)^2]^{1/2}$.

The total velocity $\mid u_t \mid$ can be expressed as

$$\mid u_t \mid = [U^2 + V^2 + (u^w)^2 + 2Uu^w \cos\theta + 2Vu^w \sin\theta]^{1/2} \tag{2.110}$$

The local wave orbital velocity u^w is purely oscillating in time

$$u^w = u_m \cos\sigma t \tag{2.111}$$

where u_m is the maximum wave orbital velocity at the bottom

$$u_m = \frac{\sigma \mid a \mid}{\sinh kh} \tag{2.112}$$

The time averaged bottom shear stresses in the x and y directions then become

$$\overline{\tau_{bx}} = \rho \frac{f}{T} \int_0^T (U + u_m \cos\theta \cos\sigma t) \mid u_t \mid dt \tag{2.113}$$

$$\overline{\tau_{by}} = \rho \frac{f}{T} \int_0^T (V + u_m \sin\theta \cos\sigma t) \mid u_t \mid dt \tag{2.114}$$

Alternative, for computational convenience, it can be rewritten as

$$\overline{\tau_{bx}} = \rho \frac{f}{2\pi} \int_0^{2\pi} (U + u_m \cos\theta \cos\sigma t) \mid u_t \mid d(\sigma t) \tag{2.115}$$

$$\overline{\tau_{by}} = \rho \frac{f}{2\pi} \int_0^{2\pi} (U + u_m \sin\theta \cos\sigma t) \mid u_t \mid d(\sigma t) \tag{2.116}$$

These integrals can be calculated by applying Simpson's rule. The serious problem by applied the above bottom friction model is the computational time. A simplified model is introduced with

$$\overline{\tau_{bi}} = \rho f \mid u'_t \mid U_i \tag{2.117}$$

where

$$\mid u'_t \mid = \sqrt{U^2 + V^2} + u_m$$

since there is no interaction term between wave orbital velocity and mean current velocity. In the component form the above equation gives

$$\overline{\tau_{bx}} = \rho f \mid u'_t \mid U \tag{2.118}$$

$$\overline{\tau_{by}} = \rho f \mid u'_t \mid V \tag{2.119}$$

The difference between the two models (2.107) and (2.117) is minor for cases $U \gg u_m$ as shown by the example in Fig.2.4, in which the same bottom friction coefficient is used (the testing conditions refer to Fig.5.3 in chapter 5), but the saving in computational time is more than 60%. In fact the small difference can be offset by increasing the bottom friction coefficient in (2.117) to account for the absence of u_m term. Equation (2.117) will be used in our model.

Another very important factor is selection of the friction coefficient f. Based on field observations and laboratory experiments Longuet-Higgins (1970) suggested a value about 0.01 for long-shore current calculations. The bottom friction coefficient for waves alone presents a more difficult situation. For smooth turbulent flow over fixed bed, Kamphuis(1975) gave

$$f = \frac{1}{\sqrt{R_e}} \tag{2.120}$$

where R_e is Reynolds number, $R_e = \frac{|a|^2\omega}{\nu}$ and ν is the kinematic viscosity.

For rough turbulent flow, friction coefficient no longer depends upon Reynolds number. Investigations were conducted by Jonsson(1966)and Grant & Madsen(1979). The most commonly used relation is

$$f = \begin{cases} \frac{1}{2}\exp[5.213(\frac{r}{a'})^{0.194} - 5.977] & \frac{r}{a'} < 0.63 \\ 0.15 & \frac{r}{a'} \geq 0.63 \end{cases} \tag{2.121}$$

where r is the roughness of the bed and $a' = \mid a \mid$. Equation (2.121) is an approximate explicit solution given by Swart (1974) to an implicit, semi-empirical formula by Jonsson and Carlsen (1976).

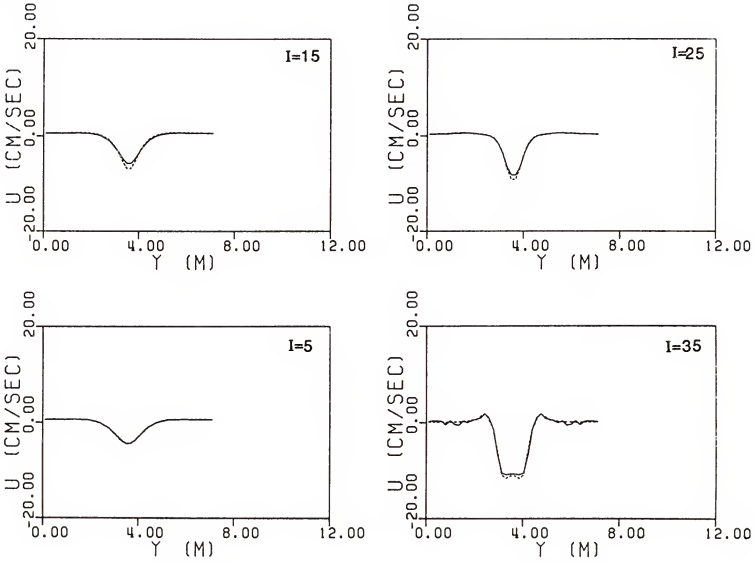

Figure 2.4: Velocity Profiles for different friction models — (2.107); - - - (2.117)

The situation becomes further complicated once combined wave with current, the state of the art of modeling such flows is rather rudimentary. The total velocity in (2.107) becomes much larger than the wave orbital velocity in the present case of very strong current. The actual values of f used in the model will be adjusted as a function of (a, T) based on experimental results to be discussed in chapter 4.

In application, the bottom friction coefficient may be treated differently in x and y directions, in the present study, the bottom friction coefficient in y direction is taken as one half of the value in x (or main) direction.

Lateral Mixing

Lateral mixing due to turbulent diffusion is a complicated flow phenomenon. Rigorous mathematical treament is beyond the state of art. Figure 2.5 shows the effects of lateral mixing on longshore current distribution (Longuet-Higgins, 1970 a.b). The common assumption is that turbulent mixing is proportional to the local mean velocity gradient. Following Longuet-Higgins' formulation on longshore current mixing, the lateral shear stress is written as

$$\overline{\tau}_\ell = \rho\epsilon_y \frac{\partial U}{\partial y} + \rho\epsilon_x \frac{\partial V}{\partial x} \tag{2.122}$$

where ϵ_x and ϵ_y are the horizontal eddy viscosities in the x and y direction respectively. We define

$$\epsilon_i = \epsilon_{wi} + \epsilon_{ci} \qquad i = x, y \tag{2.123}$$

where ϵ_{wi} and ϵ_{ci} are the eddy viscosities of wave and current, respectively , which are assumed to be independent. The inclusion of ϵ_{ci} is based on the fact that even though there is no wave, the flow from the inlet still generates turbulence. As the simplest possible approach, Longuet-Higgins proposed a model for ϵ_{wx}, that is proportional to the distance offshore, x, multiplied by velocity scale

$$\epsilon_{wx} = Nx\sqrt{gh} \tag{2.124}$$

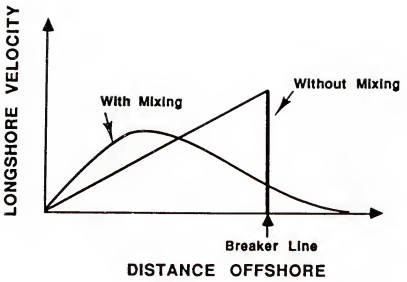

Figure 2.5: Longuet-Higgen's Longshore Current Profiles

where N is a dimensionless constant whose limits Longuet-Higgins gave as

$$0 \leq N \leq 0.016 \tag{2.125}$$

Following Ebersole and Dalrymple (1979), N is chosen as 0.01 and ϵ_{wx} is allowed to vary linearly with x to the breaking line. From this point seaward the coefficient remains at this constant value. There is no elaborate consideration of ϵ_{wy}. Ebersole and Dalrymple assumed a constant value and here it is chosen as half the value of ϵ_{wx} throughout the field.

The eddy viscosity ϵ_{ei}, theoretically, will change from point to point. One of the formulas was due to Von Kàrmàn's similarity hypothesis:

$$\epsilon_{ex} = m_1^2 \mid \frac{dV}{dx} \mid \tag{2.126}$$

$$\epsilon_{ey} = m_2^2 \mid \frac{dU}{dy} \mid \tag{2.127}$$

where

$$m_1 = k\frac{dV}{dx}/\frac{d^2V}{dx^2} \quad \text{and} \quad m_2 = k\frac{dU}{dy}/\frac{d^2U}{dy^2}$$

and $k = 0.4$ is Von Kàrmàn's constant. In the numerical calculation, these coefficients go to infinit near a point of inflection. An upper-limit value should be imposed. Alternatively, both eddy viscosities can be treated as constants. Figure 2.6 give the effects of eddy viscosities on the velocity profiles (the testing conditions refer to Fig.5.3 in chapter 5). It shows that they have only minor difference between constant 0.001 m^2/sec and Von Kàrmàn's mixing model with upper-limit equal to 0.001 m^2/sec. Therefore in this investigation, instead of Eqs.(2.126) and (2.127) the constant eddy viscosity is selected.

2.2.6 Wave Breaking Criterion

When waves enter shallow water, they will eventually become unstable and break, dissipating the energy in the form of turbulence and work against bottom friction. For a very mildly sloping beach, spilling breaker occurs and the simplest criterion predicted by solitary wave theory is (McCowan (1894))

$$\gamma = (\frac{H}{D})_b = 0.78 \tag{2.128}$$

where D is total water depth and subscript b denotes the value at breaking.

Dally et al. (1984) proposed that the decay of energy flux with distance in the surf zone is proportional to the excess of energy flux above a stable value, given the relation

$$\frac{\partial}{\partial x}(Ec_g) = -\frac{q}{D}[Ec_g - (Ec_g)_s] \tag{2.129}$$

where q is a constant related to the rate of energy decay. The quantity $(Ec_g)_s$ is the stable energy flux for a broken wave in water of total depth D. The last term in the wave equation (2.93) which appears only after wave breaking

$$2(cc_g k_1 + \sigma_1 U)WA$$

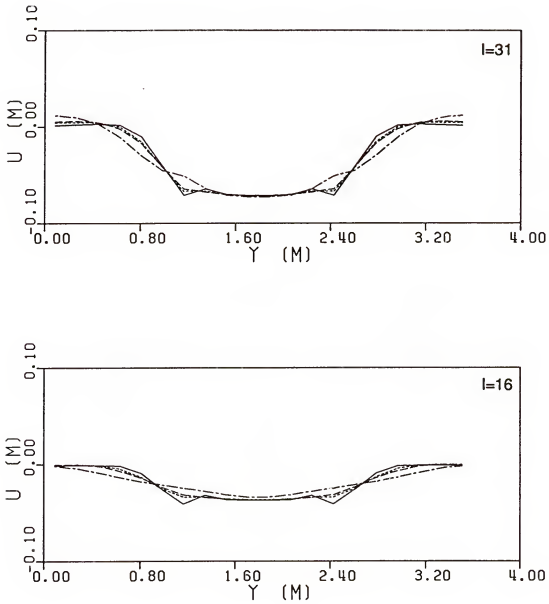

Figure 2.6: Variations of Eddy Vicosity Coefficients. — = 0. ; ··· =0.001; -·- =0.01; - - - Von Kàrmàn's Model with upper-limit =0.001. unit= m^2/s

can now be completely defined as

$$W = \frac{q}{2D}(1 - \frac{\gamma^2 D^2}{4|A|^2} \tag{2.130}$$

by virtue of Eqs. (2.128) and (2.129). The value of q is chosen as 0.4 following Kirby and Dalrymple (1986).

2.3 Summary

In this chapter, the analytical model of a current-wave-topographic interaction system is formulated under the assumption of strong current and slowly varying bottom. Basic equations together with essential terms are developed. They are summarized as follows:

Depth-Integrated Continuity Equation

$$\frac{\partial \overline{\eta}}{\partial t} + \frac{\partial UD}{\partial x} + \frac{\partial VD}{\partial y} = 0 \tag{2.131}$$

Depth-Integrated Momentum Equation in X-Direction

$$\frac{\partial U}{\partial t} + U\frac{\partial U}{\partial x} + V\frac{\partial U}{\partial y} = -g\frac{\partial \overline{\eta}}{\partial x} - \frac{1}{\rho D}\frac{\partial S_{xx}}{\partial x} - \frac{1}{\rho D}\frac{\partial S_{xy}}{\partial y} + \frac{1}{\rho}\frac{\partial \overline{\tau}_\ell}{\partial y} - \frac{1}{\rho D}\overline{\tau}_{bx} \tag{2.132}$$

Depth-Integrated Momentum Equation in Y-Direction

$$\frac{\partial V}{\partial t} + U\frac{\partial V}{\partial x} + V\frac{\partial V}{\partial y} = -g\frac{\partial \overline{\eta}}{\partial y} - \frac{1}{\rho D}\frac{\partial S_{xy}}{\partial x} - \frac{1}{\rho D}\frac{\partial S_{yy}}{\partial y} + \frac{1}{\rho}\frac{\partial \overline{\tau}_\ell}{\partial x} - \frac{1}{\rho D}\overline{\tau}_{by} \tag{2.133}$$

in which we have substituted (2.131) into (2.21) and (2.22), where

$$[S_{ij}] = \begin{bmatrix} S^0_{xx} & S^0_{xy} \\ S^0_{xy} & S^0_{yy} \end{bmatrix} = \begin{bmatrix} E[n(\cos^2\theta + 1) - \frac{1}{2}] & \frac{1}{2}En\sin 2\theta \\ \frac{1}{2}En\sin 2\theta & E[n(\sin^2\theta + 1) - \frac{1}{2}] \end{bmatrix} \tag{2.134}$$

$$\overline{\tau}_\ell = \rho\epsilon_y\frac{\partial U}{\partial y} + \rho\epsilon_x\frac{\partial V}{\partial x} \tag{2.135}$$

$\epsilon_i = \epsilon_{wi} + \epsilon_{ci}$; ϵ_{ci} is a constant and ϵ_{wx} is given by

$$\epsilon_{wx} = Nx\sqrt{gD} \quad \text{with} \quad N = 0.01;$$

$$\epsilon_{wy} = \frac{1}{2}\epsilon_{wx}$$

$$\overline{\tau_{bi}} = \rho f \mid u'_t \mid U_i \tag{2.136}$$

$$\mid u'_t \mid = \sqrt{U^2 + V^2} + u_m \tag{2.137}$$

$$u_m = \frac{\sigma \mid a \mid}{\sinh kh}$$

Wave Equation

$$2(cc_g k_1 + \sigma_1 U)A_x + 2\sigma_1 V A_y - i(cc_g - V^2)A_{yy} + \sigma_1^2[(\frac{cc_g k_1 + U\sigma_1}{\sigma_1^2})_x$$
$$+(\frac{V}{\sigma_1})_y + icc_g(k_1^2 - k^2) + 2i(cc_g k_1 + \sigma_1 U)(k_0 - k_1)]A + i(\sigma_0^2 - \sigma^2)A$$
$$-\frac{(i-1)gk^2}{\cosh^2 kh}\sqrt{(\frac{\nu}{2\omega})}A + 2(cc_g k_1 + \sigma_1 U)WA = 0 \tag{2.138}$$

where

$$\sigma_0 = [gk(1 + f_1\epsilon^2 D_k)\tanh(kh + f_2\epsilon)]^{1/2}$$

$$f_1 = \tanh^5 kh$$

$$f_2 = (kh/\sinh kh)^4$$

$$D_k = \frac{\cosh 4kh + 8 - 2\tanh kh}{8\sinh^4 kh}$$

$$\begin{cases} W = 0 & \text{before wave breaking} \\ W = \frac{q}{2D}(1 - \frac{\gamma^2 h^2}{4|A|^2}) & \text{after wave breaking, } \gamma = 0.39 \text{ and } q = 0.4 \end{cases} \tag{2.139}$$

When waves enter the surf zone, the last term in (2.138) will be brought into calculation till waves reach stable condition.

The dispersion relation used in this model is

$$\omega = \sigma + Uk_1 + Vk_2 \tag{2.140}$$

and the wave angle is included in the complex wave amplitude A.

CHAPTER 3
NUMERICAL SCHEME

In this chapter, the numerical schemes for solving the continuity, momentum and wave equations are presented, along with boundary and initial conditions.

The numerical scheme requires (1) the definition of a grid system with a system which provides a systematic method for identifying variables of interest and (2) the conversion of the governing equations into finite difference forms.

3.1 Grid System and Definition of Variables

A rectangular grid mesh was established over the area of interest as shown in Fig.3.1, where x and y denote the onshore and longshore direction, respectively. Two kinds of variables are employed in the computation: the grid-center variable and the grid-side variable. Practically all the quantities of interest are represented by the grid-center form which expresses the value at the center of the grid and has the following notation:

$$X^n_{i,j}$$

where X is the grid-center variable, the subscripts i, j represent the ith grid side in the x-direction and the jth grid side in the y-direction, respectively, and the superscript n represents the nth time step. The grid-side variable expresses the value of the quantity along any grid side. The only variable that appeared in this form in the present study is the velocity vector; it is denoted by a subscript s to differentiate it from the grid-center value and has the following form:

$$(Y_s)^n_{i,j}$$

Y_s is the vector quantity along a grid side: the subscripts are such that i denotes the ith grid point in the x-direction on the left of the vector and j denotes the jth grid point in the y-direction on the right of the vector.

In the present study, the grid-side velocity vector was applied in the continuity and momentum equations and a grid-center velocity vector was applied in the wave equation. The definitions of grid-side and grid-center variables are shown in Fig.3.2

3.2 Finite Difference Scheme for Combined Continuity- Momentum Equation

The Crank-Nicolson finite difference scheme in double sweep form is applied here to solve the continuity and momentum equations and later also to solve the wave equation.

3.2.1 Linearized Implicit Model

A variety of numerical schemes are presently available to solve the equations for nearshore hydrodynamics similar to those developed in Chapter 2. Ebersole and Dalrymple (1979) presented an explicit model for nearshore circulation which requires small time steps due to the stability criterion, thus relatively long computational time. Vemulakonda (1982) presented an implicit model allowing for much larger time steps. Both models adopt a three time level schemes. Butler (1981) and Sheng(1981)proposed a two time level implicit model. This method not only saves computational time but also shortens the development of the difference scheme for the governing equations. To demonstrate the structure of their model, the simplified linearized equations are discussed here. The depth averaged linearized continuity and momentum equations are

$$\frac{\partial \overline{\eta}}{\partial t} + \frac{\partial Q_x}{\partial x} + \frac{\partial Q_y}{\partial y} = 0 \tag{3.1}$$

$$\frac{\partial Q_x}{\partial t} = -gD\frac{\partial \overline{\eta}}{\partial x} \tag{3.2}$$

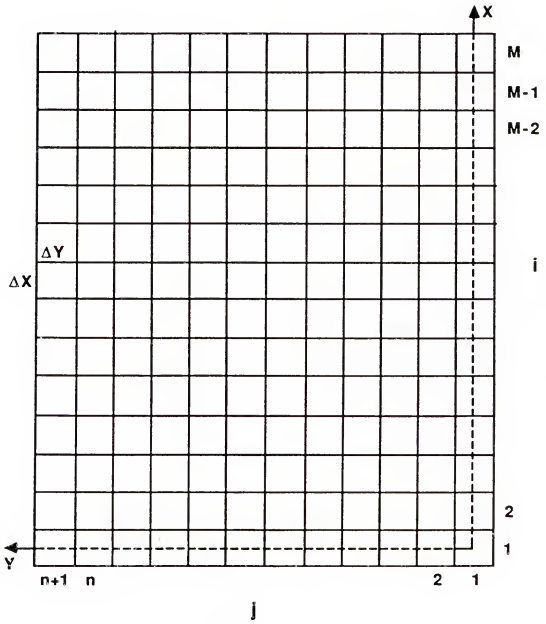

Figure 3.1: Grid Scheme

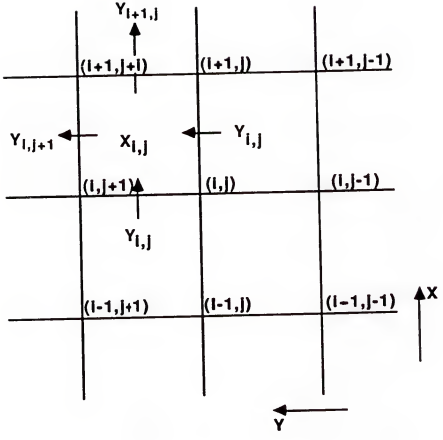

Figure 3.2: Definition of $X^n_{i,j}$ and $(Y_s)^n_{i,j}$

$$\frac{\partial Q_y}{\partial t} = -gD\frac{\partial \overline{\eta}}{\partial y} \tag{3.3}$$

where $Q_x = UD$ and $Q_y = VD$. U and V in this section denote the grid-side values. In matrix form, linearized equations can be rewritten as

$$W_t + AW_x + BW_y = 0 \tag{3.4}$$

where

$$W = \begin{pmatrix} \overline{\eta} \\ Q_x \\ Q_y \end{pmatrix} \qquad A = \begin{pmatrix} 0 & 1 & 0 \\ gD & 0 & 0 \\ 0 & 0 & 0 \end{pmatrix} \qquad B = \begin{pmatrix} 0 & 0 & 1 \\ 0 & 0 & 0 \\ gD & 0 & 0 \end{pmatrix}$$

Sheng (1981) implemented a two time level fully implicit scheme in computing the external model in his three dimensional mode.

$$\frac{\overline{\eta}_{i,j}^{n+1} - \overline{\eta}_{i,j}^{n}}{\triangle t} + \frac{1}{\triangle x}[(Q_x)_{i+1,j}^{n+1} - (Q_x)_{i,j}^{n+1}] + \frac{1}{\triangle y}[(Q_y)_{i,j+1}^{n+1} - (Q_y)_{i,j}^{n+1}] = 0 \tag{3.5}$$

$$\frac{(Q_x)_{i,j}^{n+1} - (Q_x)_{i,j}^{n}}{\triangle t} + \frac{gD}{\triangle x}[\overline{\eta}_{i,j}^{n+1} - \overline{\eta}_{i-1,j}^{n+1}] = 0 \tag{3.6}$$

$$\frac{(Q_y)_{i,j}^{n+1} - (Q_y)_{i,j}^{n}}{\triangle t} + \frac{gD}{\triangle y}[\overline{\eta}_{i,j}^{n+1} - \overline{\eta}_{i,j-1}^{n+1}] = 0 \tag{3.7}$$

or in the matrix form

$$\frac{1}{\triangle t}(W^{n+1} - W^{n}) + (\frac{A}{\triangle x}\delta_x + \frac{B}{\triangle y}\delta_y)W^{n+1} = 0 \tag{3.8}$$

where δ_x and δ_y are central spatial difference operators which provide the differentiated quantities at the same points as the time difference quantities. Equation(3.8) involves only the (n+1) time level in the last two terms, i.e., the whole equation is staggered in time.

Rearranging (3.8) by time levels, we obtain

$$(1 + 2\beta_x + 2\beta_y)W^{n+1} = W^{n} \tag{3.9}$$

where

$$\beta_x = \frac{\triangle t}{2\triangle x}A\delta_x; \qquad \beta_y = \frac{\triangle t}{2\triangle y}B\delta_y$$

By adding the quantity of $4\beta_x\beta_y(W^{n+1}-W^n)$, which has a second order truncation error as

$$(\triangle t)^2 AB\frac{\partial^3 W}{\partial t\partial x\partial y}$$

we have

$$(1+2\beta_x)(1+2\beta_y)W^{n+1}=(1+4\beta_x\beta_y)W^n \tag{3.10}$$

This factorized finite difference equation is still a second order approximation to the differential equation (3.4). The advantage of using (3.10) lies in the fact that the solution of the factorized form can be split into two separate one dimensional operations. To achieve this, we introduce an intermediate value, W^*, such that

$$(1+2\beta_x)W^*=(1-2\beta_y)W \tag{3.11}$$

$$(1+2\beta_y)W^{n+1}=W^*+2\beta_y W \tag{3.12}$$

From now on, quantities without the time level denoted are the values at time level n. Equation (3.10) is recoverable from (3.11) and (3.12) by eliminating W^*.

A double sweep method is used to solve (3.11) and (3.12). At the first sweep, the values at time level n are known we solve for W^*. The full solution W^{n+1} then is obtained based upon known W^* values. After some manipulations, the first sweep in x direction gives

$$\begin{cases} \overline{\eta}^* - \overline{\eta} + \frac{\triangle t}{\triangle x}\delta_x Q_x^{n+1} + \frac{\triangle t}{\triangle y}\delta_y Q_y = 0 \\ \\ Q_x^{n+1} - Q_x + \frac{\triangle t}{\triangle x} g D\delta_x\overline{\eta}^* = 0 \end{cases} \tag{3.13}$$

and the second sweep in the y direction yields

$$\begin{cases} \overline{\eta}^{n+1} - \overline{\eta}^* + \frac{\triangle t}{\triangle y}\delta_y Q_y^{n+1} - \frac{\triangle t}{\triangle y}\delta_y Q_y = 0 \\ \\ Q_y^{n+1} - Q_y + \frac{\triangle t}{\triangle y} g D\delta_y\overline{\eta}^{n+1} = 0 \end{cases} \tag{3.14}$$

On the first sweep, U^{n+1} and $\overline{\eta}^*$ are found, and on next sweep the values of V^{n+1} and $\overline{\eta}^{n+1}$ are obtained. Therefore, after one loop, the quantities at time level $n+1$ are known. The

advantages of this scheme are (a) the finite difference equations are brief, at second sweep (3.14) there is no Q_x involved; (b) a significant savings in computation time is realized with large time steps and less computations.

3.2.2 Numerical Scheme for the Full Equations

Following the above model, the full equations (2.131), (2.132) and (2.133) in chapter 2 can be written in numerical form as (see Appendix C)

x-sweep

$$\begin{cases} \overline{\eta}^* - \overline{\eta} + \frac{\triangle t}{\triangle x}\delta_x(U^{n+1}D) + \frac{\triangle t}{\triangle y}\delta_y(VD) = 0 \\ (1 + \triangle t c_x)U^{n+1} - U + \frac{\triangle t}{\triangle x}g\delta_x\overline{\eta}^* + \triangle t m_1 = 0 \end{cases} \tag{3.15}$$

y-sweep

$$\begin{cases} \overline{\eta}^{n+1} - \overline{\eta}^* + \frac{\triangle t}{\triangle y}\delta_y(V^{n+1}D) - \frac{\triangle t}{\triangle y}\delta_y(VD) = 0 \\ (1 + \triangle t c_y)V^{n+1} - V + \frac{\triangle t}{\triangle y}g\delta_y\overline{\eta}^{n+1} + \triangle t m_2 = 0 \end{cases} \tag{3.16}$$

where $c_x U$ and $c_y V$ are bottom shear stresses in x and y direction, respectively. By (2.136) in chapter 2, we have

$$c_x = \frac{f}{D} \mid u_t' \mid_x \quad \text{and} \quad c_y = \frac{f}{D} \mid u_t' \mid_y$$

where $\mid u_t' \mid_i$ is the total velocity defined in (2.137) and here is specified in each direction. m_1 and m_2 are the remaining terms in Eqs. (2.132) and (2.133).

Again, on the x sweep the solutions for $\overline{\eta}^*$ and U^{n+1} are obtained; these up-dated values are brought into the y sweep to obtain $\overline{\eta}^{n+1}$ and V^{n+1}. Writing the above two set of equations in detail, we have

a) X-Sweep

Continuity equation

$$\begin{aligned} &\frac{1}{\triangle t}(\overline{\eta}^*_{i,j} - \overline{\eta}_{i,j}) + \frac{1}{2\triangle x}[U^{n+1}_{i+1,j}(D_{i+1,j} + D_{i,j}) - U^{n+1}_{i,j}(D_{i,j} + D_{i-1,j})] \\ &+ \frac{1}{2\triangle y}[V_{i,j+1}(D_{i,j+1} + D_{i,j}) - V_{i,j}(D_{i,j} + D_{i,j-1})] = 0 \end{aligned} \tag{3.17}$$

X-Direction Momentum Equation

$$\frac{1}{\Delta t}(U_{i,j}^{n+1} - U_{i,j}) + \frac{U_{i,j}}{2\Delta x}(U_{i+1,j} - U_{i-1,j}) + \frac{(V_{i,j+1} + V_{i,j} + V_{i-1,j+1} + V_{i-1,j})}{8\Delta y}$$
$$(U_{i,j+1} - U_{i,j-1}) = -\frac{g}{\Delta x}(\overline{\eta}_{i,j}^{*} - \overline{\eta}_{i-1,j}^{*}) - \frac{2}{\rho(D_{i,j} + D_{i-1,j})}\frac{1}{\Delta x}[(S_{xx})_{i,j} - (S_{xx})_{i-1,j}]$$
$$-\frac{1}{\rho(D_{i,j} - D_{i-1,j})}\frac{1}{2\Delta y}[(S_{xy})_{i,j+1} - (S_{xy})_{i,j-1} + (S_{xy})_{i-1,j+1} - (S_{xy})_{i-1,j-1}]$$
$$-\frac{f}{(D_{i,j} + D_{i-1,j})}|\,(u_t)_{i,j}\,|_x U_{i,j}^{n+1} + (FL_{yy})_{i,j} + (FL_{yx})_{i,j} \tag{3.18}$$

where

$$|\,(u_t)_{i,j}\,|_x = |(u_m)_{i,j} + (u_m)_{i-1,j}| + 2(u_x)i,j$$

u_m is wave orbital velocity as defined in (1.112) in chapter 2.

$$(u_x)_{i,j} = \{U_{i,j}^2 + [0.25(V_{i,j} + V_{i,j+1} + V_{i-1,j} + V_{i-1,j+1})]^2\}^{1/2}$$

$$(FL_{yy})_{i,j} = \frac{1}{4(\Delta y)^2}\{(U_{i,j+1} - U_{i,j}[((\epsilon_{wy})_{i,j} + (\epsilon_{wy})_{i,j+1} + (\epsilon_{wy})_{i-1,j} + (\epsilon_{wy})_{i-1,j+1})$$
$$+2((\epsilon_{cy})_{i,j} + (\epsilon_{cy})_{i,j+1})] - (U_{i,j} - U_{i,j-1})[((\epsilon_{wy})_{i,j} + (\epsilon_{wy})_{i,j-1}$$
$$+(\epsilon_{wy})_{i-1,j} + (\epsilon_{wy})_{i-1,j-1}) + 2((\epsilon_{cy})_{i,j} + (\epsilon_{cy})_{i,j-1})]\}$$

$$(FL_{yx})_{i,j} = \frac{1}{4\Delta x\Delta y}\{(V_{i,j+1} - V_{i-1,j+1})[((\epsilon_{wx})_{i,j+1} + (\epsilon_{wx})_{i,j} + (\epsilon_{wx})_{i-1,j}$$
$$+(\epsilon_{wx})_{i-1,j+1}) + 2((\epsilon_{cx})_{i,j+1} + (\epsilon_{cx})_{i-1,j+1})] - (V_{i,j} - V_{i-1,j})[((\epsilon_{wx})_{i,j}$$
$$+(\epsilon_{wx})_{i-1,j} + (\epsilon_{wx})_{i,j-1} + (\epsilon_{wx})_{i-1,j-1}) + 2((\epsilon_{cx})_{i,j} + (\epsilon_{cx})_{i-1,j})]\}$$

b) Y-Sweep

Continuity Equation

$$\frac{1}{\Delta t}(\overline{\eta}_{i,j}^{n+1} - \overline{\eta}_{i,j}^{*}) + \frac{1}{2\Delta y}[V_{i,j+1}^{n+1}(D_{i,j+1} + D_{i,j})_{*} - V_{i,j}^{n+1}(D_{i,j} + D_{i,j-1})_{*}]$$
$$-\frac{1}{2\Delta y}[V_{i,j+1}(D_{i,j+1} + D_{i,j})_{*} - V_{i,j}(D_{i,j} + D_{i,j-1})_{*}] = 0 \tag{3.19}$$

Y-Direction Momentum Equation

$$\frac{1}{\Delta t}(V_{i,j}^{n+1} - V_{i,j}) + \frac{(U_{i,j}^{n+1} + U_{i+1,j}^{n+1} + U_{i,j-1}^{n+1} + U_{i+1,j-1}^{n+1})}{8\Delta x}(V_{i+1,j} - V_{i-1,j}) + \frac{V_{i,j}}{2\Delta y}$$

$$(V_{i,j+1} - V_{i,j-1}) = -\frac{g}{\Delta y}(\overline{\eta}^{n+1}_{i,j} - \overline{\eta}^{n+1}_{i,j-1}) - \frac{1}{\rho(D_{i,j} - D_{i,j-1})_*}\frac{1}{2\Delta x}[(S_{xy})_{i+1,j}$$
$$-(S_{xy})_{i-1,j} + (S_{xy})_{i+1,j-1} - (S_{xy})_{i-1,j-1}] - \frac{2}{\rho(D_{i,j} + D_{i,j-1})_*}\frac{1}{\Delta y}((S_{yy})_{i,j}$$
$$-(S_{yy})_{i,j-1} - \frac{f}{2(D_{i,j} + D_{i,j-1})_*}|\,(u_t)_{i,j}\,|_y V^{n+1}_{i,j} + (FL_{xy})_{i,j} + (FL_{zz})_{i,j} \qquad (3.20)$$

where the bottom shear stress coffficient has taken as half the value of that in x the direction as stated in (2.2.5), and

$$|\,(u_t)_{i,j}\,|_y = [(u_m)_{i,j} + (u_m)_{i,j-1}] + 2(u_y)i,j$$
$$(u_x)_{i,j} = \{V^2_{i,j} + [0.25(U^{n+1}_{i,j} + U^{n+1}_{i+1,j} + U^{n+1}_{i,j-1} + U^{n+1}_{i+1,j-1})]^2\}^{1/2}$$

$$(FL_{zx})_{i,j} = \frac{1}{4(\Delta x)^2}\{(V_{i+1,j} - V_{i,j}[[(\epsilon_{wx})_{i+1,j} + (\epsilon_{wx})_{i,j} + (\epsilon_{wx})_{i+1,j-1} + (\epsilon_{wx})_{i,j-1}$$
$$+2((\epsilon_{cx})_{i+1,j} + (\epsilon_{cx})_{i,j})] - (V_{i,j} - V_{i-1,j})[[(\epsilon_{wx})_{i,j} + (\epsilon_{wx})_{i-1,j}$$
$$+(\epsilon_{wx})_{i,j-1} + (\epsilon_{wx})_{i-1,j-1}) + 2((\epsilon_{cx})_{i,j} + (\epsilon_{cx})_{i-1,j})]\}$$

$$(FL_{zy})_{i,j} = \frac{1}{4\Delta x\Delta y}\{(U^{n+1}_{i+1,j} - U^{n+1}_{i+1,j-1})[[(\epsilon_{wy})_{i+1,j} + (\epsilon_{wy})_{i+1,j-1} + (\epsilon_{wy})_{i,j}$$
$$+(\epsilon_{wy})_{i,j-1}) + 2((\epsilon_{cy})_{i+1,j} + (\epsilon_{cy})_{i+1,j-1})] - (U^{n+1}_{i,j} - U^{n+1}_{i-1,j})[[(\epsilon_{wy})_{i,j}$$
$$+(\epsilon_{wy})_{i,j-1} + (\epsilon_{wy})_{i-1,j} + (\epsilon_{wy})_{i-1,j-1}) + 2((\epsilon_{cy})_{i,j} + (\epsilon_{cy})_{i,j-1})]\}$$

In (3.17) to (3.20), the quantities with no time level are at time level n; and the subscript $(_*)$ outside the bracket in(3.19) and (3.20) denotes up-dated values, i.e., $D_* = h + \overline{\eta}^*$. Also we have used the latest x direction velocity, U^{n+1}, in the y sweep to accelerate the convergence. In application, the (ϵ_{cx}) and (ϵ_{cy}) are considered as constants as dicussed in chapter 2.

3.2.3 Method of Calculation and Boundary Conditions

A double sweep method has been developed in each direction,i.e., in both x-sweep and y-sweep. The advantage of this sweep method lies in the fact that it gives an explicit formula at each sweep to calculate the results.

Collecting the terms from (3.17) to (3.20) by time level, so that the unknown quantities are to the left and the known qantities are to the right, we have

X-Sweep

$$\begin{cases} \overline{\eta}^*_{i,j} + P_{i,j} U^{n+1}_{i+1,j} - P_{i-1,j} U^{n+1}_{i,j} = C_{i,j} \\ A_{i,j} U^{n+1}_{i,j} + R1\, \overline{\eta}^*_{i+1,j} - R1\, \overline{\eta}^*_{i,j} = B_{i,j} \end{cases} \tag{3.21}$$

Y-Sweep

$$\begin{cases} \overline{\eta}^{n+1}_{i,j} + Q_{i,j} V^{n+1}_{i,j+1} - Q_{i,j-1} V^{n+1}_{i,j} = Z_{i,j} \\ R_{i,j} V^{n+1}_{i,j} + R2\, \overline{\eta}^{n+1}_{i,j} - R2\, \overline{\eta}^{n+1}_{i,j-1} = S_{i,j} \end{cases} \tag{3.22}$$

where the quatities without superscripts are at time level n. The definitions of undefined quantities are given in Appendix D, which also shows the details of the following derivation.

The x sweep equations, after some manipulations, can be reorganized as

$$\begin{cases} \overline{\eta}^*_{i,j} = F1_i + E1_i U^{n+1}_{i,j} \\ U^{n+1}_{i,j} = F2_{i-1} + E2_{i-1} \overline{\eta}^*_{i-1,j} \end{cases} \tag{3.23}$$

where

$$\begin{aligned} F1_i &= \frac{C_{i,j} - P_{i,j} F2_i}{1 + P_{i,j} E2_i} \\ E1_i &= \frac{P_{i-1,j}}{1 + P_{i,j} E2_i} \\ F2_i &= \frac{B_{i+1,j} - R1 F1_{i+1}}{A_{i+1,j} + R1 E1_{i+1}} \\ E2_i &= \frac{R1}{A_{i+1,j} + R1 E1_{i+1}} \end{aligned}$$

The boundary conditions state that at the shoreline (i=idry), the velocities should be equal to given velocities in the inlet section and they disappear elsewhere, and the mean water displacement $\overline{\eta}$, assumes to be identically equal zero. Therefore, the first sweep will solve coefficients $F1$, $F2$, $E1$ and $E2$ starting from i=idry till offshore line (i=1). Once those coefficients are determined, the second sweep will directly yield results of $\overline{\eta}^*$ and U^{n+1} starting from i=1 (offshore boundary) till i=iwet, where iwet = idry-1, is the last grid at

which water depth has non-zero positive value. The offshore boundary condition is given at deep water, i=1, by specifying the mean water displacement to be zero. This is approximate assumption to maintain a steady state mean flow in the region of concern with no increase or decrease of water mass. A more rigorous condition is to allow for water level variation at the offshore boundary such that the change in hydrostatic force is balanced by the net momentum flux and bottom shears in the x-direction.

The lateral boundary conditions basically have three kinds for the concerned region: the symmetric free boundary conditions; the no-flow boundary conditions and the non-symmetric free boundary conditions. They will be specified for specific problems later.

The y sweep is similar to the x sweep and (3.22) can be rewritten as

$$\begin{cases} \overline{\eta}_{i,j}^{n+1} = F3_j + E3_j V_{i,j}^{n+1} \\ V_{i,j}^{n+1} = F4_{j-1} + E4_{j-1}\overline{\eta}_{i,j-1}^{n+1} \end{cases} \tag{3.24}$$

where

$$\begin{aligned} F3_j &= \frac{Z_{i,j} - Q_{i,j}F4_j}{1 + Q_{i,j}E4_j} \\ E3_j &= \frac{Q_{i,j-1}}{1 + Q_{i,j}E4_j} \\ F4_j &= \frac{S_{i,j+1} - R2F3_{j+1}}{R_{i,j+1} + R2E3_{j+1}} \\ E4_j &= \frac{R2}{R_{i,j+1} + R2E3_{j+1}} \end{aligned}$$

The first sweep will determine $F3$, $E3$, $F4$ and $E4$, then the following sweep will give the values of $\overline{\eta}^{n+1}$ and V^{n+1}. The shoreline boundary condition for V is set equal to zero at i=idry; and offshore boundary condition at i=1 supposes that it satisfies the mass conservation, i.e., $(VD)_x = 0$. The lateral boundary conditions will be discussed for different situations later.

3.2.4 Stability Criteria

The stability criteria of these schemes can not be established theoretically. In general, the stability criterion for explicit scheme can be guided by the following inequality:

$$\triangle t \leq \frac{\sqrt{(\triangle x)^2 + (\triangle y)^2}}{\mid u_t \mid + \sqrt{gD}} \tag{3.25}$$

where $\mid u_t \mid$ is the magnitude of total velocity. For application, it becomes

$$\triangle t \leq Min.[\frac{\triangle x, \triangle y}{\sqrt{gD}}] \tag{3.26}$$

for $\mid u_t \mid \ll \sqrt{gD}$

Actually, the critical time step, $\triangle t$, in our study by using a two time level implicit model is at least one order larger than that given by (3.26).

3.3 Finite Difference Scheme for the Wave Equation

The final form of wave equation (2.138) in chapter 2 is mixed parabolic-hyperbolic partial differential equation. The advantage of parabolic type partial differential equation is that the marching method can be used in step by step calculation. Booij (1981) proposed a parabolic model following on Radder (1979). Then the wave field can be split into a transmitted and a reflected field. In his parabolic approach, the reflected field is completely neglected. Kirby (1983) gave another approximation, after assuming that the complex amplitude can absorb the difference between real and image wave directions for small angle incident waves, and also assuming that wave amplitudes are changing more rapidly in y direction than in x direction for slowly varying topography. Both of those assumptions have been introduced in our derivation of the wave equation.

For the parabolic partial differential equation, the Crank-Nicolson finite difference scheme is applied. For simplicity, (2.138) in chapter 2 can be rewritten as

$$A_x + C_0 A_y - iC_1 A_{yy} + \frac{1}{C_2}\frac{\partial C_2}{2\partial x}A + \frac{1}{C_2}\frac{\partial C_3}{\partial y}A + (C_4 + iC_5)A = 0 \tag{3.27}$$

where

$$
\begin{aligned}
C_0 &= \frac{2\sigma_1 V}{P} \\
C_1 &= \frac{cc_g - V^2}{P} \\
C_2 &= \frac{P}{\sigma_1^2} \\
C_3 &= \frac{V}{\sigma_1} \\
C_4 &= R + W \\
C_5 &= \frac{1}{P}[cc_g(k_1^2 - k^2)] + (k_0 - k_1) - R + \frac{1}{P}(\sigma_0^2 - \sigma^2)
\end{aligned}
$$

in which

$$
\begin{aligned}
P &= 2(cc_g k_1 + \sigma_1 U) \\
R &= \frac{gk^2}{P\cosh^2 kh}\sqrt{\frac{\nu}{2\omega}}
\end{aligned}
$$

As the waves enter the surf zone, the second term in C_4 will be added into calculation. The quantity of $\mid A \mid^2$ in σ_0^2 is the value evaluated at last iteration, unlike Kirby who specified this value at the same iteration. The values of velocity components U and V are grid-center values in this calculation.

The Crank-Nicolson finite difference scheme constructs Eq.(3.27) as

$$
\begin{aligned}
&\frac{A_{i+1,j} - A_{i,j}}{\triangle x} + \frac{1}{4\triangle y}[(C_0)_{i+1,j}(A_{i+1,j+1} - A_{i+1,j-1}) + (C_0)_{i,j} \\
&(A_{i,j+1} - A_{i,j-1})] - \frac{i}{2(\triangle y)^2}[(C_1)_{i+1,j}(A_{i+1,j+1} - 2A_{i+1,j} + A_{i+1,j-1}) + (C_1)_{i,j} \\
&(A_{i,j+1} - 2A_{i,j} + A_{i,j-1})] + \frac{1}{2\triangle x}\frac{((C_2)_{i+1,j} - (C_2)_{i,j})}{((C_2)_{i+1,j} + (C_2)_{i,j})}(A_{i+1,j} + A_{i,j}) \\
&+\frac{1}{4\triangle y}[\frac{((C_3)_{i+1,j+1} - (C_3)_{i+1,j-1})}{(C_2)_{i+1,j}}A_{i+1,j} + \frac{((C_3)_{i,j+1} - (C_3)_{i,j-1})}{(C_2)_{i,j}}A_{i,j}] \\
&+\frac{1}{2}[((C_4)_{i+1,j} + i(C_5)_{i+1,j})A_{i+1,j} + ((C_4)_{i,j} + i(C_5)_{i,j})A_{i,j}] = 0
\end{aligned}
\tag{3.28}
$$

A similar double sweep method is used to solve (3.28), resulting in

$$
A_{i,j} = R2_{j-1} + R1_{j_1}A_{i,j-1} \tag{3.29}
$$

The definitions of $R1$, $R2$ and other details are also given in Appendix C.

The boundary conditions are stated as follows:

a) at offshore, i=1, the wave amplitudes are specified in complex forms;

b) at shoreline, i=idry, the wave amplitudes are supposed to die off completely;

c) the lateral boundary conditions can be considered as

$$A_y = ik \sin\theta A \tag{3.30}$$

which assumes that the waves travel mainly in the x direction on a slowly varying topography and Snell's law is valid for first order correction. The finite difference form of (3.30) gives

$$A_{i,j+1} = A_{i,j} \frac{1+Q}{1-Q} \tag{3.31}$$

where

$$Q = (ik \sin\theta \frac{\triangle y}{2})_{i,j+1}$$

The local wave propagation angle θ, as discussed in chapter 2, can be found through the complex wave amplitude. By Eq.(2.92) of chapter 2, we have

$$\ln(\frac{A^{i+1}a^i}{A^i a^{i+1}}) = i(k_1 - k_0)\triangle x \tag{3.32}$$

$$\ln(\frac{A^{j+1}a^{j-1}}{A^{j-1}a^{j+1}}) = i2k_2\triangle y \tag{3.33}$$

where the double primes in Eq.(2.92) have been dropped. The local wave angles are included both in k_1 and k_2, so that either of above equations can be used to obtain θ.

3.4 Method of Solution

With the specified initial and boundary conditions, the finite difference equations (3.21), (3.22) and (3.28) can be solved in a loop of iteration.

The initial condition is assumed to be the state of rest. The velocity field, both U and V components as well as the mean free surface displacement, $\overline{\eta}$, are initially set equal to zero. A bottom topography is input into the model. The initial wave amplitude field is calculated

by solving the wave energy equation with velocities equal to zero, which corresponds to Snell's law for plane beach before waves break.

To avoid "shock loading" the model, both wave amplitude and velocities of inlet discharge are built up from zero to their termination value over a number of iterations. We choose 100 iterations to set up those values by using the hyperbolic tangent function

$$F = F_0 \tanh(IT/25) \tag{3.34}$$

where F is either wave amplitude or velocity of inlet discharge; F_0 is their termination values; IT is the number of iteration. The approach declares that the termination value will be reached as total iteration is up to 100, while $\tanh 4$ approaches the value of unity.

The program will run till the variables U, V, $\overline{\eta}$ and A reach their steady state. The convergency is also checked by the balance of total discharge in and out of the controlled boundary.

There are two coefficients to be determined in a running case: one is the bottom friction coefficient and the other is the eddy viscosity coefficient. For fixed inlet discharge, the eddy viscosity is assumed to be constant, but the bottom friction coefficient may vary for different combinations of wave and current. Further explanations on how to select these two coefficients are given in the next two chapters.

CHAPTER 4
PERFORMANCE OF THE MODEL

To evaluate the performance of the numerical model, a number of tests were run, mainly utilizing existing numerical models of simple cases as bench marks. Little attempt was made to compare directly with existing experimental data for two reasons:

(1) Experimental data that can be used to test the model to its full term, i.e., current-wave interaction due to inlet on sloping beach, does not exist.

(2) The bench mark numerical models selected here usually already did their comparisons with laboratory data, whenever available. Since the purpose of the present model is not to seek improvement of any specific numerical model but rather to extend the capabilities to new applications, it is deemed suffcient for verification purpose to compare with numerical results only.

4.1 Wave Setup on Plane Beach

The model was run for a case of normal incident wave on a plane smooth beach. The conditions were as follows: T=1.14 sec, deep water wave height $H_0 = 6.45$ cm and beach slope = 0.082. This was the same case used by Ebserole and Dalrymple (1979) to compare with laboratory data by Bowen, Inman and Simmons (1968). Since it is a two dimensional case, we have selected $m = 52$ in the x- direction (on-offshore) with $\triangle x = 0.25m$ and $n = 4$ in the y-direction (longshore) with $\triangle y = 0.4m$. The water depth at the deep water end in the numerical model was about 1 m and the mean water level displacement due to set down can be neglected. The results are shown in Fig.4.1. The wave height was computed on the basis of linear wave shoaling and the wave equation as expressed by (2.138) was used for wave height computation. The data from Bowen, Inman and Simmons (1968) were also plotted for comparisons. Apparently, these two approaches are similar except around

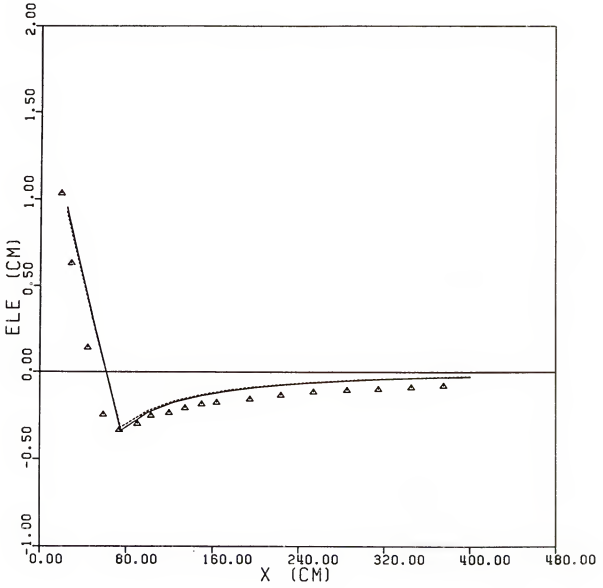

Figure 4.1: Set-up on a Plane Beach. —— Eq.(2.138); - - - Linear Wave; △ Data

breaking line.

4.2 Open Lateral Boundary Conditions and Longshore Current Distributions on a Plane Beach

Two typical open boundary conditions can be specified for the present numerical model. One of them is the periodic lateral boundary conditions, which requires that

$$Q(i,1) = Q(i,N+1)$$

$$Q(i,2) = Q(i,N+2)$$

$$Q(i,3) = Q(i,N+3)$$

and so forth, where Q is any quantity of interest. This boundary condition can obviously be applied to topographies with periodicity such as the example given by Ebsersole and Dalrymple (1979), but can also be relaxed to apply to an arbitrary topography that has no periodicity as long as the boundaries are chosen far enough away from the area of interest and there is no source or sink in the area.

In the case where a source or sink exists, such as the present study with an inlet, the periodic lateral boundary condition can no longer be applied as the out-flow from downstream would not be balanced by the in-flow from the upstream. An approximate free boundary condition in this case is to let

$$\frac{\partial Q}{\partial y} = 0$$

at far enough distance on both upstream and downstream. The above boundary condition implies no longshore variations far away from the area of interest.

A typical example for open-boundary-condition computation is the longshore current generated by obliquely incident waves. The problem was studied analytically by Longuet-Higgins (1970). The case illustrated here is for the conditions: beach slope = 0.075; incident wave angle = 5°; bottom friction coefficient = 0.01; wave height = 0.02 m and wave period = 1 second. The results are shown in Fig.4.2.

If there is no lateral mixing effects at all, the velocity decreases rapidly from maximum to zero at breakline. The apparent existence of velocities outside the breaker zone is due to the fact that the advective acceleration terms in the differenced y momentum equation cause velocities outside the surf zone to be contaminated by velocities inside the breaking zone. The strong mixing effects are demonstrated in the other two cases: one only has the lateral mixing due to breaking with a mixing coefficient = 0.01 m^2/sec and the other includes both mixing from breaking waves with coefficient= 0.01 m^2/sec and flow turbulence with an eddy viscosity coefficient = 0.005 m^2/sec.

4.3 Nearshore Circulation

In this example, currents induced by waves over irregular bottom topography are computed. The bottom topography is slightly modified from that used by Noda et al. (1974) and Ebersole and Dalrymple (1979) and is generated by the following equation:

$$h = s \cdot x[\,1 + Ae^{-(x/20)^{\frac{1}{3}}} \sin^{10} \frac{\pi}{\lambda}(y - \sqrt{x}\tan\beta)\,] \tag{4.1}$$

where

s: beach slope = 0.025

x: distance from shoreline

λ: periodic beach length = 104 m

A: amplitude of bottom variation = 10 m

β: = 30°

in which $\sqrt{x}$ is used instead of x on the right hand side as in the original equation by Noda. This modification is necessary to reduce the variations on the lateral boundary conditions. We choose m=40 in x-direction with $\triangle x = 5.0$ m and n=27 in y-direction with $\triangle y = 4.0$ m. The other parameters are given as

$$T = 4.0sec.; \qquad a_0 = 0.75m; \qquad \theta = 5°; \qquad f = 0.012$$

breaking mixing coefficient = $0.01m^2/sec.$

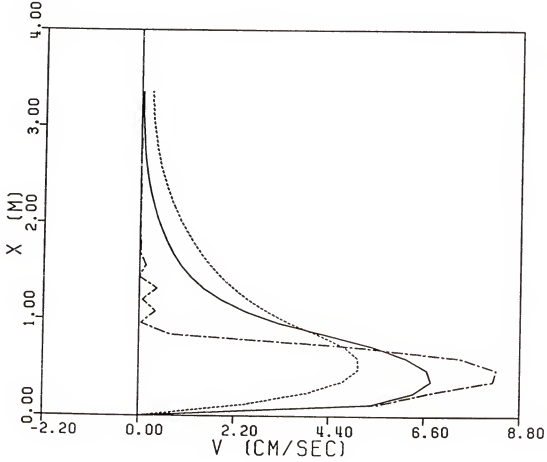

Figure 4.2: Lonshore Current Generated by Obliquely Incident Waves. -- no mixing; —— breaking mixing coeff.=$0.01m^2/s$; - - - breaking mixing coeff. =$0.01m^2/s$ and eddy vis. coeff.=$0.005m^2/s$

The resulting velocity field is shown in Fig.4.3. Although this case offers no direct comparison with the result by Ebersole and Dalrymple, the flow patterns are similar and the current field is physically plausible.

4.4 Combined Refraction, Diffraction and Current Interaction Case

This example deals with the wave refraction problem as illustrated in the previous three cases, but also the combined effects of refraction and diffraction under the influence of topography and the interaction with current. A case of a submerged circular shoal with a parabolic configuration resting on a beach is studied. Similar topography is commonly seen around inlet where an ebb shoal is located outside an inlet. This idealized topography was first investigated by Radder (1979) and then by Kirby and Dalrymple (1983) on a flat bottom with normal incident waves. Therefore, the numerical model was first run at the same condition used by Radder. Then, the case of obliquely incident waves was considered with the shoal on a plane beach. Finally, the model was treated with the presence of an inlet to the above configuration.

4.4.1 The Circular Shoal on a Flat Bottom

Radder (1979) suggested two configurations of shoals in his study of parabolic wave equation. Configuration I, of a circular shoal on a flat bottom is represented by the depth profile

$$\begin{cases} h = h_m + e_0 r^2 & r < R \\ h = h_0 & r \geq R \end{cases} \tag{4.2}$$

where

$$r^2 = (x - x_m)^2 + (y - y_m)^2$$

$$e_0 = (h_0 - h_m)/R^2$$

x_m and y_m are the coordinates of the center of the shoal, and h_m is the water depth at that point; h_0 is the water depth at the flat bottom area. The portion of $r < R$ prescribes a

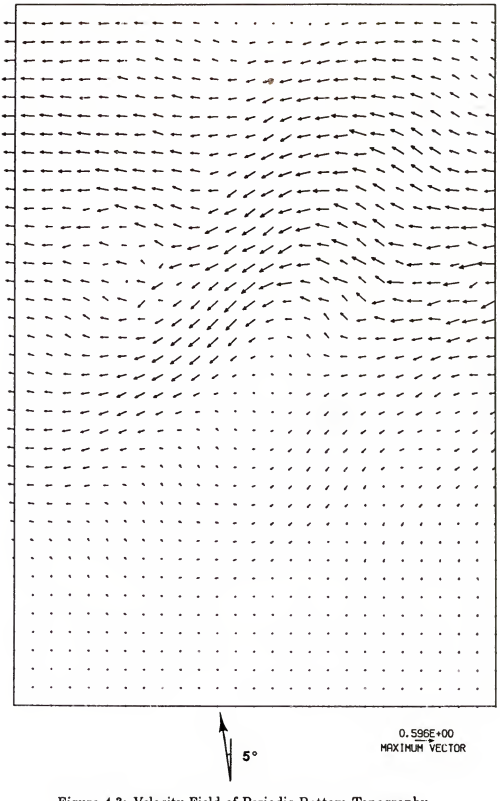

Figure 4.3: Velocity Field of Periodic Bottom Topography

parabolic curve. The numerical values selected are

$$h_m/R = 0.0625; \qquad h_0/R = 0.1875; \qquad L_0/R = 0.5$$

where L_0 is the wave length in the flat bottom area.

For such a configuration, the wave rays of a linear refraction approximation are focus into cusped caustics. Peregrine (1983) and Kirby and Dalrymple (1983) discussed this case and have shown that two jumps in wave condition fan out in approximately the same manner as the caustics emanating from the region of the cusp. The region between the jump conditions, directly in the lee of the submerged shoal, would then be dominated by waves of approximately uniform amplitude propagating in the incident wave direction.

The grid spacings used by Radder are described as

$$\triangle y/\triangle x = 0.5; \quad \text{and} \quad L_0/\triangle x = 1, 2, 4 \text{ and } 8.$$

and it is noted here that the larger the value of $L_0/\triangle x$, the better the resolution. For the shoal studied here, $L_0 = 0.25m$ is used, the corresponding $L_0/\triangle y = 2.5$. The center of the shoal, with the radius $R = 10\triangle x(5\triangle y)$ is located along the line of symmetry with respect to the y-axis.

Without consideration of current, the wave energy equation becomes

$$2cc_g k_1 A_x - icc_g A_{yy} + [(k_1 cc_g)_x + icc_g(k_1^2 - k^2) + i2(k_1 cc_g)(k_0 - k_1)]A$$
$$+i(\sigma_0^2 - \sigma^2)A - \frac{(i-1)gk^2}{\cosh^2 kh}\sqrt{(\frac{\nu}{2\omega})}A + (2cc_g k_1)WA = 0 \qquad (4.3)$$

Following Kirby and Dalrymple (1983), the non-dimensional incident wave amplitudes are chosen as $k_0 A_0 = 0.16$ and 0.32 in which $k_0 = 2\pi/L_0$. The variations of wave amplitudes along the center line $(y/R = 0)$ in the x direction are shown in Fig.4.4 in which $x/R = 0$ starts from the fore-edge of the shoal with the center of shoal located at $x/R = 1.0$. For both cases, in the neighborhood of the center of the shoal the wave amplitudes drop significantly below the incident wave amplitude. The peak value of $k_0 A_0 = 0.32$ is less than half the value of $k_0 A_0 = 0.16$; it indicates the effects of nonlinearity with the increase of wave steepness.

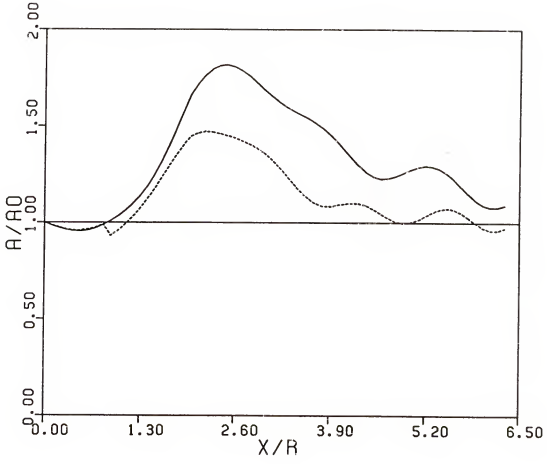

Figure 4.4: Wave Amplitude Variations along Centerline —— $A_0k_0 = 0.16$; - - - $A_0k_0 = 0.32$

In other words, the wave energy is much easier to be trapped and harder to decay for the shorter waves at the line of symmetry. Also, there is a slight phase shift in the position of maximum wave amplitudes. Figures 4.5 and 4.6 gives the wave amplitude variations in the longshore direction at the location of $x/R = 3.0$, 4.0, 5.0 and 6.0, respectively. $y/R = 0$ is the symmetric center line of the shoal. These plots show that as waves travel downstream from the shoal the influence zone becomes wider. The spreading of the influence zone for both cases are almost the same. Since wave amplitudes for $k_0 A_0 = 0.16$ have a large amplification at $y/R = 0$, which can also be shown in Fig.4.4, they drop rapidly to below the incident wave amplitude to keep the wave energy balance.

These results are similar to those described by Kirby and Dalrymple (1983).

4.4.2 Circular Symmetric Shoal on Plane Beach

In the case of the circular shoal located at the center of a uniform sloping beach as shown in Fig.4.7, the water depth, referring to Fig.4.8, is prescribed by the following formulas:

$$\begin{cases} h = x\tan\alpha & r > R\cos\alpha \\ h = x\tan\alpha - h' & r \le R\cos\alpha \end{cases} \tag{4.4}$$

where

$$r^2 = (x - x_n)^2 + (y - y_n)^2,$$

$$h' = h''/\cos\alpha,$$

$$h'' = \frac{-B + \sqrt{B^2 - 4C}}{2},$$

$$B = \frac{R^2}{h_n \tan^2\alpha} - \frac{2r}{\sin\alpha} \quad \text{and}$$

$$C = \frac{r^2}{\sin^2\alpha} - \frac{R^2}{\tan^2\alpha}.$$

The values used in the examples are: $R = 0.7521m$; $h_n = 0.085m$; $\triangle x = \triangle y = 0.15m$ and the center of shoal is located at grid point i=17 and j=13.

The model is first run for a case with no inlet and then for a case with the presence of an inlet. In both cases, the input waves form an angle of 5° with the normal of the shoreline.

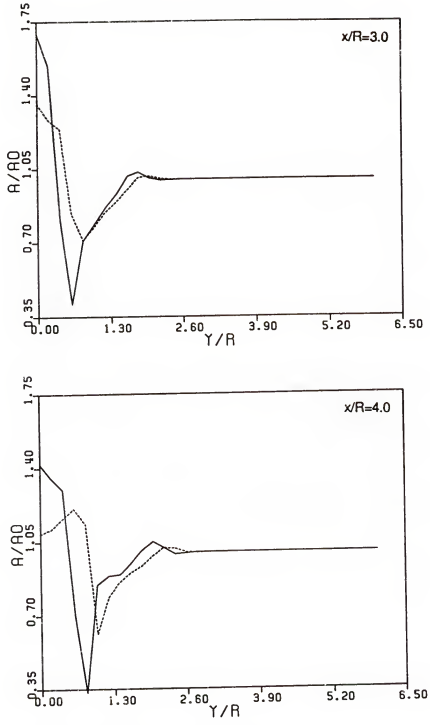

Figure 4.5: Wave Amplitude Variations across Centerline —— $A_0k_0 = 0.16$; - - - $A_0k_0 = 0.32$

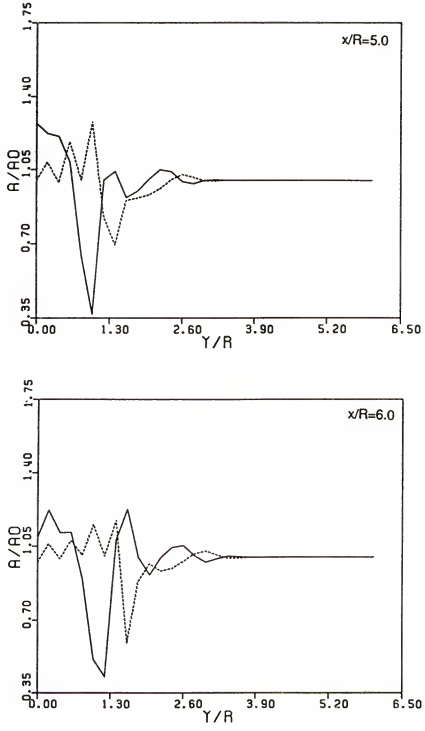

Figure 4.6: Wave Amplitude Variations across Centerline —— $A_0k_0 = 0.16$; - - - $A_0k_0 = 0.32$

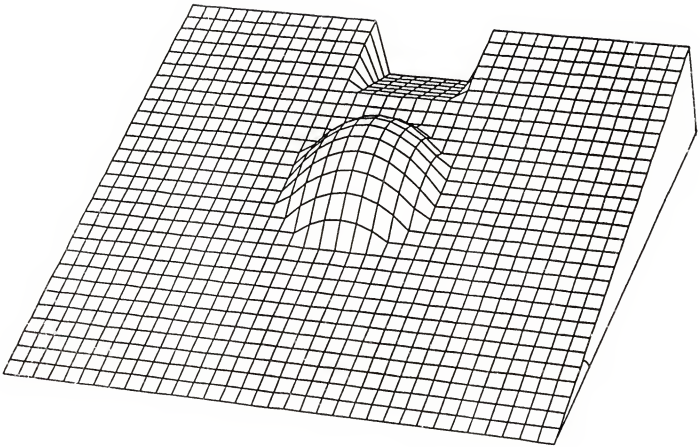

Figure 4.7: Bottom Topography : a Circular Shoal with Parabolic Configuration on the Plane Beach

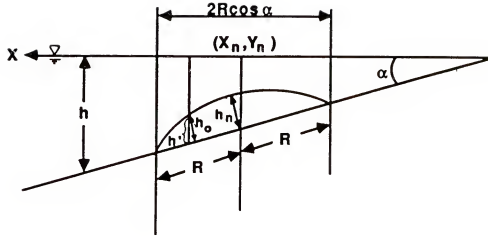

Figure 4.8: Description of Water Depth

The other input conditions are

$$T = 1.0sec.; \qquad a_0 = 0.02m; \qquad \alpha = 0.075; \qquad f = 0.01$$

breaking mixing coefficient $= 0.01m^2/sec.$

For the case of no inlet, the eddy viscosity coefficient is equal to zero and for the case with inlet, a value of $0.005m^2/sec$ is used. The inlet discharge is equal to $0.007m^3/sec.$

The velocity field with no inlet is shown in Fig.4.9. Waves break at the top of the shoal. The current induced by the waves is characterized by a strong onshore flow over the shoal consistent with the wave incident angle; at the lee side of the shoal, the flow splits into two directions, one upstream and one downstream. The upstream flow develops into two vortexes rotating in opposite directions; the downstream flow forms a longshore flow system with two portions. This longshore current pattern at the downstream boundary is sketched in Fig.4.10.

The velocity field with the inlet is shown in Fig.4.11. The effects of inlet flow are seen

to be quite pronounced. First of all, the two upstream vortices are strengthened and pushed farther offshore. Secondly, the downstream longshore current system is also strengthened with a flow reversal close to the shoreline, which is caused by the lower mean water surface elevation at the mid-section of the shoreline in the shadow of the shoal and also caused by the lower pressure due to the higher velocities in the inlet, and the influence is extended further offshore which is due to the fact that the momentum of the inlet discharge pushes the flow into the lower pressure region. The mean water surface elevation is also lowered in this region. The longshore current distribution at the downstream boundary for the case with inlet is also shown in Fig.4.10. The location of null flow on the lee side of the shoal is now being pushed seaward onto the shoal due to the inlet flow momentum.

Figures 4.12 and 4.13 show the contour lines of wave amplitudes. The unit in these figures is 10^{-4} meter. For the case of no inlet, the wave refraction effect causes the waves to focus on the shoal and this leads to wave breaking and a low region just leeward of the shoal crest. The diffraction effect, on the other hand causes waves to focus on the leeward of the shoal and creates a local high region there.

The effects of current are most pronounced in the center region between the inlet and the shoal. The local high region behind the shoal as mentioned above is enhanced considerably. The waves at the location of inlet entrance are also steepened and the heights increased.

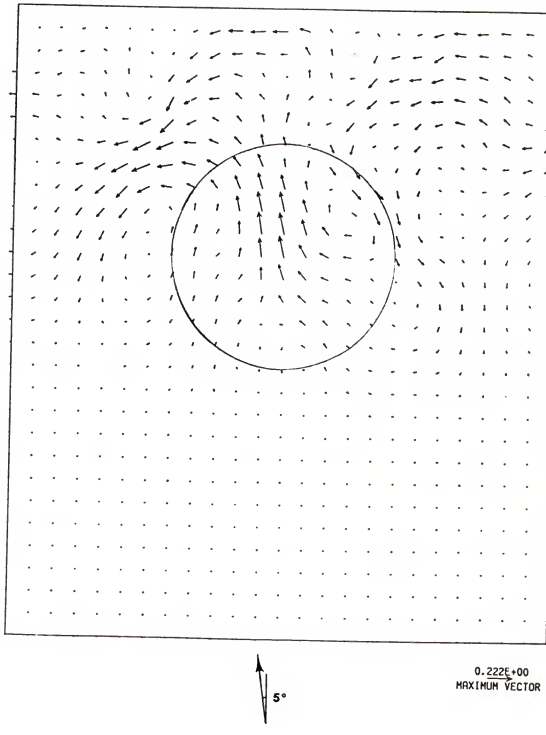

Figure 4.9: Velocity Vector Field for Circular Shoal Located on the Plane Beach (no inlet)

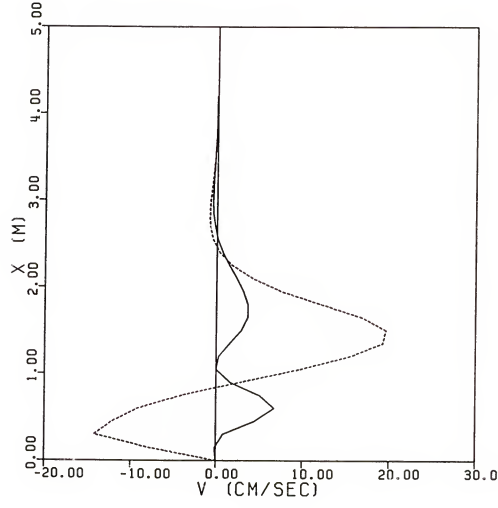

Figure 4.10: Longshore Current Distributions at Lowest Boundary. —— No Inlet; - - - with Inlet

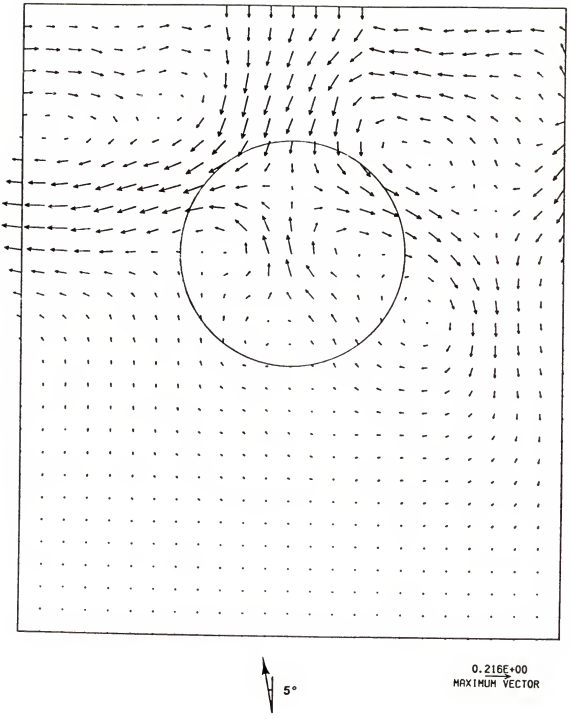

Figure 4.11: Velocity Vector field for Circular Shoal Located on the Plane Beach with Current from Inlet

Figure 4.12: Contour Plot of Wave Amplitudes on the Circular Shoal Located on the Plane Beach (no inlet)

Figure 4.13: Contour Plot of Wave Amplitudes on the Circular Shoal Located on the Plane Beach with Current from Inlet

CHAPTER 5
EXPERIMENTAL COMPARISONS

In order to test the validity of the numerical model, laboratory experiments were conducted in a square basin in the laboratory of the Coastal and Oceanographic Department, University of Florida. The experimental set up, procedures and results together with numerical simulations are reported in this chapter.

5.1 Purpose of Experiments

Although there are many theoretical studied in recent years on the subject of wave-current interaction, laboratory experiments and field data are scarce. Ismail-Awadalla (1981) conducted laboratory experiments in wave-current interaction on a flat bottom with a nozzle injecting dye against the normal incident waves. The results demonstrated the physical phenomenon of current-wave interaction but were not sufficiently quantitative to verify numerical models.

In the present experiments, we focus on a beach-inlet system, where the phenomena of wave transformation over a gentle slope, coupled with the effects of a non-uniform current from an inlet can be studied. There are four basic quantities to be investigated: mean velocities: U in x direction and V in y direction; the mean water surface displacements $\overline{\eta}$ and the wave amplitudes A. Since $\overline{\eta}$ is a small quantity and requires a long time to establish a steady value, the effects of wave reflection in the wave basin preclude meaningful measurements. Only wave amplitude and current field were investigated.

5.2 Facilities and Instruments

5.2.1 The Laboratory Facilities

The experiments were conducted in a square 7.22 m by 7.22 m wave basin with a depth of 0.8 m as shown in Fig.5.1 and 5.2. A fixed plane beach was constructed of cement with 1:13.3 slope (or s = 0.075). The toe of the beach was 0.85 m from the wave generator. The inlet was located at the center of the beach end. It was 1.44 m wide and the bottom was horizontal. The total length from the leading edge of the inlet to the diffuser was 1.2 m as shown in Fig.5.2. For all cases tested the water depth was kept 0.369 m measured from the bottom of the basin. Thus, the water depth was 0.045 m in the inlet. A grid system was established as shown in Fig.5.3 to facilitate numerical computation and laboratory measurement. The grid size is 0.12 m x 0.18 m. There are 43 grids in the x-direction and 40 in y-direction. The inlet was located at the center of basin from j = 17 to j = 24. The leading edge of the inlet was at i = 37. The toe of the sloping beach was located at i = 1.

Waves were generated by a flap type wave generator. The bottom of the flap was elevated 0.2 m above the bottom to permit the excess water from the inlet to return freely under it. The wave generator was driven by a D.C. motor. Wave period and amplitude were controlled by adjusting the frequency of the motor and the eccentricity of the linkage. Uniformly long crested waves can be obtained for small amplitude waves. Cross waves would appear as the wave amplitudes became larger. Standing waves also existed under certain circumstance due to the short distance from the toe of the beach to the wave flap.

To prevent the leakage of wave energy from behind the wavemaker, horse hair mats were placed between the wave paddle and the wall, so that the wave motion behind the paddle was greatly reduced. On the other hand, due to space limitation, wave energy absorber could not be placed at the beach end. Therefore, reflection of waves was serious at times.

The current system consisted of a pipe system, a flow filter, a diffuser and a reservoir. As shown in Fig.5.1, a 2.5 horsepower centrifugal pump located between the flow filter and the diffuser was used to transport the water. The flow filter situated behind the wave flap

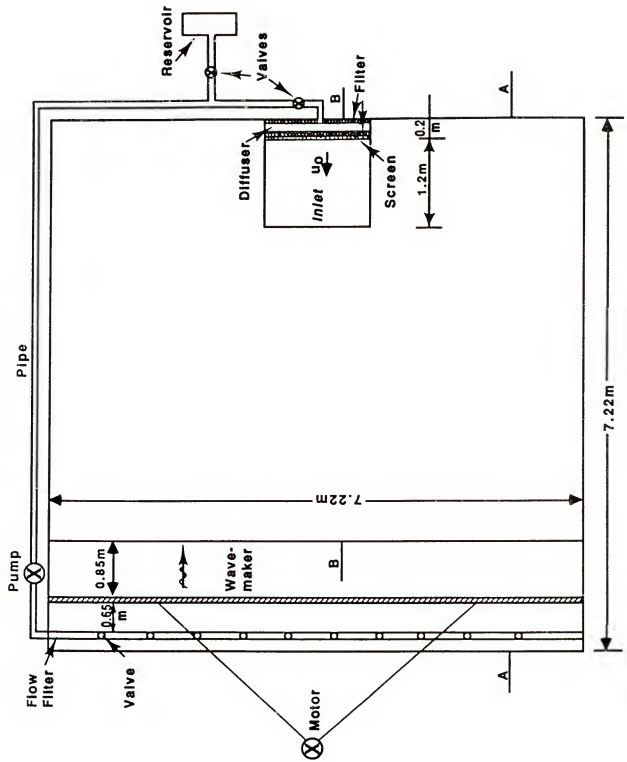

Figure 5.1: Plan View of Wave Tank

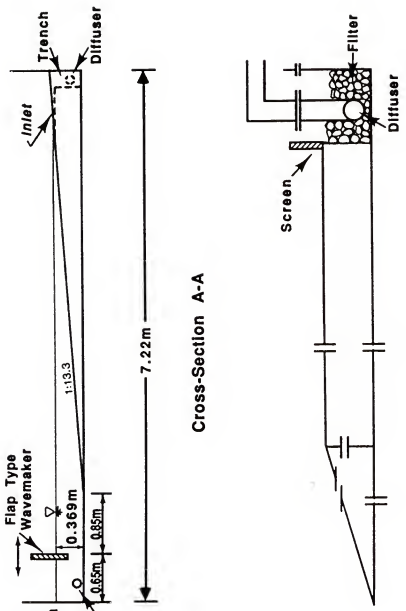

Figure 5.2: Cross-Section Views of Wave Tank

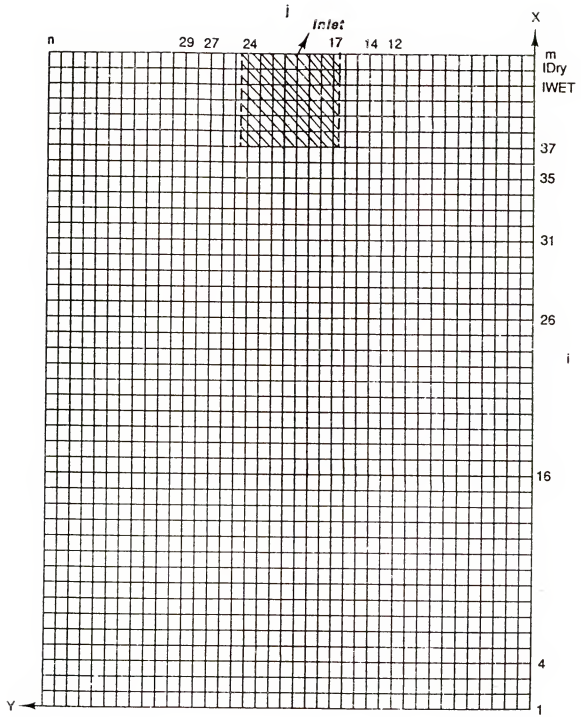

Figure 5.3: Cross-Sections of Measurement

has ten control valves, allowing the water to flow naturally to the recirculation pipe without disturbing natural flow condition. A diffuser with a length 1.4 m was installed in a trench at the end of the inlet. It was a section of pipe with a series of different sized holes to distribute the flow uniformly. The gap around the diffuser was filled in with pebbles and a filter screen made by two layer a net filter with horse hair in between was set up in front of the trench to promote uniform flow across the inlet. However, the distance between the diffuser and the intersection of the shoreline and the inlet entrance was only 0.6 m. It was very difficult to attain a uniform flow condition for such a short distance. After many fine tunings, an acceptable uniform flow condition was finally reached. Fig.5.4 shows the velocity distribution in the inlet at the cross-section that intersects the shoreline. The adopted final velocity distribution was 7/25/86 profile.

5.2.2 Instrumentation

The main properties measured included wave characteristics and current. Four resistance type wave gages were used to measured the spatial distributions of wave heights and periods. Current was measured by a Marsh-Mcburney type electro-magnetic current meter. In addition to wave and current, the discharge from the inlet was monitored by a commercial flow meter manufactured by Sitnet Scientific. The wave gage was calibrated statically by varying the gage submergence stepwise. It was found that the gage could not maintain linearity for the full gage length. Therefore, gage calibration was finally done for each location prior to each test. The current meter was supplied with calibration but was further calibrated, verified and adjusted by towing test in a long flume in the same laboratory. The flow meter was also calibrated by measuring the discharge filling in a reservoir. Fig.5.5 shows the calibration curves of the three instruments; the results were consistent and stable.

A 6-channel strip chart recorder was used to display the data. The wave gage signal was first amplified before feeding into recorder. The current meter signal was time-integrated to eliminate short term fluctuations. The layout of the instrument arrangement is shown in Fig.5.6

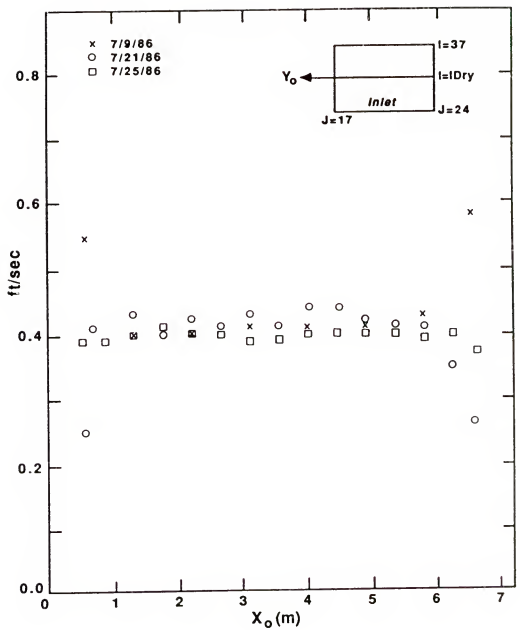

Figure 5.4: Velocity Distribution at I=Idry

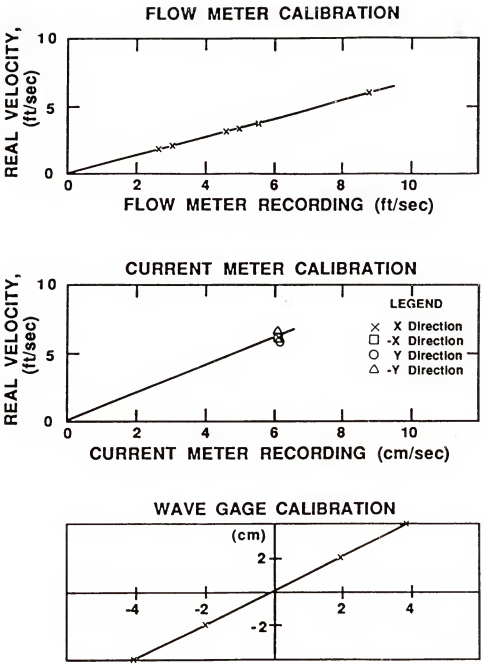

Figure 5.5: Instrument Calibrations

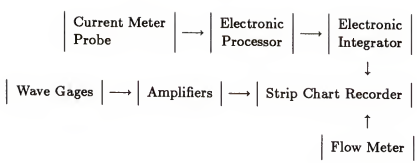

Figure 5.6: Instrument Connections

5.3 Experimental Arrangement and Measurements

The selections of test conditions ideally should fulfill the following criteria:

1. Inlet and beach configurations representative of nature.

2. Waves and current conditions in conformance with the basic assumptions in the analytical model.

3. Test conditions covering a wide spectrum.

Due to the limitations of the basin facility, compromises are made. The beach slope was restricted to 1:13.3 which is somewhat steeper than most of the natural beaches along the east coast of the United States. The inlet dimensions were such that the depth to width ratio was 1:32, which was common for the inlet along Barrier Island and the model size when scaled up 100 times roughly represents a typical natural inlet. The test range on wave conditions was unfortunately rather limited owing to the inability of the wave maker to produce clean large amplitude waves. Thus, the selected incident wave amplitudes were all quite small. The range of wave period (or length) variation, was also limited because of the size of the basin and the strong reflection due to the beach and the current filter at the end of the inlet.

Six different cases were tested. The corresponding conditions are given in Table 5.1. The Ursell number is an indicator of wave nonlinearity. The values selected here were to insure that the Stokes theory remains valid at least in the constant depth region. The ratios

of current velocity to wave celerity at the exit of the inlet ranged from 1:5.5 to 1:7.7 which were within the range that the basic assumption in the wave energy equation is not violated.

Measurements were performed along sections parallel to the y-axis as shown in Fig.5.3, waves were measured along six sections at i = 4, 16, 26, 31, 35 and 37. Current, owing to the rapidly diminishing strength from the inlet exit, were measured along three cross-sections only at i = 26, 31 and 35. At each station, relocation at a minimum of five vertical locations were measured, each with a time-averaged value of 3-5 minutes. Since the inlet discharge is perpendicular to the y coordinate, the velocity component in the y-direction, V, was small. No attempt was made to measure this component.

Table 5.1: Test Condition

$Q_0(m^3/s)$	$H_0(m)$	$T(sec)$	a_0k_0	k_0h_0	U_r
	0.0097	0.87	0.027	2.03	0.25
0.0056	0.0088	1.16	0.015	1.27	0.58
	0.0097	1.36	0.013	1.02	0.99
	0.0123	0.87	0.039	2.03	0.32
0.0076	0.0095	1.16	0.017	1.27	0.62
	0.0097	1.36	0.013	1.02	0.99

in which

Q_0: Total discharge from inlet;

H_0: Incident wave height at water depth h_0;

T : Wave period;

a_0: Incident wave amplitude = $H_0/2$;

k_0: Incident wave number at water depth h_0;

h_0: Maximum water depth = 0.369 m.;

U_r: Ursell number = $\frac{H_0L_0^2}{h_0^3}$ in which L_0 is the wave length at depth h_0.

5.4 Experimental Results and Numerical Comparisons

The experimental results were presents here together with numerical computations to offer one to one comparisons. Since only wave amplitudes and x-component of the mean

current velocities were measured in the experiments, the comparisons were also restricted to these two parameters. Other flow properties such as current fields, wave height distributions and stream lines were presented in numerical computations only. The conditions were steady state, which, in the numerical computation, normally took 500 iterations with a time step of 0.5 second. The grid system, both mesh size and grid layout, was identical for the numerical and physical models.

The numerical model requires that the mean water level at the offshore boundary be specified. Due to the small a_0k_0 values used in the experiments, the actual water surface elevation under the influence of set down is difficult to established. Therefore, the sensitivity of the numerical model due to slight variations of mean water level was tested. The results of current velocity and wave height profile along the onshore direction are shown in Fig.5.7 and 5.8, for $\overline{\eta} = 0$ and $\overline{\eta} = -\frac{a^2k}{2\sinh 2kD}$ (the set down value of linear wave theory). The other input conditions are: $H_0 = 1$ cm, $T = 1$ sec., $Q_0 = 0.0019\ m^3$/sec, m = 13, $\triangle x = 0.12$ m, n = 6, $\triangle y = 0.18$ m and the inlet located at j = 3 and 4. The results shown in these figures are for those on the plane beach (j = 2) and along the inlet (j = 3). The differences due to the two boundary conditions are so small that in the subsequent computations, the offshore boundary water level displacement is set equal to zero.

The grid size in the x-direction controls the accuracy and the rate of convergency. A value of $\triangle x = 0.12$ m was selected after several numerical trails. Figure 5.9 compares the velocity and wave profiles for the same testing condition with $\triangle x = 0.12$ m and 0.06 m, respectively. For $\triangle x = 0.06$ m the computational time doubles that for $\triangle x = 0.12$ m. The maximum difference between the results is less than 8 %.

5.4.1 Wave Shoaling on Plane Beach

The first case compared was the wave shoaling on plane beach. The test conditions were: $H_0 = 1.23$, 0.95, 0.97 cm and $T = 0.87$, 1.16, 1.36 sec., respectively. The results are shown in Fig.5.10 with calculations from both linear shoaling and the full equation (2.138). Both calculations underestimated the shoaling, particularly for longer period waves. The

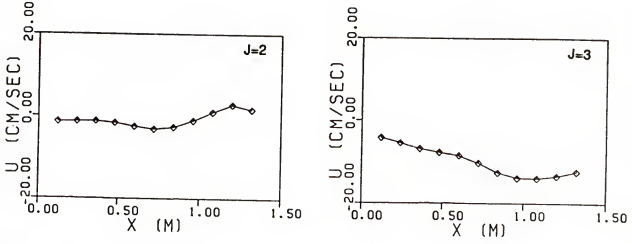

Figure 5.7: Velocity Variations along the Beach, — $\eta(1,j)=0$; $\diamond\ \eta(1,j)=-a^2/(2\sinh kh)$

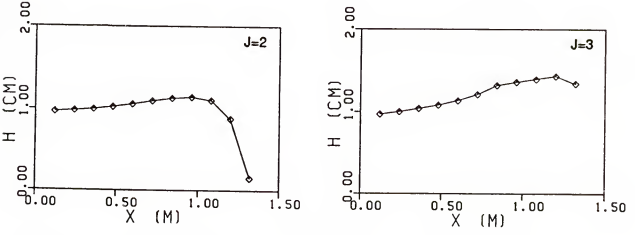

Figure 5.8: Wave Height Variations along the Beach, — $\eta(1,j) = 0$; $\diamond$ $\eta(1,j)=-a^2/(2\sinh kh)$

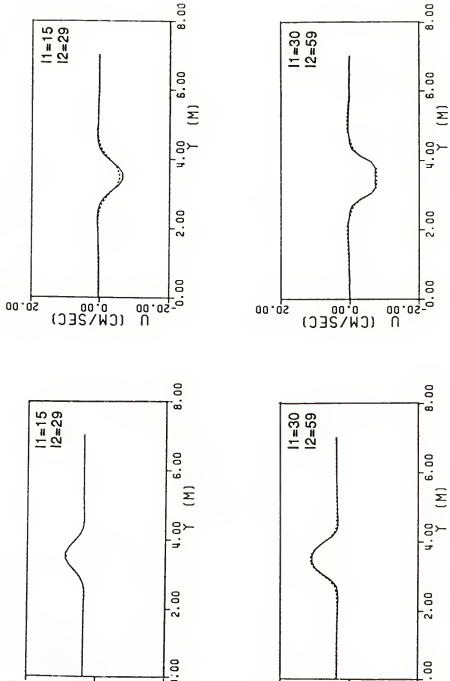

Figure 5.9: Comparisons between m = 43 with $\Delta x = 0.12$ m, ——; and m = 83 with $\Delta x = 0.06$ m, - - - at I1 = 15,30 for m =43 and I2 = 29,59 for m = 83

full equation actually predicts smaller shoaling values than the linear equation. This is a main shortcoming of wave equation presented in the present form as it is derived by using Stokes parameter to rank the order of magnitude. After wave breaking, the full equation is more consistent with the trend of the experimental data.

5.4.2 Flow Field due to Inlet on Sloping Beach with no Waves

The second set of experiments was conducted with inlet flow discharging onto a beach but no incoming waves. Two cases with discharge equal to 0.0056 m^3/sec and 0.0076 m^3/sec were examined. The results of velocity distributions were given in Fig.5.11 and 5.12, respectively. The computed velocity profiles based upon the numerical model were fitted to the experimental data at the offshore outer cross sections i = 26 and 31 by adjusting the bottom friction coefficient (f) and the eddy viscosity coefficient (ϵ_e). The reason for selecting the outer cross sections for the matching is that both frictional and diffusive effects will not be fully recognized until the flow leaves the inertial dominated phase. The values for f and ϵ_e obtained from obtained from the best data fit are as follows:

For $Q_0 = 0.0056 m^3/sec$

$f = 0.005$ and $\epsilon_e = 0.003 m^2/sec$

For $Q_0 = 0.0076 m^3/sec$

$f = 0.003$ and $\epsilon_e = 0.005 m^2/sec$

The computed velocity distributions are in good agreement with the data both in magnitude and spreading even though the magnitude is somewhat force fitted. Both experimental data and calculated profile revealed the flow reversal characteristics at the outer edges of the jet as the result of an adverse force gradient when the inlet flow enter a sloping beach.

The magnitudes and the trend of variations of both the bottom friction coefficient and the viscosity coefficient obtained here are reasonable. The bottom friction coefficient is smaller for the larger discharge case. This is because the Reynolds numbers in the inlet are in the order of 4,000 to 5,000 and the friction coefficient in this range is expected to

decrease as the velocity increases. The eddy viscosity coefficient is a flow property affected by the mean velocity gradients; one expects the higher the velocity gradient the larger the eddy viscosity. Therefore, the values obtained here are consistent.

5.4.3 Inlet on Sloping Beach with Waves

The ultimate purpose of the present study is the development and verification of a numerical model that is capable of solving the kinematic and dynamic flow properties of an inlet-beach-wave system. Therefore, the measurements of this category are of paramount importance to test the validity of the numerical model.

As mentioned before, a total of six different combinations of current and wave conditions were tested. The effect of waves on current field modifications and influence of current on wave properties are discussed here separately.

(1) Current Field Modification

The experimental results of current profiles for the six cases are given in Fig.5.13 to 5.24. The calculated values from the numerical model are also plotted. The solid line is the computed profile with the same input conditions as the experiment. The dotted line is the corresponding profile without input waves. In these computations, the eddy viscosity coefficients were adopted from previous experiments where no waves were imposed and are assumed to be a function of inlet discharge only. The rationale behind such a choice is based on the physical reasoning that the lateral mixing caused by turbulence generated by current gradient will not be significantly affected by an oscillatory wave field and on the observed fact that the computed velocity profile is not sensitive to small changes of this coefficient. The bottom friction coefficient, on the other hand, by virtue of its definition (see Eq.(2.136)) is expected to vary with the wave induced bottom velocity. Therefore, the same method employed in the no wave case is used here by matching the profiles at outer cross sections through adjusting the bottom friction coefficient. Here the values of f and ϵ_c deduced from experimental and numerical comparison are summarized in the following table. The variations and characteristics of f will be discussed later.

Table 5.2: The values of ϵ_e and f in the Tests

case	discharge (m^3/sec)	H_0 (cm)	T (sec)	$\epsilon_e(m^2/sec)$	f
a	0.0056	0.97	0.87	0.003	0.011
b	0.0056	0.88	1.16	0.003	0.013
c	0.0056	0.97	1.36	0.003	0.015
d	0.0076	1.23	0.87	0.005	0.012
e	0.0076	0.95	1.16	0.005	0.010
f	0.0076	0.97	1.36	0.005	0.0105

Overall the experimental date agreed well with the laboratory results. Again, the agreement on the current magnitude was somewhat artificial because of the adjustment made on the friction coefficients. Therefore, the agreement of the shape of the distribution is more indicative of the validity of the numerical model. For all the cases tested, the influence of waves on the current field was small. In general, an opposing wave field reduces the centerline velocity of the jet flow from the inlet but causes the jet to spread wider. Return flows appear at the outer edges of the jet. In the far field, a weak undulating current field outside the jet zone is developed. This current field, undulating in the lateral direction, becomes more prominent for higher discharge, an indication that it might be strongly influenced by the lateral mixing. To reduce the possibility of numerical instability on the unsteady nature, the numerical iterations were raised up to 900 with practically the same results.

As stated before the current strength at the center portion of the jet is reduced under the influence of the opposing waves. When the wave height increases, the velocity distribution can no longer maintain bell shaped and the center portion becomes concaved as clearly shown in cases *a* and *d* in the numerical calculations. Experimental results also displayed such behavior, only more pronounced. In case *f*, for instance, the experimental results showed a very prominent concave shape whereas the numerical prediction only revealed a very mild indentation.

Another experimental observation is the seemingly strong three dimensional flow pattern along the edges of the jet where return flow developed near the surface layer.

To illustrate the change of the complete velocity field, contour plots of current

magnitude for all the cases are shown in Figs.5.25 to 5.34. All the contour lines are expressed in non- dimensional velocity defined as $u/(Q_0/A)$ where $u = \sqrt{U^2 + V^2}$ is the magmitude of velocity, Q_0 is the inlet discharge and A is the inlet cross-sectional area. Figure 5.25 shows a case of an inlet of $Q_0 = 0.0056m^3/sec$ discharging into a basin of flat bottom with constant water depth of 0.045 m and bottom friction coffficient equal to zero. In this case, the flow behaves more or less like a two-dimensional submerged jet. The core of the jet contains a clear out-shot tongue. The extent of the tongue is an indicator of a flow regime dominated by inertial force. The core ends, of course, where the zone of diffusion reaches the centerline of the jet. Downstream from this section, the magnitude of the velocity diminishes as the jet expands laterally due to entrainment. The velocity distribution is bell shaped with discernable similarity profiles as the jet continually expands into downstream section. Figure 5.26 shows a similar case with the exception that bottom friction is present ($f = 0.01$). The presense of bottom friction greatly retards the jet flow and results in much rapid lateral mixing. The velocity vectors are also plotted for both cases.

For the situation that a jet expands into a sloping beach, such as that in the present experiment, it appears that the jet contracts first then expands gradually with pulsatory nature. It is apparent that similarity velocity profile can not be maintained. The pulsatory nature of the jet profile could be the consequence of two competing mechanisms: the lateral diffusion mechanism prompts the jet to expand but the cross-sectional expansion due to water depth deepening, on the other hand, creates vertical vortex and causes the jet expansion in the vertical direction at the expense of lateral contraction.

The apparent effects of opposing waves are the retardation of the advancing jet and the wider spreading of the current field. The over all effects on the jet appear to be mild.

As mentioned earlier, the values of bottom friction coefficient were obtained by the best data fitting at outer cross sections i = 26 and 31. These values are list in Table 5.3 together with other pertinent parameters. Since in the present model the bottom shear stress is computed by a pair of simplified quadratic equations (Eqs.(2.118) and (2.119)) in which

the wave obital velocity appears only as a linear quantity, it is expected that the associated friction coefficient should be affected by the relative magnitude of this wave orbital velocity to the ambient current velocity. The values of f are plotted against u_m/U_i in Fig.5.35 in which U_i is the discharge velocity at inlet and the definition of u_m is

$$u_m = \frac{a_i \omega}{\sinh kh}$$

where a_i is the wave amplitude at inlet given by linear shoaling and h is the still water depth at inlet, k is wave number at inlet with no current. It appears that f in the simplified bottom stress equation is linearly proportional to u_m/U_i. The results so obtained are completely consistent with the physical phenomenon.

Table 5.3: Bottom Friction Coefficients Used in the Model

case	$T(sec)$	a_0 (cm)	u_m (cm/s)	U_0 (cm/s)	u_m/U_0	f_w
a	0.87	0.485	6.58	8.64	0.76	0.011
b	1.16	0.440	6.20	8.64	0.72	0.013
c	1.36	0.485	6.92	8.64	0.80	0.015
d	0.87	0.615	8.35	11.73	0.71	0.012
e	1.16	0.475	6.69	11.73	0.57	0.010
f	1.36	0.485	6.92	11.73	0.59	0.0105

(2)Wave Field Modification

In contrast to the good agreement between measured and computed velocity field, the wave amplitudes were mostly underestimated by the numerical model. This, as explained earlier, is mainly due to the limitation of the wave equation in the form used in the present model, i.e., to include the effects of refraction, diffraction and shoaling on the same order of magnitude.

In the experiment, owing to the finite basin size, the presence of inlet and current influenced the wave field of the entire basin including the boundary wave heights. In the numerical computation, the measured wave amplitudes at the offshore boundary are used as input. Table 5.4 provides the boundary heights as measured. The centerline of the basin is in between grid 20 and 21. For normal incident waves, the field is symmetrical.

Table 5.4: Incident Wave Height

case	Q_0 (m^3/sec)	T (sec)	H_0 (cm)	H_{17}	H_{18}	H_{19}	H_{20}
a	0.0056	0.87	0.97	1.00	1.03	1.06	1.07
b	0.0056	1.16	0.88	0.88	0.89	0.92	0.965
c	0.0056	1.36	0.97	0.97	0.98	0.99	0.99
d	0.0076	0.87	1.23	1.27	1.33	1.42	1.44
e	0.0076	1.16	0.95	0.97	0.98	1.05	1.08
f	0.0076	1.36	0.97	0.99	0.99	1.13	1.15

Therefore, we have $H_{21} = H_{20}$, $H_{22} = H_{19}$ and so on. The wave heights of unspecified grid are considered to be equal to H_0, where H_0 is the original incident wave height.

Figures 5.36-5.41 give the measured data plotted against the numerical values. Both numerical and experimental results revealed that the wave-current interaction has a very prominent effect on the local wave height, particular in the zone directly influenced by the jet. The counter current in the center of the jet obviously enhances the wave height whereas the return current near the edge of the jet causes the waves to diminish somewhat. Therefore, the shape of the wave height profile is very similar to that of the current. Figure 5.42 shows the variations of the non-dimensional wave heights along the centerline of the basin for the six cases tested. As can be seen, the combined shoaling and current-wave interaction causes the waves to increase their amplitudes significantly as they progress toward the inlet. The numerical results showed more than doubling the amplitude for cases of strong current. The experimental results were even higher, with amplification reaching as high as threefold.

The agreement between experimental and numerical results is considered fair for weak current and in deep water and becomes progressively worse with longer incoming wave period, shallower depth and stronger counter current. The breaking criterion used in the numerical model proves to be inadequate under strong current condition. Experimental evidence showed that waves break earlier than predicted.

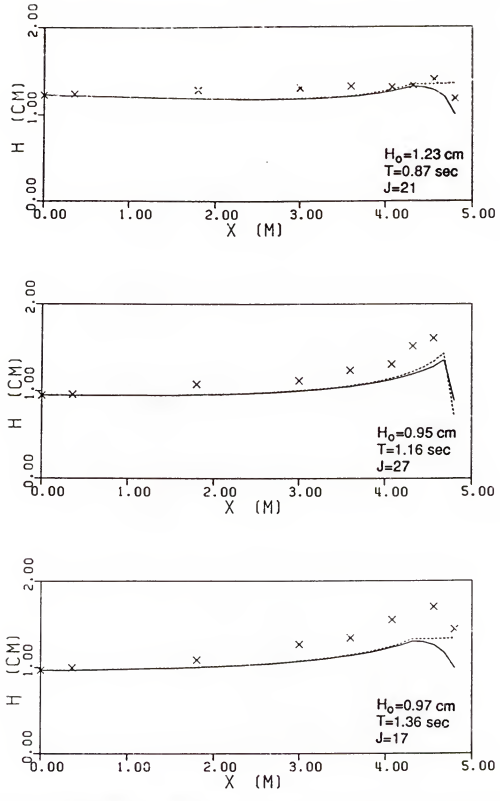

Figure 5.10: Wave Height Variations along the Beach (no current), — – Wave Eq. (2.138); - - - Linear Shoaling; x Measured Data

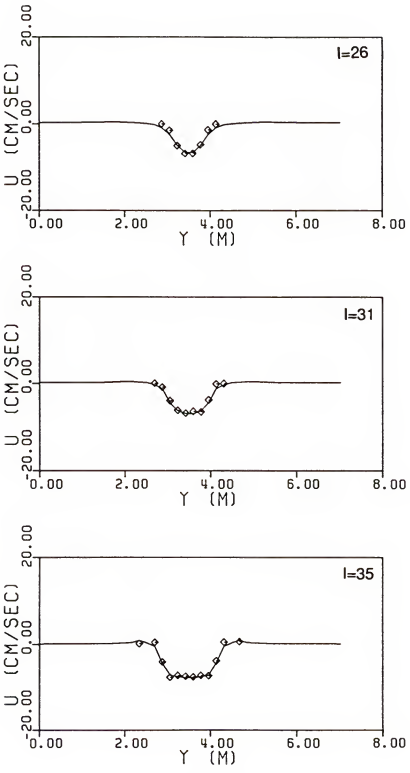

Figure 5.11: Velocity profiles for $Q_0 = 0.0056 m^3/sec.$ (no waves)

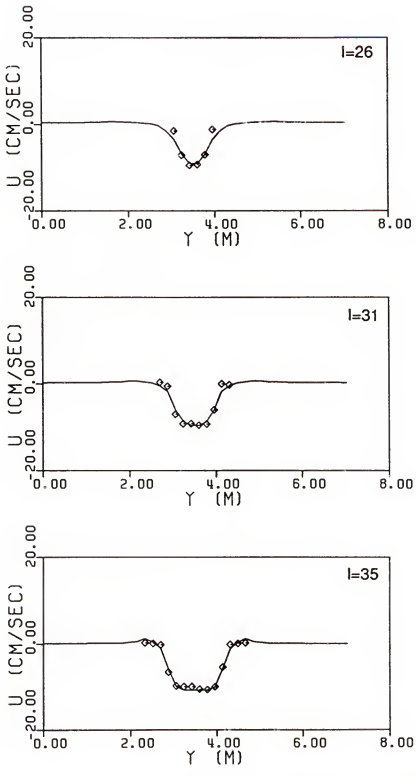

Figure 5.12: Velocity profiles for $Q_0 = 0.0076 m^3/sec.$ (no waves)

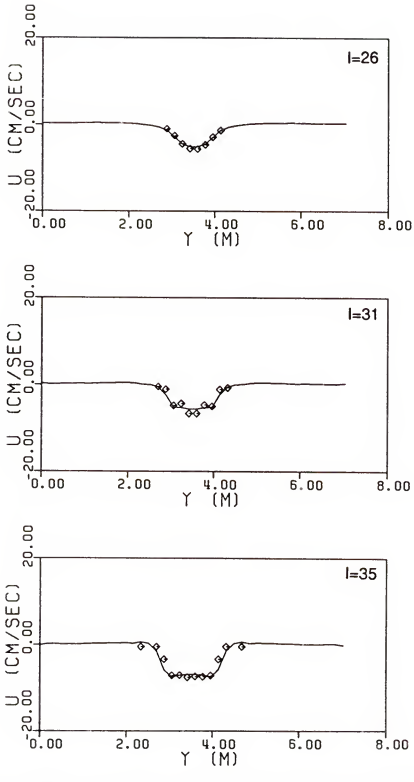

Figure 5.13: Variation of x-Component Velocity. Case a: $Q_0 = 0.0056m^3/s$; T = 0.87 sec.; $H_0 = 0.97$ cm. — Numerical Model; ⋄ Measured Data

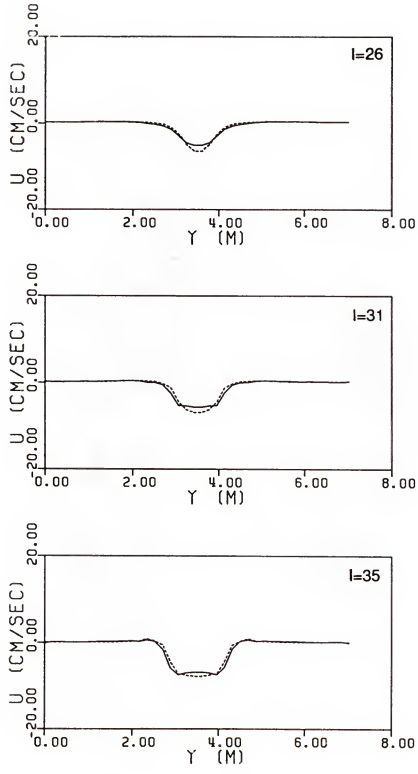

Figure 5.14: Comparisons of Calculating Velocities between with and without Waves. Case a: $Q_0 = 0.0056 m^3/s$, T = 0.87 sec.; $H_0 = 0.97$ cm. —— with Waves; - - - no Waves

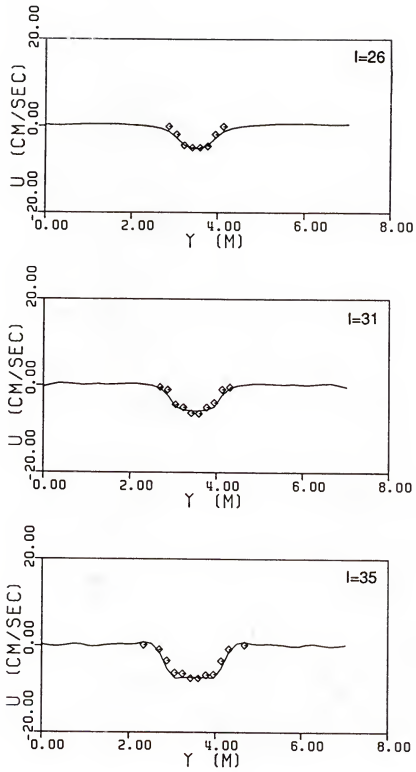

Figure 5.15: Variation of x-Component Velocity. Case b: $Q_0 = 0.0056 m^3/s$; T = 1.16 sec.; $H_0 = 0.88$ cm. —— Numerical Model; ◇ Measured Data

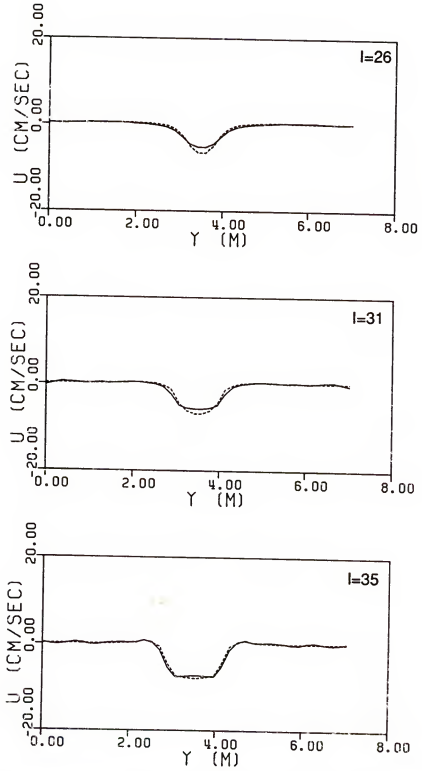

Figure 5.16: Comparisons of Calculating Velocities between with and without Waves. Case b: $Q_0 = 0.0056 m^3/s$, T = 1.16 sec.; $H_0 = 0.88$ cm. —— with Waves; - - - no Waves

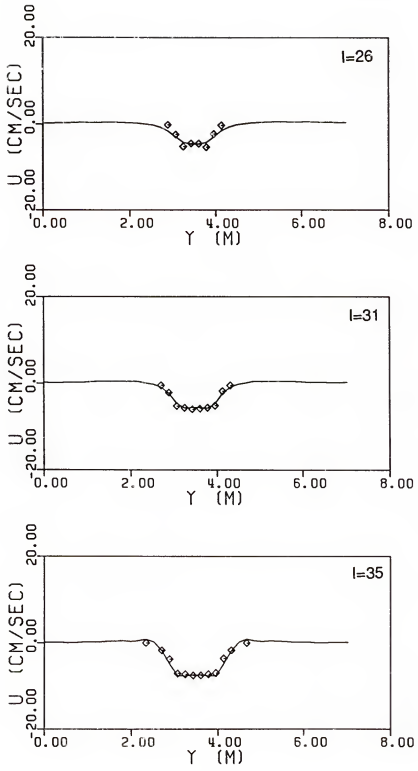

Figure 5.17: Variation of x-Component Velocity. Case c: $Q_0 = 0.0056 m^3/s$; T = 1.36 sec.; $H_0 = 0.97$ cm. —— Numerical Model; ◇ Measured Data

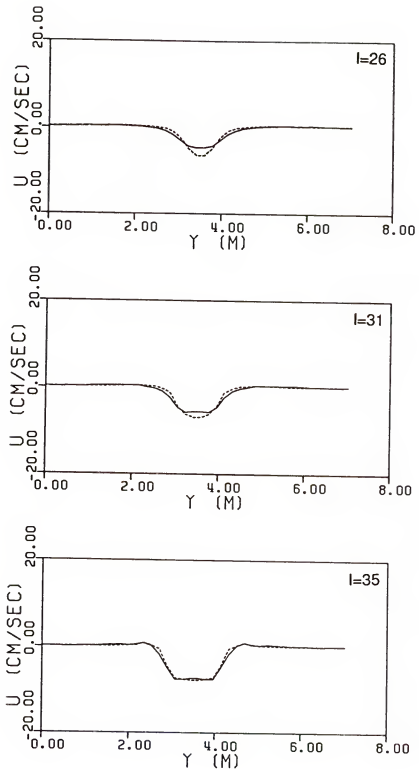

Figure 5.18: Comparisons of Calculating Velocities between with and without Waves. Case c: $Q_0 = 0.0056 m^3/s$, T = 1.36 sec.; $H_0 = 0.97$ cm. —— with Waves; - - - no Waves

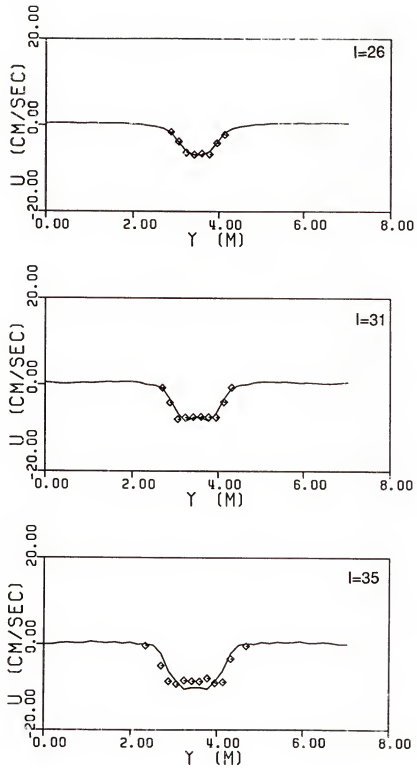

Figure 5.19. Variation of x-Component Velocity Case d: $Q_0 = 0.0076 m^3/s$; T = 0.87 sec.; $H_0 = 1.23$ cm. —— Numerical Model; ◇ Measured Data

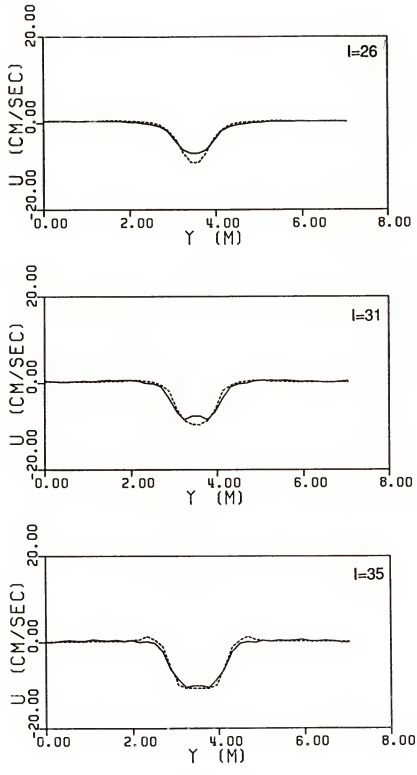

Figure 5.20: Comparisons of Calculating Velocities between with and without Waves. Case d: $Q_0 = 0.0076m^3/s$, T = 0.87 sec.; $H_0 = 1.23$ cm. —— with Waves; - - - no Waves

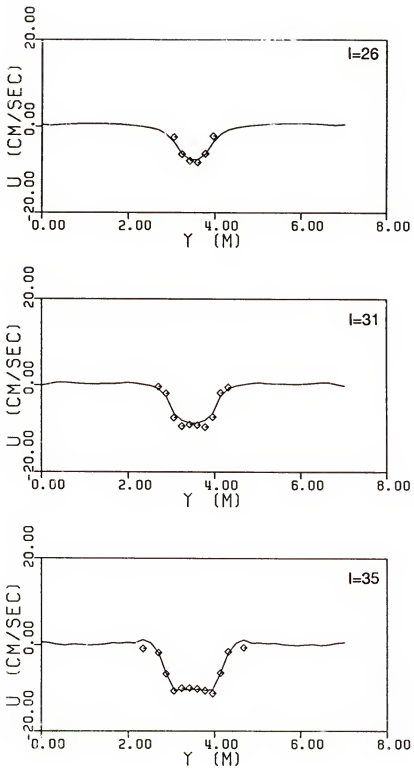

Figure 5.21: Variation of x-Component Velocity. Case e: $Q_0 = 0.0076m^3/s$; T = 1.16 sec.; $H_0 = 0.95$ cm. —— Numerical Model; ◇ Measured Data

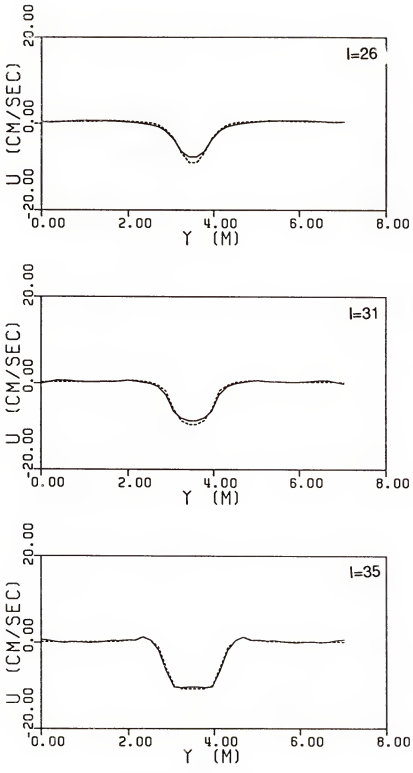

Figure 5.22: Comparisons of Calculating Velocities between with and without waves. Case e: $Q_0 = 0.0076m^3/s$, T = 1.16 sec.; $H_0 = 0.95$ cm. —— with Waves; - - - no Waves

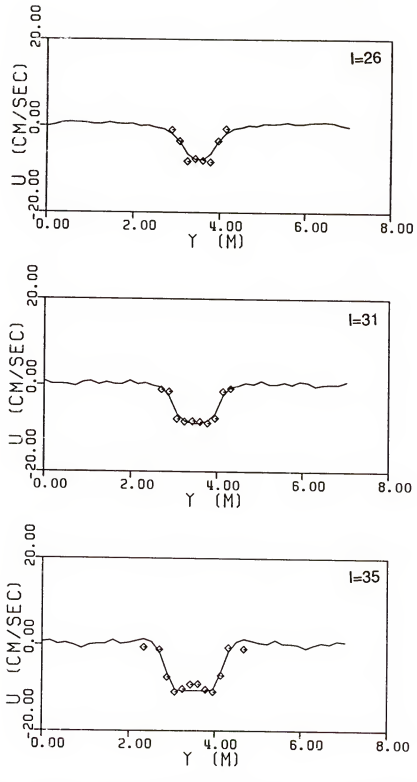

Figure 5.23: Variation of x-Component Velocity. Case f: $Q_0 = 0.0076m^3/s$; T = 1,36 sec.; $H_0 = 0.97$ cm. —— Numerical Model; ⋄ Measured Data

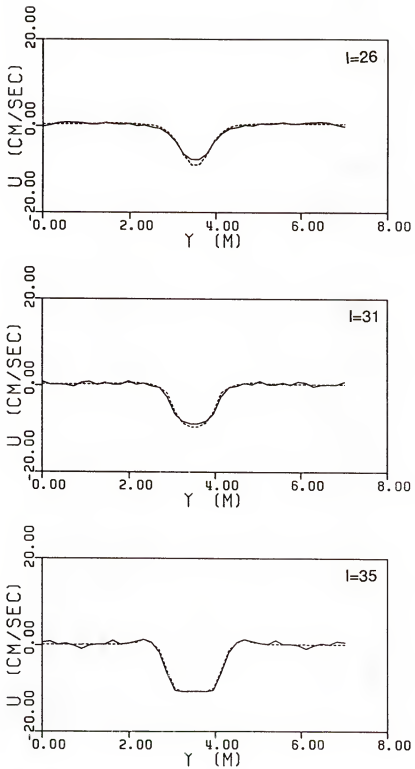

Figure 5.24: Comparisons of Calculating Velocities between with and without Waves. Case f: $Q_0 = 0.0076 m^3/s$, T = 1.36 sec.; $H_0 = 0.97$ cm. —— with Waves; - - - no Waves

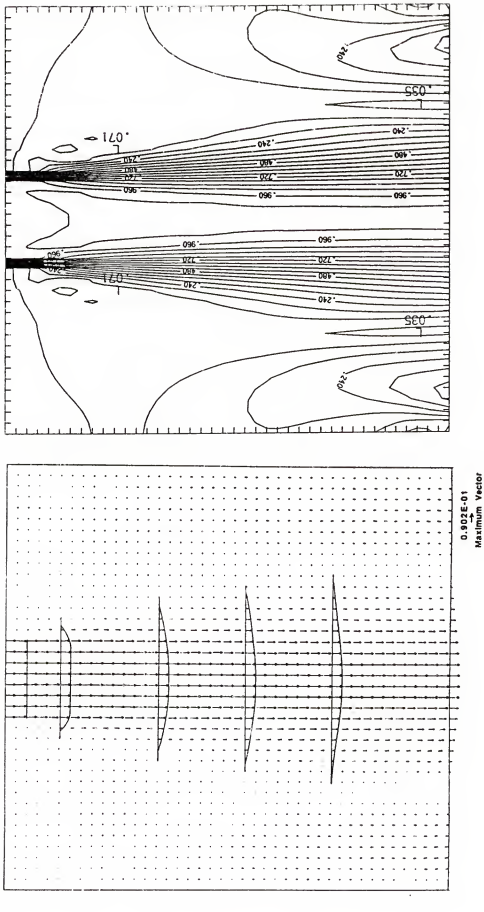

Figure 5.25: Velocity Field and Contour Lines in Flat Bottom. f = 0

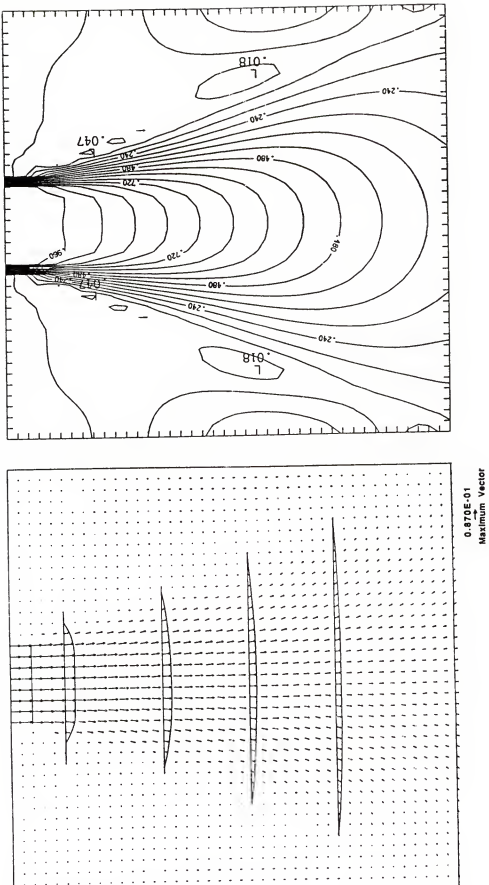

Figure 5.26: Velocity Field and Contour Lines in Flat Bottom. f = 0.01

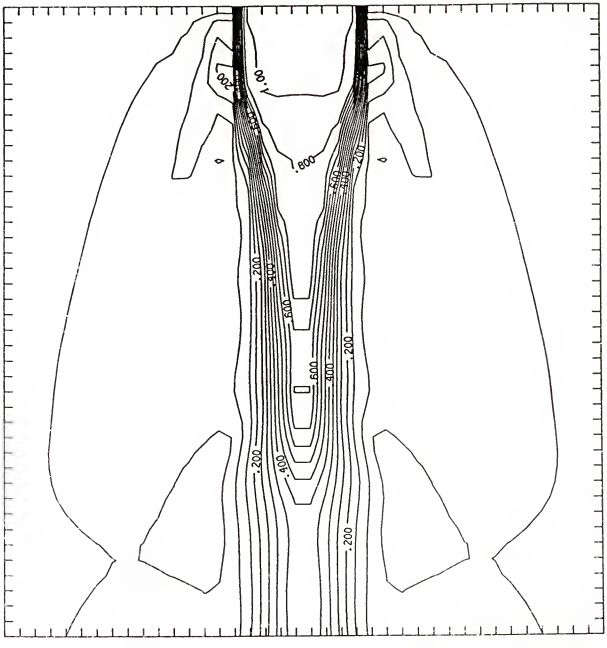

Figure 5.27: Contour Plot of Velocity. Case i. $Q_0 = 0.0056 m^3/s$ (no waves)

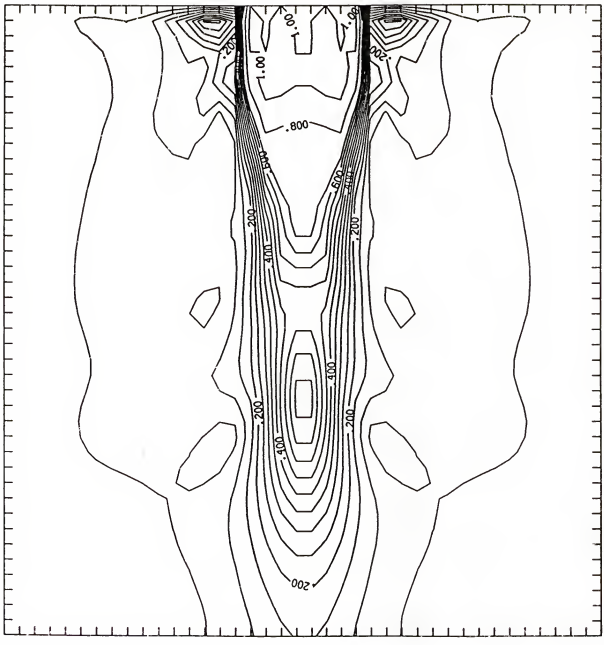

Figure 5.28: Contour Plot of Velocity. Case a: $Q_0 = 0.0056 m^3/s$; T = 0.87; $H_0 = 0.97$ cm

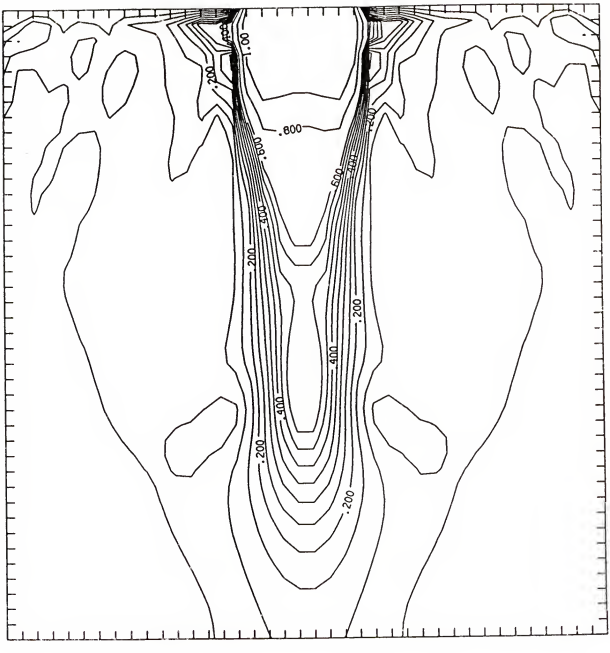

Figure 5.29: Contour Plot of Velocity. Case b: $Q_0 = 0.0056 m^3/s$; T = 1.16; $H_0 = 0.88$ cm

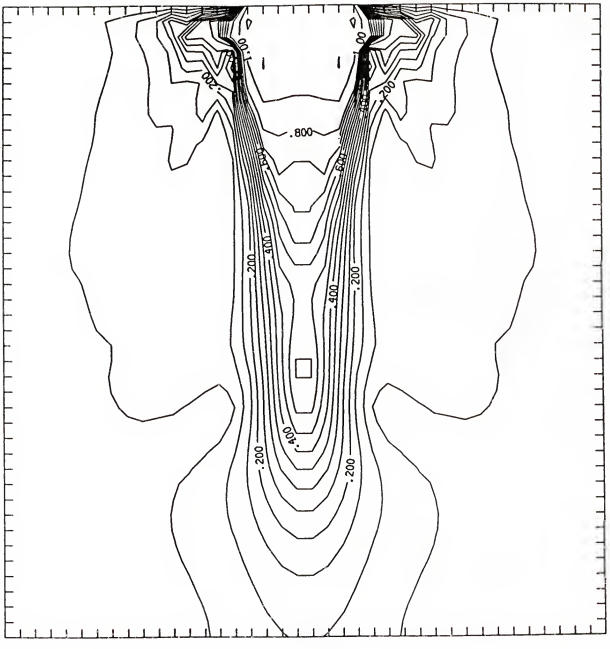

Figure 5.30: Contour Plot of Velocity. Case c: $Q_0 = 0.0056 m^3/s$; T = 1.36; $H_0 = 0.97$ cm

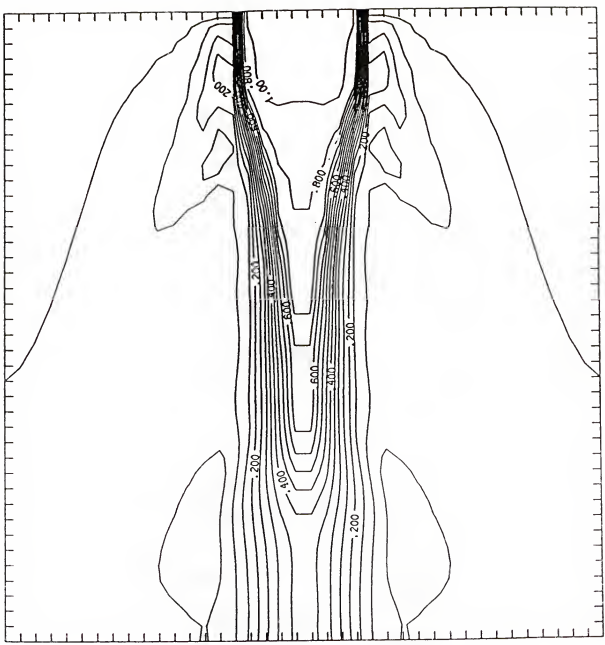

Figure 5.31: Contour Plot of Velocity. Case ii: $Q_0 = 0.0076m^3/s$ (no waves)

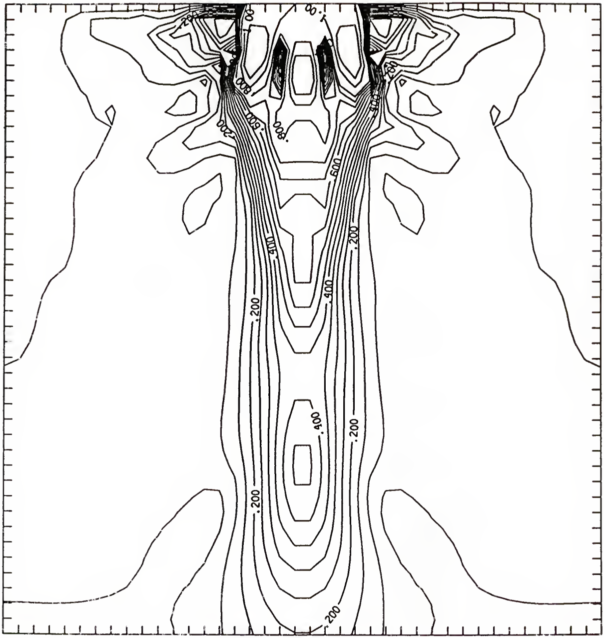

Figure 5.32: Contour Plot of Velocity. Case d: $Q_0 = 0.0076 m^3/s$; T = 0.87; H_0 = 1.23 cm

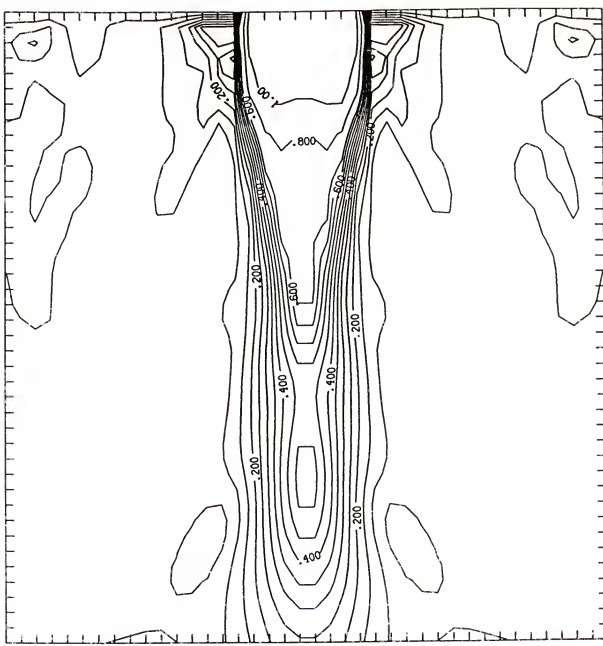

Figure 5.33: Contour Plot of Velocity. Case e: $Q_0 = 0.0076 m^3/s$; T = 1 16; H_0 = 0.95 cm

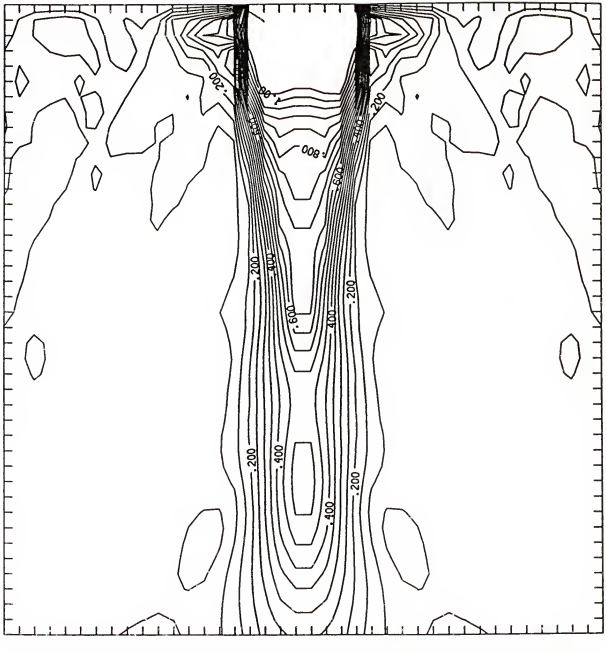

Figure 5.34: Contour Plot of Velocity. Case f: $Q_0 = 0.0076m^3/s$; T = 1.36; $H_0 = 0.97$ cm

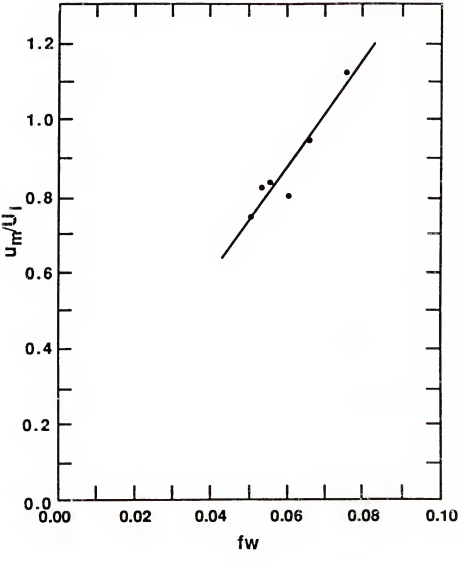

Figure 5.35: Bottom Friction Coefficients f as Function of u_m/U_i

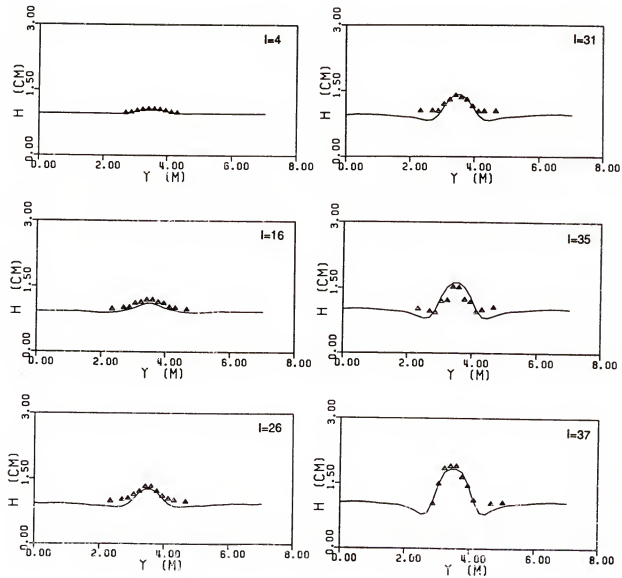

Figure 5.36: Wave Amplitude Variations. Case a: $Q_0 = 0.0056 m^3/s$; T = 0.87 sec.; H_0 = 0.97 cm. —— Numerical Model; △ Data

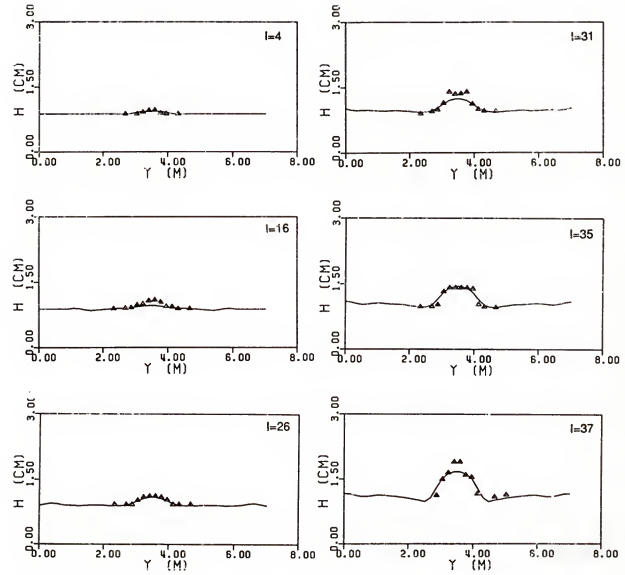

Figure 5.37: Wave Amplitude Variations. Case b: $Q_0 = 0.0056m^3/s$; T = 1.16 sec., H_0 = 0.88 cm. —— Numerical Model; $\triangle$ Data

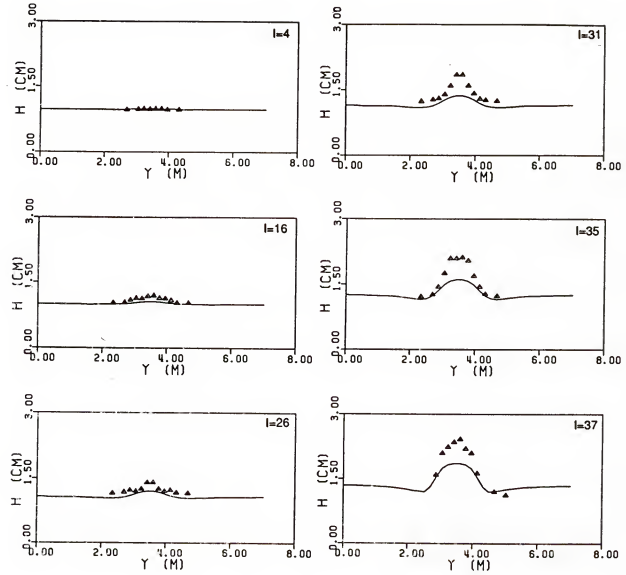

Figure 5.38: Wave Amplitude Variations. Case c: $Q_0 = 0.0056m^3/s$; T = 1.36 sec.; H_0 = 0.97 cm. —— Numerical Model; Δ Data

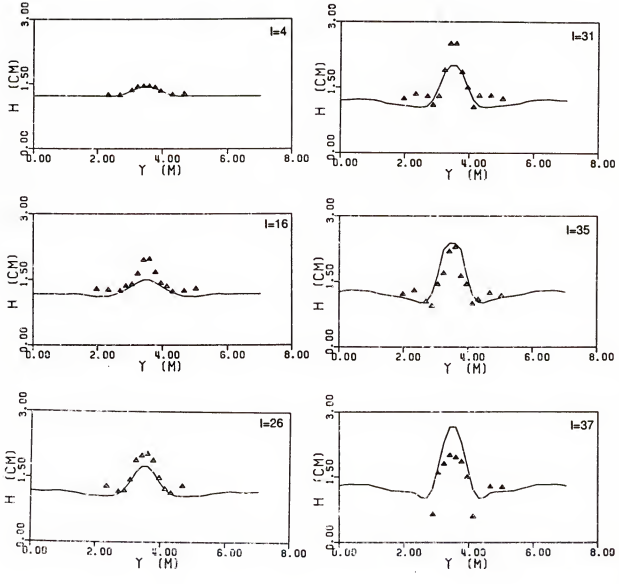

Figure 5.39: Wave Amplitude Variations. Case d: $Q_0 = 0.0076 m^3/s$; T = 0.87 sec.; H_0 = 1.23 cm. —— Numerical Model; Δ Data

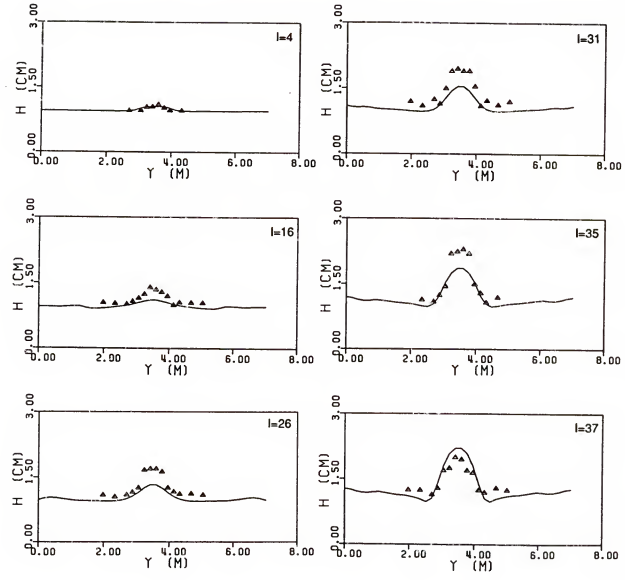

Figure 5.40: Wave Amplitude Variations. Case e: $Q_0 = 0.0076m^3/s$; T = 1.16 sec.; H_0 = 0.95 cm. —— Numerical Model; Δ Data

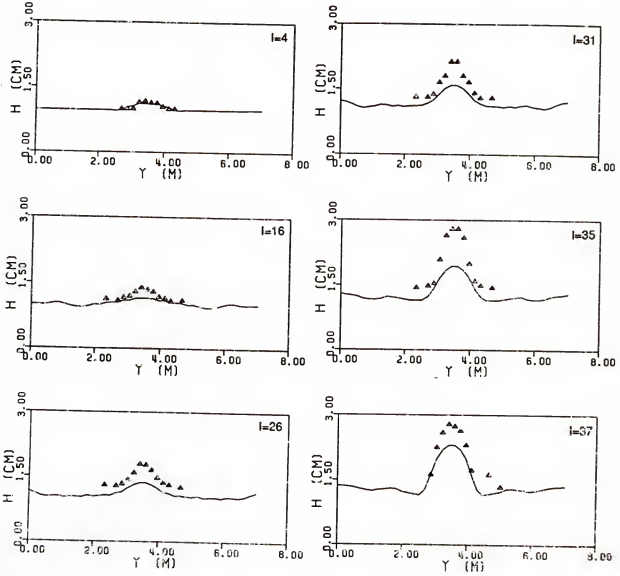

Figure 5.41: Wave Amplitude Variations. Case f: $Q_0 = 0.0076m^3/s$; T = 1.36 sec.; H_0 = 0.97 cm. —— Numerical Model; Δ Data

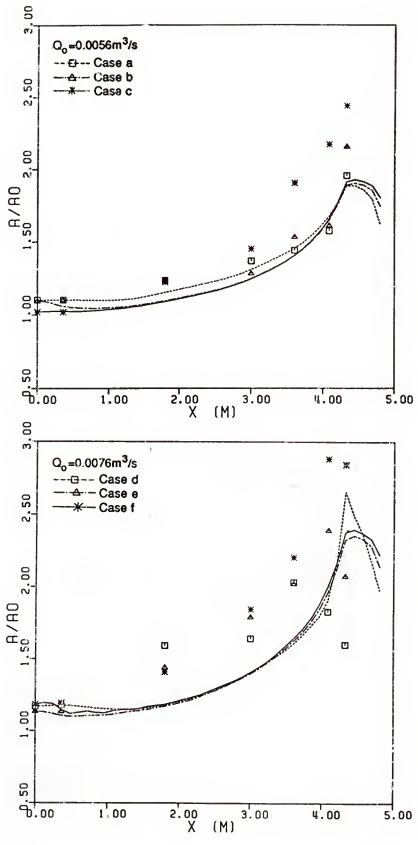

Figure 5.42: Wave Amplitude Variations along Centerline

CHAPTER 6
CONCLUSIONS AND RECOMMENDATIONS

The main objective of the present study is to develop a numerical model capable of predicting the hydrodynamics in the vicinity of an ocean inlet, which is a complicated system owing to the interactions of spatially non-uniform current with waves over changing topographies. The study entails three major endeavors: theoretical formulation, numerical modeling and experimental verification.

The theoretical formulation includes the derivations of four basic equations: the depth-averaged continuity equation, two depth-averaged momentum equations and the wave equation. The derivation of the first three equations is straight forward and follows closely the procedures employed by Ebersole and Dalrymple (1979). The wave equation, on the other hand, is extremely complex and has to be dealt with care and tailored to the physical system it intended to represent.

The wave equation derived here retained the important effects of refraction, diffraction, current-wave interaction and energy dissipation. The wave reflection effect is not considered under the assumption of slowly varying topography. Two different method - variational principle and perturbation method - are used which yield identical final form of the wave equation. One primary magnitude scale, ϵ, and two auxiliary magnitude scales, μ and δ are introduced. ϵ is the commonly known Stokes wave steepness parameter; μ is a spatial scale parameter representing the relative horizontal spatial gradient over one wave length and finally, δ is a strength parameter indicating the relative strength of mean current to wave celerity. In the present model, the wave equation is subject to the following constraints:

$$\frac{\delta}{\epsilon^{-2}} = 1; \qquad \frac{\mu}{\epsilon^2} = 1$$

which imply slowly varying topography, strong mean current and small incident wave angle. The final form of the equation is consistent to $0(\epsilon^3)$ and contains all pertinent terms to that order. Therefore, consistency (or homogeneity) and completeness are the emphasis in the present derivation.

The equations form a set of nonlinear partial differential equations dependent upon time and space. The numerical method developed to solve these equations is based upon Crank-Nicolson finite difference scheme in a double spatial sweep form. A two time level implicit model developed by Sheng (1981) is incorporated into both the x-sweep and the y-sweep. To implement the model requires specification of the bottom friction coefficient, lateral diffusion coefficient as well as the boundary conditions of waves and current.

Performance of the model is evaluated against existing numerical models including cases of wave set-up on a plane beach, longshore current distributions due to an oblique waves on a plane beach, wave-induced nearshore circulation over an irregular topography and wave diffraction over a circular shoal. Examples are also given to demonstrate the model's capability of providing nearshore current and wave interaction for an inlet-beach system, which is the ultimate goal of this study.

Finally, laboratory experiments were conducted to calibrate and verify the numerical model and to evaluate the two empirical coefficients - bottom friction and lateral diffusion - required as input to the model. The laboratory conditions are intended to represent the typical coastal inlets along the eastern seaboard of the United States. Owing to the limitation of the facility, only a limited range of inlet current strength and wave conditions were tested. By adjusting diffusion and friction coefficients, the numerical model could duplicate the current profiles satisfactorily. However, the model invariably underpredicts the wave shoaling against current. This is partially due to the inherent weakness of the governing wave equation and partially due to the inadequate breaking criterion. The lateral diffusion coefficient and the bottom friction coefficient so evaluated by force fitting the current profiles are found to be reasonable and their variations can be explained on plausible physical

reasoning. Both physical and numerical models reveal that, in the range of commonly encountered inlet conditions, the effects of current on waves are much more pronounced than the other way around. In the physical model, wave amplification as high as threefold is observed while numerical prediction also yields values more than doubling the incident wave heights. Topography is still the dominant factor governing the current pattern. The effects of bottom friction appear to be more pronounced than the lateral diffusion in retarding the inlet flow and causing wide spreading of the jet.

The numerical model developed here should prove to be a useful tool for better understanding of inlet dynamics and as a basis to develop a sediment transport model. The emphasis on the inclusion of wave diffraction effects necessitates compromising on wave shoaling prediction as well as imposing stricter restrictions on the incoming wave angle. Although the limit on mild slope criterion cannot be clearly established, it is believed that the model is able to accommodate common prototype nearshore topographies without numerical errors.

Although the numerical model seems to yield sensible results, the verification is inadequate and incomplete for two reasons: most of existing numerical models used as bench mark here are themselves not adequately verified and the physical model experiments conducted in this study are too restricted due to facility and instrument limitations.

It is recommended here that the first and foremost task is to expand the laboratory experiments to verify the numerical model with particular emphasis on current measurements. Field data on current in the vicinity of inlet should also prove to be invaluable as we now have the preliminary tool to interpret them.

APPENDIX A
WAVE EQUATION DERIVED BY USING PERTURBATION METHOD

Appendix A gives a derivation of the wave equation based on perturbation method. It follows Chu and Mei (1970), but under the consideration of strong current. On the other hand, instead of unsteady time scale, steady time scale is considered, it means that no slow derivative is related to time.

Governing equations read

$$\nabla^2\phi = 0 \qquad -h_0 \le z \le \eta$$

$$\phi_z = \eta_t + \nabla_h\phi \cdot \nabla_h\eta \qquad z = \eta$$

$$\phi_t + g\eta + \tfrac{1}{2} \mid \nabla\phi \mid^2 = 0 \qquad z = \eta$$

$$\phi_z + \nabla_h\phi \cdot \nabla_h h_0 = 0 \qquad z = -h$$

where

$$\phi = \phi_c + \phi',$$

$$\eta = \eta_0 + \eta'$$

and ϕ_c and η_0 represent current alone, ϕ' and η' are wave quantities which have the order $\le 0(\epsilon)$, h_0 is still water depth. ∇ and ∇_h are again the three dimensional and horizontal gradient operators, respectively. As in chapter 2, introduce a shifting coordinate about z axis, which define as

$$z' = z - \eta_0$$

$$z + h_0 = z' + h'$$

$$\frac{\partial}{\partial z} = \frac{\partial}{\partial z'}$$

Dropping the primes on z and h for convience, governing equations are replaced by

$$\nabla^2\phi = 0 \qquad -h_0 \le z \le \eta' \tag{A.1}$$

$$\phi_z = \eta'_t + \nabla_h\phi\cdot\nabla_h\eta' + \nabla_h\phi\cdot\nabla_h\eta_0 \qquad z=\eta' \tag{A.2}$$

$$\phi_t + g(\eta_0+\eta') + \tfrac{1}{2}\mid\nabla\phi_c\mid^2 + \tfrac{1}{2}\mid\nabla\phi\mid_*^2 = 0 \qquad z=\eta' \tag{A.3}$$

$$\phi_z + \nabla_h\phi\cdot\nabla_h h = 0 \qquad z=-h \tag{A.4}$$

in which

$$\mid\nabla\phi\mid_*^2 + \mid\nabla\phi_c\mid^2 = \mid\nabla\phi\mid^2$$

$$\mid\nabla\phi\mid_*^2 = \mid\nabla\phi'\mid^2 + 2\nabla\phi'\cdot\nabla\phi_c$$

$\nabla_h\phi_c(x,y)$ and $\eta_0(x,y)$ are $0(1)$ under strong current assumption as did in chapter 2.

$$\nabla_h\phi_c = U\hat{i} + V\hat{j}$$

From the kinetic free surface boundary condition $z' = z - \eta_0$ we get

$$\mathbf{u}\cdot\nabla_h\,\eta_0 = 0 \qquad \text{from (A.2)}$$

Collecting $0(1)$ terms in (A.3) gives

$$\eta_0 = -\frac{1}{2g}\mid\nabla_h\phi_c\mid^2 \tag{A.5}$$

which is same as (2.64) in chapter 2; finally the governing equations for wave motion are given by

$$\nabla^2\phi = 0 \qquad -h_0 \le z \le \eta' \tag{A.6}$$

$$g\phi_z + \phi_{tt} + (\frac{\partial}{\partial t} + \tfrac{1}{2}\nabla\phi\cdot\nabla)\mid\nabla\phi\mid_*^2 = 0 \qquad z=\eta' \tag{A.7}$$

$$\phi_t + g\eta' + \tfrac{1}{2}\mid\nabla\phi\mid_*^2 = 0 \qquad z=\eta' \tag{A.8}$$

$$\phi_z + \nabla_h\phi\cdot\nabla_h h = 0 \qquad z=-h \tag{A.9}$$

in which we have substituted (A.3) into (A.2) to make (A.7) only contains function ϕ. Introducing a slowly varying coordinates, i.e.

$$x = x + \mu x = X + X_2$$

$$y = \mu^{1/2}y + \mu y = Y_1 + Y_2$$

where μ is slowly changing parameter, $\mu = \epsilon^2$ as defined in chapter 2, so that

$$\frac{\partial}{\partial x} = \frac{\partial}{\partial X} + \epsilon^2 \frac{\partial}{\partial X_2}$$
$$\frac{\partial}{\partial y} = \epsilon \frac{\partial}{\partial Y_1} + \epsilon^2 \frac{\partial}{\partial Y_2}$$

Assuming that ϕ and η have the forms

$$\phi = \epsilon^{-2}\phi_c(X_2, Y_2) + \sum_{n=1}^{3}\sum_{m=-n}^{n} \epsilon^n \phi^{(n,m)}(Y_1, Y_2, X_2, z)e^{im\psi} \tag{A.10}$$

$$\eta = \eta_0(X_2, Y_2) + \sum_{n=1}^{3}\sum_{m=-n}^{n} \epsilon^n \eta^{(n,m)}(Y_1, Y_2, X_2, z)e^{im\psi} \tag{A.11}$$

where ψ is phase function which is defined under assumption that waves mainly propagate in x-direction and let complex amplitude absorbs the different between real phase and imaginal main phase. In supercripts n is the orders of magnitudes and m is the harmonics, m can not be great than n.

$$\psi = \int^x k_1 dx - \omega t$$
$$k_1 = k\cos\theta$$
$$k_2 = k\sin\theta$$

We have assumed that incident wave angle is small, therefore

$$k^2 = k_1^2 + k_2^2 = k_1^2 + 0(\epsilon^2)$$

Substituting (A.10) and (A.11) into (A.6) through (A.9), after taking Tailor series about $z = 0$, we orginize equations as

$$(\frac{\partial}{\partial z^2} - m^2 k_1^2)\phi^{(n,m)} = F^{(n,m)} \qquad -h \le z \le 0 \tag{A.12}$$

$$\phi_z^{(n,m)} = B^{(n,m)} \qquad z = -h \tag{A.13}$$

$$(g\frac{\partial}{\partial z} - m^2\omega^2)\phi^{(n,m)} = G^{(n,m)} \qquad z = 0 \tag{A.14}$$

$$\eta^{(n,m)} = H^{(n,m)} \qquad z = 0 \tag{A.15}$$

The $F^{(n,m)}$, $B^{(n,m)}$, $G^{(n,m)}$ and $H^{(n,m)}$ are given as follows. It is noted of that $|\nabla_h\phi_c|^2$ is removed from $|\nabla\phi|_*^2$.

(a) $G^{(n,m)}$

Define $f^{(n,m)} = [|\nabla\phi|_*^2]^{(n,m)}$

$$\begin{aligned}\nabla\phi &= \phi_{cX_2}\hat{i} + \phi_{cY_2}\hat{j} + \sum_n\sum_m \epsilon^n\{[imk_1\phi^{(n,m)} + \epsilon^2\phi_{X_2}^{(n,m)}]\hat{i} + [\epsilon\phi_{Y_1}^{(n,m)} \\ &\quad + \epsilon^2\phi_{Y_2}^{(n,m)}]\hat{j} + \phi_z^{(n,m)}\hat{k}\}e^{im\psi}\end{aligned}$$

$$\begin{aligned}f^{(n,m)} &= -\delta m_1m_2k_1^2\phi^{(n_1,m_1)}\phi^{(n_2,m_2)} + 2imk_1\phi_{cX_2}\phi^{(n,m)} + 2\phi_{cX_2}\phi_{X_2}^{(n-2,m)} \\ &\quad + 2im_1k_1\phi^{(n_1,m_1)}\phi_{X_2}^{(n_2-2,m_2)} + \delta\phi_{X_2}^{(n_1-2,m_1)}\phi_{X_2}^{(n_2-2,m_2)} + 2\phi_{cY_2} \\ &\quad \phi_{Y_1}^{(n-1,m)} + \delta\phi_{Y_1}^{(n_1-1,m_1)}\phi_{Y_1}^{(n_2-1,m_2)} + 2\phi_{cY_2}\phi_{Y_2}^{(n-2,m)} + 2\phi_{Y_1}^{(n_1-1,m_1)} \\ &\quad \phi_{Y_2}^{(n_2-2,m_2)} + \delta\phi_{Y_2}^{(n_1-2,m_1)}\phi_{Y_2}^{(n_2-2,m_2)} + \delta\phi_z^{(n_1,m_1)}\phi_z^{(n_2,m_2)}\end{aligned}$$

where δ is defined as

$$\delta = \begin{cases} 1 & n_1 - k_1 = n_2 - k_2;\ \ m_1 = m_2 \\ 2 & \text{otherwise} \end{cases}$$

where $(n_1 - k_1) + (n_2 - k_2) = n$ and $m_1 + m_2 = m$ in which $k_i = 0, 1, 2$.

The common term ϵ^n in $f^{(n,m)}$ has been dropped. Writing in details, we have

$$\begin{aligned}f^{(0,0)} &= 0 \\ f^{(1,0)} &= 0 \\ f^{(1,1)} &= 2ik_1\phi_{cX_2}\phi^{(1,1)} \\ f^{(1,-1)} &= -2ik_1\phi_{cX_2}\phi^{(1,-1)} \\ f^{(2,0)} &= 2k_1^2\phi^{(1,1)}\phi^{(1,-1)} + 2\phi_z^{(1,1)}\phi_z^{(1,-1)} + \phi_z^{(1,0)}\phi_z^{(1,0)} + 2\phi_{cY_2}\phi_{Y_1}^{(1,0)} \\ f^{(2,1)} &= 2\phi_z^{(1,1)}\phi_z^{(1,0)} + 2ik_1\phi_{cX_2}\phi^{(2,1)} + 2\phi_{cY_2}\phi_{Y_1}^{(1,1)} \\ f^{(2,2)} &= -k_1^2\phi^{(1,1)}\phi^{(1,1)} + \phi_z^{(1,1)}\phi_z^{(1,1)} + 4ik_1\phi_{cX_2}\phi^{(2,2)} \\ f^{(3,1)} &= 4k_1^2\phi^{(2,2)}\phi^{(1,-1)} + 2\phi_z^{(2,2)}\phi_z^{(1,-1)} + 2\phi_z^{(2,0)}\phi_z^{(1,1)} + 2\phi_z^{(2,1)}\phi_z^{(1,0)} \\ &\quad + 2ik_1\phi_{cX_2}\phi^{(3,1)} + 2\phi_{cX_2}\phi_{X_2}^{(1,1)} + 2\phi_{cY_2}\phi_{Y_1}^{(2,1)} + 2\phi_{cY_2}\phi_{Y_2}^{(1,1)}\end{aligned}$$

Next define

$$Q^{(n,m)} = \{[\frac{\partial}{\partial t} + \frac{1}{2}(\phi_x \frac{\partial}{\partial x} + \phi_y \frac{\partial}{\partial y} + \phi_z \frac{\partial}{\partial z})] \mid \nabla\phi \mid_*^2\}^{(n,m)}$$

Expanded as

$$\begin{aligned} Q^{(n,m)} &= -im\omega f^{(n,m)} + \frac{1}{2}\phi_{cX_2}[ik_1 m f^{(n,m)} + f_{X_2}^{(n-2,m)}] + \frac{1}{2}\phi_{cY_2}[f_{Y_1}^{(n-1,m)} \\ &\quad + f_{Y_2}^{(n-2,m)}] - \frac{1}{2}k_1^2 m_1 m_2 \phi^{(n_1,m_1)} f^{(n_2,m_2)} + \frac{1}{2}\phi_{Y_1}^{(n_1-1,m_1)} f_{Y_1}^{(n_2-1,m_2)} \\ &\quad + \frac{1}{2}ik_1 m_1 \phi^{(n_1,m_1)} f_{X_2}^{(n_2-2,m_2)} + \frac{1}{2}\phi_z^{(n_1,m_1)} f_z^{(n_2,m_2)} + \frac{1}{2}ik_1 m_2 \\ &\quad \phi_{X_2}^{(n_1-2,m_1)} f^{(n_2,m_2)} + [\dots]^{(n-3,m)} \end{aligned}$$

Term by term, yield

$$\begin{aligned} Q^{(0,0)} &= 0 \\ Q^{(1,0)} &= 0 \\ Q^{(1,1)} &= -i\omega f^{(1,1)} + \frac{1}{2}\phi_{cX_2} ik_1 f^{(1,1)} \\ Q^{(1,-1)} &= i\omega f^{(1,-1)} - \frac{1}{2}\phi_{cX_2} ik_1 f^{(1,-1)} \\ Q^{(2,0)} &= \frac{1}{2}\phi_z^{(1,-1)} f_z^{(1,1)} + \frac{1}{2}\phi_z^{(1,1)} f_z^{(1,-1)} + \frac{1}{2}k_1^2[\phi^{(1,1)} f^{(1,-1)} + \phi^{(1,-1)} f^{(1,1)}] \\ Q^{(2,1)} &= -i\omega f^{(2,1)} + \frac{1}{2}ik_1\phi_{cX_2} f^{(2,1)} + \frac{1}{2}\phi_{cY_2} f_{Y_1}^{(1,1)} + \frac{1}{2}\phi_z^{(1,0)} f_z^{(1,1)} \\ Q^{(2,2)} &= -2i\omega f^{(2,2)} + ik_1\phi_{cX_2} f^{(2,2)} - \frac{1}{2}k_1^2\phi^{(1,1)} f^{(1,1)} + \frac{1}{2}\phi_z^{(1,1)}\phi_z^{(1,1)} \\ Q^{(3,1)} &= -i\omega f^{(3,1)} + \frac{1}{2}ik_1\phi_{cX_2} f^{(3,1)} + \frac{1}{2}\phi_{cX_2} f_{Y_2}^{(1,1)} + \frac{1}{2}\phi_{cY_2} f_{Y_1}^{(2,1)} \\ &\quad + \frac{1}{2}\phi_{cY_2} f_{Y_2}^{(1,1)} + k_1^2[\phi^{(1,-1)} f^{(2,2)} + \phi^{(2,2)} f^{(1,-1)}] + \frac{1}{2}[\phi_z^{(1,1)} f_z^{(2,0)} \\ &\quad + \phi_z^{(1,0)} f_z^{(2,1)} + \phi_z^{(1,-1)} f_z^{(2,2)} + \phi_z^{(2,2)} f_z^{(1,-1)} + \phi_z^{(2,0)} f_z^{(1,1)}] \end{aligned}$$

Finally, expanding $Q^{(n,m)}$ in Tailor series about $z = 0$, we obtain

$$G^{(n,m)} = -Q^{(n,m)} - [\eta'(\phi_{tt} + g\phi_z + Q)_z]^{(n,m)} - \frac{1}{2}[\eta'^2(\phi_{tt} + g\phi_z + Q)_{zz}]^{(n,m)} + \cdots$$

Writing in detail, we have

$$\begin{aligned} G^{(n,m)} &= -Q^{(n,m)} - \eta^{(1,m_1)}[-m_2^2\omega^2\phi + g\phi_z + Q]_z^{(n_2-1,m_2)} - \eta^{(2,m_1)}[-m_2^2\omega^2\phi \\ &\quad + g\phi_z + Q]_z^{(n_2-2,m_2)} - \varsigma^{(2,m_1)}[-m_2^2\omega^2\phi + g\phi_z + Q]_{zz}^{(n_2-2,m_2)} + \cdots \end{aligned}$$

where

$$\varsigma^{(n,m)} = \frac{1}{2}\eta^{(n_1,m_1)}\eta^{(n_2,m_2)}$$

The expansions of $\varsigma^{(n,m)}$ are as follows:

$$\varsigma^{(2,0)} = \frac{1}{2}\eta^{(1,0)}\eta^{(1,0)} + \eta^{(1,1)}\eta^{(1,-1)}$$

$$\varsigma^{(2,1)} = \eta^{(1,0)}\eta^{(1,1)}$$

$$\varsigma^{(2,-1)} = \eta^{(1,-1)}\eta^{(1,0)}$$

$$\varsigma^{(2,2)} = \frac{1}{2}\eta^{(1,1)}\eta^{(1,1)}$$

The formations of $G^{(n,m)}$ are given as follows:

$$\begin{aligned}
G^{(0,0)} &= 0 \\
G^{(1,0)} &= 0 \\
G^{(1,1)} &= -Q^{(1,1)} \\
G^{(1,-1)} &= -Q^{(1,-1)} \\
G^{(2,0)} &= -Q(2,0) - \eta^{(1,0)}[\,g\phi_x + Q\,]_x^{[1,0)} - \eta^{(1,-1)}[\,-\omega^2\phi + g\phi_x + Q\,]_x^{(1,1]} \\
&\quad -\eta^{(1,1)}[\,-\omega^2\phi + g\phi_x + Q\,]_x^{(1,-1)} \\
G^{(2,1)} &= -Q^{(2,1)} - \eta^{(1,1)}g\phi_{xx}^{(1,0)} - \eta^{(1,0)}[\,-\omega^2\phi + g\phi_x + Q\,]_x^{(1,1]} \\
G^{(2,2)} &= -Q^{(2,2)} - \eta^{(1,1)}[\,-\omega^2\phi + g\phi_x + Q\,]_x^{(1,1]} \\
G^{(3,1)} &= -Q^{(3,1)} - \eta^{(1,0)}[\,-\omega^2\phi + g\phi_x + Q\,]_x^{(2,1]} - \eta^{(1,1)}[\,g\phi_x + Q\,]_x^{[2,0)} - \eta^{(1,-1)} \\
&\quad [\,-4\omega^2\phi + g\phi_x + Q\,]_x^{(2,2]} - \eta^{(2,1)}g\phi_{xx}^{(1,0)} - \eta^{(2,2)}[\,-\omega^2\phi + g\phi_x + Q\,]_x^{(1,-1)} \\
&\quad -\eta^{(2,0)}[\,-\omega^2\phi + g\phi_x + Q\,]_x^{(1,1]} - \varsigma^{(2,0)}[\,-\omega^2\phi + g\phi_x + Q\,]_{xx}^{(1,1]} \\
&\quad -\varsigma^{(2,1)}g\phi_{xxx}^{[1,0)} - \varsigma^{(2,2)}[\,-\omega^2\phi + g\phi_x + Q\,]_x^{(1,-1)}
\end{aligned}$$

(b) $B^{(n,m)}$

$$\begin{aligned}
B^{(n,m)} &= -[\,\nabla_h\phi\cdot\nabla_h h\,]^{(n,m)} \\
&= -[\,\phi_{cX_2}h_{X_2} + \phi_{cY_2}\,]^{(2,0)} - imk_1h_{X_2}\phi^{(n-2,m)} - h_{Y_2}\phi_{Y_1}^{(n-3,m)}
\end{aligned}$$

Thus

$$B^{(1,0)} = B^{(1,1)} = B^{(1,-1)} = 0$$

$$B^{(2,0)} = -\nabla_h h \cdot \nabla_h \phi_c$$

$$B^{(2,1)} = B^{(2,2)} = 0$$

$$B^{(3,1)} = -imk_1 h_{X_2} \phi^{(1,1)} \quad \text{for slip bottom boundary condition}$$

or

$$B^{(3,1)} = -(1+i)\sqrt{\frac{\nu}{2\omega}} \nabla_h{}^2 \phi^{(1,1)} + \nabla_h \phi^{(1,1)} \cdot \nabla_h h \quad \text{for non-slip bottom}$$

boundary condition

The non-slip bottom boundary condition is given in Appendix B after following Liu (1986).

(c) $F^{(n,m)}$

$$F^{(n,m)} = -\nabla_h{}^2 \phi_c^{(2,0)} - [\, imk_{1X_2}\phi + 2imk_1\phi_{X_2} + \phi_{Y_1Y_1}\,]^{(n-1,m)} - [\cdots]^{(n-3,m)}$$

Writing in detail, yield

$$F^{(1,1)} = F^{(1,-1)} = 0$$

$$F^{(2,0)} = -\nabla_h{}^2 \phi_c$$

$$F^{(2,1)} = F^{(2,2)} = 0$$

$$F^{(3,1)} = -[\, ik_{1X_2}\phi + 2ik_1\phi_{X_2} + \phi_{Y_1Y_1}\,]^{(1,1)}$$

(d) $H^{(n,m)}$

$$H^{(n,m)} = -\frac{1}{g}[\, \phi_t + \frac{1}{2} \mid \nabla\phi \mid_*^2 \,]^{(n,m)}$$

Expanding above equation in Tailor series about $z = 0$, we obtain

$$\begin{aligned} H^{(n,m)} \;=\; & \frac{1}{g}[\, im\omega\phi - \frac{1}{2} f\,]^{(n,m)} + \frac{1}{g}\eta^{(1,m_1)}[\, im_2\omega\phi - \frac{1}{2} f\,]_z^{(n_2-1,m_2)} + \frac{1}{g}\eta^{(2,m_1)} \\ & [\, im_2\omega\phi - \frac{1}{2} f\,]_z^{(n_2-2,m_2)} + \frac{1}{g}\zeta^{(2,m_1)}[\, im_2\omega\phi - \frac{1}{2} f\,]_{zz}^{(n_2-2,m_2)} + \cdots \end{aligned}$$

Therefore

$$H^{(1,0)} = 0$$

$$H^{(1,1)} = \frac{1}{g}[\,i\omega\phi - \frac{1}{2}f\,]^{(1,1)}$$

$$H^{(1,-1)} = -\frac{1}{g}[\,i\omega\phi + \frac{1}{2}f\,]^{(1,-1)}$$

$$H^{(2,0)} = -\frac{1}{2g}f^{(2,0)} - \frac{1}{g}\eta^{(1,1)}[\,i\omega\phi + \frac{1}{2}f\,]_z^{(1,-1)} + \frac{1}{g}\eta^{(1,-1)}[\,i\omega\phi - \frac{1}{2}f\,]_z^{(1,1)}$$

$$H^{(2,1)} = \frac{1}{g}[\,i\omega\phi - \frac{1}{2}f\,]^{(2,1)} + \frac{1}{g}\eta^{(1,0)}[\,i\omega\phi - \frac{1}{2}f\,]_z^{(1,1)}$$

$$H^{(2,2)} = \frac{1}{g}[\,2i\omega\phi - \frac{1}{2}f\,]^{(2,2)} + \frac{1}{g}\eta^{(1,1)}[\,i\omega\phi - \frac{1}{2}f\,]_z^{(1,1)}$$

The solutions will be given in the form of combinations for different orders and harmonics.

(1) $n = 1, m = 0$

The governing equations are given as

$$\phi_{zz}^{(1,0)} = F^{(1,0)} = 0 \qquad -h \le z \le 0$$

$$\phi_z^{(1,0)} = B^{(1,0)} = 0 \qquad z = -h$$

$$g\phi_z^{(1,0)} = G^{(1,0)} = 0 \qquad z = 0$$

$$\eta^{(1,0)} = H^{(1,0)} = 0 \qquad z = 0$$

The solutions are simply obtained as

$$\eta^{(1,0)} = 0 \tag{A.16}$$

$$\phi_z^{(1,0)} = \phi_{zz}^{(1,0)} = 0 \tag{A.17}$$

(2) $n = 1, m = 1$

$$\phi_{zz}^{(1,1)} - k_1^2\phi^{(1,1)} = 0 \qquad -h \le z \le 0$$

$$\phi_z^{(1,1)} = 0 \qquad z = -h$$

$$g\phi_z^{(1,1)} - \omega^2\phi^{(1,1)} = -2k_1\omega\phi_{cX_2}\phi^{(1,1)} + k_1^2\phi_{cX_2}^2\phi^{(1,1)}$$

or

$$g\phi_z^{(1,1)} - (\omega - k_1\phi_{cX_2})^2\phi^{(1,1)} = 0 \qquad z = 0$$

$$\eta^{(1,1)} = \frac{i}{g}\phi^{(1,1)}[\,\omega - k_1\phi_{cX_2}\,] \qquad z = 0$$

Those give

$$\phi^{(1,1)} = -i\frac{g}{2\sigma_1}a\frac{\cosh k_1(h+z)}{\cosh k_1 h}e^{i\psi} + c.c \tag{A.18}$$

$$\eta^{(1,1)} = \frac{a}{2}e^{i\psi} + c.c \tag{A.19}$$

with the definition of the apparent dispersion relation

$$\begin{aligned}\omega &= \sqrt{gk_1\tanh k_1 h} + k_1\phi_{cX_2} \\ &= \sigma_1 + k_1\phi_{cX_2}\end{aligned}$$

in which a is a complex wave amplitude and $c.c$ is the complex conjugate; k_1 and k_2 are wave numbers in x and y direction, respectively. The linear dispersion relation discussed in chapter 2 gives

$$\begin{aligned}\omega &= \sqrt{gk\tanh kh} + k_1\phi_{cX_2} + k_2\phi_{cY_2} \\ &= \sigma + k_1\phi_{cX_2} + k_2\phi_{cY_2}\end{aligned}$$

Therefore, we have

$$\sigma_1 = \sigma + k_2\phi_{cY_2} = \sigma + 0(\epsilon)$$

By introducing the error for less than $0(\epsilon^2)$, equation (A.8) can be revised as

$$\phi^{(1,1)} = -i\frac{g}{2\sigma_1}a\frac{\cosh k(h+z)}{\cosh kh}e^{i\psi} + c.c \tag{A.20}$$

It is important to note that when we insert (A.20) back into Laplace equation, we get

$$\phi^{(1,1)}_{zz} - k_1^2\phi^{(1,1)} = (k^2 - k_1^2)\phi^{(1,1)} \sim o(\epsilon^3) \tag{A.21}$$

It entirely satisfies governing equation at order of $0(\epsilon)$, but the left hand side will be induced at the order of $0(\epsilon^3)$.

(3) $n = 1, m = -1$

$$\phi^{(1,-1)} = i\frac{g}{2\sigma_1}a\frac{\cosh k(h+z)}{\cosh kh}e^{-i\psi} + c.c \tag{A.22}$$

$$\eta^{(1,-1)} = \frac{a}{2}e^{-i\psi} + c.c \tag{A.23}$$

(4) $n = 2, m = 0$

$$\phi_{zz}^{(2,0)} = F^{(2,0)} = -\phi_{cX_2X_2} - \phi_{cY_2Y_2} \qquad -h \le z \le 0$$

$$\phi^{(2,0)} = B^{(2,0)} = -\phi_{cX_2}h_{X_2} - \phi_{cY_2}h_{Y_2} \qquad z = -h$$

$$\phi_z^{(2,0)} = G^{(2,0)} = 0 \qquad z = 0$$

$$\eta(2,0) = H^{(2,0)} = -\tfrac{1}{2g}f^{(2,0)} + \tfrac{2i}{g}\sigma_1\eta^{(1,1)}\phi_z^{(1,1)} \qquad z = 0$$

The following solvability condition must be satisfied by first above three equations:

$$\int_{-h}^{0} F^{(2,0)}dz + B^{(2,0)} = \frac{1}{g}G^{(2,0)}$$

which gives

$$\nabla_h(h\mathrm{U}) = 0 \tag{A.24}$$

or

$$h_{X_2}U_{X_2} + h_{Y_2}V_{Y_2} = 0 \tag{A.25}$$

where $\mathrm{U} = \nabla_h\phi_c$

It is continuity equation for order of $0(1)$. The last equation gives $\eta^{(2,0)}$ as

$$\eta^{(2,0)} = -\frac{|\,a\,|^2\,k}{2\sinh 2kh} + 0(\epsilon^3) \tag{A.26}$$

This is the mean water set-down related to the shifted coorinate due to radiation stresses.

(5) $n = 2, m = 1$

$$\phi^{(2,1)} - k_1^2\phi^{(2,1)} = F^{(2,1)} = 0 \qquad -h \le z \le 0$$

$$\phi_z^{(2,1)} = B^{(2,1)} = 0 \qquad z = -h$$

$$g\phi_z^{(2,1)} - \omega^2\phi^{(2,1)} = G^{(2,1)}$$

$$\text{or} \quad g\phi_z^{(2,1)} - \sigma_1^2\phi^{(2,1)} = G'^{(2,1)} = 2i\sigma_1\phi_{cY_2}\phi_{Y_1}^{(1,1)} \qquad z = 0$$

$$\eta^{(2,1)} = H^{(2,1)} = \tfrac{i\sigma_1}{g}\phi^{(2,1)} + \tfrac{1}{g}\phi_{cY_2}\phi_{Y_1}^{(1,1)} \qquad z = 0$$

in which $G'^{(2,1)}$ does not include $\phi^{(2,1)}$.

The possible solutions from above equations are $\phi^{(2,1)}$ and $\eta^{(2,1)}$ equal zeros. However, $\eta(2,1) = 0$ contradicts with that derived in chapter 2 which $\eta(2,1)$ is non-zero. But, $\eta(2,1)$ will not be involved in later calculation in this derivation, it does not affect the final formulation of wave equation.

(6) $n = 2, m = 2$

$$\phi_{zz}^{(2,2)} - 4k_1^2\phi^{(2,2)} = 0 \qquad -h \le z \le 0$$

$$\phi_z^{(2,2)} = 0 \qquad z = -h$$

$$g\phi_z^{(2,2)} - 4\omega^2\phi^{(2,2)} = G^{(2,2)} \quad \text{or}$$

$$g\phi_z^{(2,2)} - 4\sigma_1^2\phi^{(2,2)} = G'^{(2,2)} \qquad z = 0$$

$$\eta^{(2,2)} = H^{(2,2)}$$

$$= \tfrac{1}{g}[\,2i\sigma_1\phi^{(2,2)} + \tfrac{1}{2}k_1^2\phi^{(1,1)^2} - \tfrac{1}{2}\phi_z^{(1,1)^2}\,] + i\tfrac{\sigma_1}{g}\eta^{(1,1)}\phi_z^{(1,1)} \qquad z = 0$$

in which

$$G'^{(2,2)} = i(\omega+\sigma_1)[-k_1^2\phi^{(1,1)^2} + k^2\tanh^2 kh\phi^{(1,1)^2}\,] + ik_1^3\phi_{cX_2}\phi^{(1,1)^2} - ik_1\phi_{cX_2}\phi_z^{(1,1)^2}$$
$$+\omega^2\eta^{(1,1)}\phi_z^{(1,1)} - g\eta^{(1,1)}\phi_{zz}^{(1,1)} - (\omega^2 - \sigma_1^2)\eta^{(1,1)}\phi_z^{(1,1)}$$

These give results as

$$\phi^{(2,2)} = -i\frac{3\sigma\mid a\mid^2}{16}\frac{\cosh k(h+z)}{\sinh^4 kh}e^{i2\psi} + c.c + 0(\epsilon^3) \tag{A.27}$$

$$\eta(2,2) = \frac{\mid a\mid^2 k\sinh kh}{8\sinh^3 kh}(2+\cosh 2kh)e^{i2\psi} + c.c + 0(\epsilon^3) \tag{A.28}$$

exactly the same as the second order Stokes wave results.

(7) $n = 3, m = 1$

$$\phi^{(3,1)} - k_1^2\phi^{(3,1)} = F^{(3,1)} = -ik_{1X_2}\phi^{(1,1)} - 2ik_1\phi_{X_2}^{(1,1)} - \phi_{Y_1Y_1}^{(1,1)} - k_2^2\phi^{(1,1)}$$

$$-h \le z \le 0$$

$$\phi_z^{(3,1)} = B^{(3,1)} \qquad z = -h$$

$$g\phi_z^{(3,1)} - \omega^2\phi^{(3,1)} = G^{(3,1)}$$

or

$$g\phi_z^{(3,1)} - \sigma_1^2\phi^{(3,1)} = G'^{(3,1)} \qquad z = 0$$

where

$$
\begin{aligned}
G'^{(3,1)} &= -Q'^{(3,1)} - \eta^{(1,1)}[\, g\phi_{zz}^{(2,0)} + Q_z^{(2,0)}\,] - \eta^{(1,1)}[\, -4\omega^2\phi_z^{(2,2)} \\
&\quad + g\phi_{zz}^{(2,2)} + Q_z^{(2,2)}\,] - \eta^{(2,2)}[\, \omega^2\phi_z^{(1,1)} - g\phi_{zz}^{(1,1)} - Q_z^{(1,1)}\,] \\
&\quad - \eta^{(2,0)}[\, -\omega^2\phi_z^{(1,1)} + g\phi_{zz}^{(1,1)} + Q_z^{(1,1)}\,] - \varsigma^{(2,0)}[\,\cdots\,] - \varsigma^{(2,2)}[\,\cdots\,]
\end{aligned}
$$

The summations of last two brackets in $G'^{(3,1)}$ are identically equal zero.

The last term in right hand side of first equation is due to $k^2 - k_1^2 = k_2^2 = 0(\epsilon^2)$ as mentioned in case (2). $G'^{(3,1)}$ and $Q'^{(3,1)}$ are no $\phi^{(3,1)}$ term in $G^{(3,1)}$ and $Q^{(3,1)}$, respectively. Again, substituting F, B and G' into solvability condition, which is given by

$$
\int_{-h}^{0} F^{(3,1)} \frac{\cosh k(h+z)}{\cosh kh}\, dz + \frac{B^{(3,1)}}{\cosh kh} = \frac{1}{g} G'^{(3,1)} \tag{A.29}
$$

in which

$$
B(3,1) = -ik_1\phi^{(1,1)}h_{X_2} = \frac{gk_1}{2\sigma_1}\frac{1}{\cosh kh} h_{X_2} a
$$

for slip bottom boundary condition, or

$$
B^{(3,1)} = \frac{1}{2\sigma_1 \cosh kh}[\,(i-1)gk^2\sqrt{\frac{\nu}{2\omega}} - gk_1 h_{X_2}\,]a
$$

for non-slip bottom boundary condition;

$$
\begin{aligned}
&\int_{-h}^{0} F^{(3,1)} \frac{\cosh k(h+z)}{\cosh kh}\, dz = -cc_g[\,\frac{k_1 X_2}{2\sigma_1}a + \frac{k_1}{\sigma_1}a_{X_2} - \frac{k_1\sigma_1 X_2}{\sigma_1^2}a\,] \\
&-\frac{k_1}{2\sigma_1}(cc_g)_{X_2}a + \frac{gk_1}{2\sigma_1}\frac{h_{X_2}}{\cosh^2 kh}a + i\frac{cc_g}{2\sigma_1}a_{Y_1Y_1} - icc_g\frac{k_1^2 - k^2}{2\sigma_1}a
\end{aligned}
$$

and

$$
\begin{aligned}
G'^{(3,1)} &= \frac{i\sigma^3 k}{2\tanh kh} D' \mid a \mid^2 a + \frac{ig}{2\sigma_1} V^2 a_{Y_1Y_1} + gU a_{X_2} + gV a_{Y_2} \\
&\quad + (\frac{g}{2}\nabla_h \cdot \mathbf{U} - \frac{g}{2\sigma_1}\mathbf{U}\cdot\nabla_h\sigma_1)a + 0(\epsilon^4)
\end{aligned}
$$

where

$$
D' = \frac{\cosh 4kh + 8 - 2\tanh^2 kh}{8\sinh^4 kh}.
$$

Substituting those expressions into solvability condition (A.29), we obtain the governing equation combining refraction with diffraction and current.

$$2(cc_g k_1 + \sigma_1 U)a_x + 2\sigma_1 V a_y - i(cc_g - V^2)a_{yy} + [\sigma_1^2(\frac{cc_g k_1 + U\sigma_1}{\sigma_1^2})_x$$
$$+\sigma_1^2(\frac{V}{\sigma_1})_y + icc_g(k_1^2 - k^2)]a + ikcc_g k' \mid a \mid^2 a - \frac{(i-1)gk^2}{\cosh^2 kh}\sqrt{\frac{\nu}{2\omega}}a = 0 \quad \text{(A.30)}$$

where $k' = k^3 \frac{c}{c_g} D'$. The last term in the equation only exists for non-slip bottom boundary condition. It is exactly the same as we have developed in chapter 2.

APPENDIX B
NON-SLIP BOTTOM BOUNDARY CONDITION APPLIED IN WAVE EQUATION

Appendix B will present how to get non-slip boundary condition for wave equation in Appendix A.

Following Liu(1986), we assume that the total velocity near the bottom can be expressed as

$$u_i = u_{wi} + u_{ci} + u_{ri} \qquad 0 \le (z+h) \le \delta \tag{B.1}$$

where u_{ri} is rotational flow to satisfy $u_i = 0$ at bottom, subscripts w and c represent quantities of wave and current, respectively, and $\delta = \sqrt{\frac{\nu}{2\omega}}$ is boundary layer thickness.

The linearized Navier-Stokes equation gives

$$\frac{\partial u_i}{\partial t} = -\frac{1}{\rho}\frac{\partial p}{\partial x_i} + \nu\frac{\partial^2 u_i}{\partial x_j \partial x_j} \tag{B.2}$$

If there is no rotational flow, (B.2) becomes

$$\frac{\partial u_{ti}}{\partial t} = -\frac{1}{\rho}\frac{\partial p}{\partial x_i} + \nu\frac{\partial^2 u_{ti}}{\partial x_j \partial x_j} \tag{B.3}$$

where $u_{ti} = u_{wi} + u_{ci}$

Therefore from (B.2) and (B.3), we obtain

$$\frac{\partial u_{ri}}{\partial t} = \nu\frac{\partial^2 u_{ri}}{\partial x_j \partial x_j} \tag{B.4}$$

Assuming u_{ri} is periodic in time

$$u_{ri} = u_{1i} e^{-i\omega t}$$

results in

$$-i\omega u_{1i} = \nu\frac{\partial^2 u_{ri}}{\partial x_j \partial x_j} \tag{B.5}$$

where $u_{1i} = u_{1i}(x, y, z_n)$, in which z_n is the coordinate perpendicular to the bottom. Defining

$$z_n = \xi\delta, \qquad \nabla^2 \sim \frac{1}{\delta^2}\frac{\partial^2}{\partial\xi^2}, \qquad \xi = \frac{1}{\delta}(z+h)$$

(B.5) becomes

$$-iu_{1i} = 2\frac{\partial^2 u_{1i}}{\partial\xi^2} \tag{B.6}$$

Solving (B.6) with boundary conditions

$$\begin{cases} z = 0 \quad \xi \to \infty & u_{ri} = 0 \\ z = -h \quad \xi = 0 & u_{ri} = -\nabla\phi^{(1,1)} \end{cases}$$

where $\phi^{(1,1)}$ is linear wave potential as defined in Appendix A, we have

$$U_1 = \frac{\partial\phi}{\partial x}\mid_{z=-h} \exp[-\frac{(1-i)}{2\delta}(z+h)] \tag{B.7}$$

$$V_1 = \frac{\partial\phi}{\partial y}\mid_{z=-h} \exp[-\frac{(1-i)}{2\delta}(z+h)] \tag{B.8}$$

From the continuity equation, we have

$$\begin{aligned} \frac{\partial W_1}{\partial z} &= -(\frac{\partial U_1}{\partial x} + \frac{\partial V_1}{\partial y}) \\ &= (\frac{\partial^2\phi}{\partial x^2} + \frac{\partial^2\phi}{\partial y^2})_{z=-h} \exp[-\frac{(1-i)}{2\delta}(z+h)] - \frac{1}{\delta}(\frac{\partial\phi}{\partial x}\frac{\partial h}{\partial x} + \frac{\partial\phi}{\partial y}\frac{\partial h}{\partial y})_{z=-h} \\ &\quad \frac{(1-i)}{2}\exp[-\frac{(1-i)}{2\delta}(z+h)] \end{aligned} \tag{B.9}$$

After integrating with respect to z , we get

$$W_1 = -(1+i)\delta\nabla_h{}^2\phi + \nabla_h\phi\cdot\nabla_h h \qquad \text{at } z = -h \tag{B.10}$$

where $\nabla_h = \frac{\partial}{\partial x}\hat{i} + \frac{\partial}{\partial y}\hat{j}$ is two dimensional gradient operator.

If assuming

$$\delta \sim 0(\epsilon^2), \qquad \nabla_h \sim 0(\epsilon^2)$$

Equation (B.10) at order of $0(\epsilon^3)$ becomes

$$W_1 = -(1+i)\sqrt{\frac{\nu}{2\omega}}\phi^{(1,1)}_{XX} + \phi^{(1,1)}_X h_{X_2} \tag{B.11}$$

where $\frac{\partial}{\partial z} = \frac{\partial}{\partial X} + \epsilon^2 \frac{\partial}{\partial X_2}$ has been applied.

Therefore, we get finally, at bottom

$$\frac{\partial \phi^{(3,1)}}{\partial z} + W_1 = 0 \tag{B.12}$$

which is at order of $0(\epsilon^3)$.

APPENDIX C
NUMERICAL SCHEME FOR CONTINUITY-MOMENTUN EQUATION

Appendix C will give the general numerical model scheme for continuity equation and momentum equations.

Following the linearized derivation in chapter 2, we may write the entire equations of (2.11), (2.21) and (2.22) in chapter 2 as

$$\frac{\partial \overline{\eta}}{\partial t} + \frac{\partial q_x}{\partial x} + \frac{\partial q_y}{\partial y} = 0 \tag{C.1}$$

$$\frac{\partial q_x}{\partial x} = -gD\frac{\partial \overline{\eta}}{\partial x} - c_x q_x - m_x \tag{C.2}$$

$$\frac{\partial q_y}{\partial y} = -gD\frac{\partial \overline{\eta}}{\partial y} - c_y q_y - m_y \tag{C.3}$$

where

$q_x = UD$ and $q_y = VD$ are total flux in x and y direction respectively.

$c_x = \frac{f}{D} \mid u_t' \mid_x$ and $c_y = \frac{f}{D} \mid u_t' \mid_y$ as define in (2.136) in chapter 2.

m_x and m_y are the rest term in x and y momentum equations, respectively.

Casting (C.1-C.3) in difference form, we obtain

$$\frac{\overline{\eta}_{i,j}^{n+1} - \overline{\eta}_{i,j}}{\Delta t} + \frac{1}{\Delta x}(q_{x_{i+1,j}}^{n+1} - q_{x_{i,j}}^{n+1}) + \frac{1}{\Delta t}(q_{y_{i,j+1}}^{n+1} - q_{y_{i,j}}) = 0 \tag{C.4}$$

$$\frac{q_{x_{i,j}} - q_{x_{i,j}}}{\Delta t} + \frac{gD}{\Delta x}(\overline{\eta}_{i,j}^{n+1} - \overline{\eta}_{i-1,j}^{n+1}) + c_x q_{x_{i,j}}^{n+1} + m_{x_{i,j}} = 0 \tag{C.5}$$

$$\frac{q_{y_{i,j}} - q_{y_{i,j}}}{\Delta t} + \frac{gD}{\Delta y}(\overline{\eta}_{i,j}^{n+1} - \overline{\eta}_{i,j-1}^{n+1}) + c_y q_{y_{i,j}}^{n+1} + m_{y_{i,j}} = 0 \tag{C.6}$$

where the quantities without time levels denote the values at time level n.

In the matrix form, those equations become

$$W^{n+1} - W + \frac{A\Delta t}{\Delta x}\delta_x W^{N+1} + \frac{B\Delta t}{\Delta y}\delta_y W^{N+1} + C^T \Delta t W^{n+1} + \Delta t M = 0 \tag{C.7}$$

where δ_x and δ_y are central spatial differential. The matrixes W, A, B, C and M are defined

as

$$A = \begin{pmatrix} 0 & 1 & 0 \\ gD & 0 & 0 \\ 0 & 0 & 0 \end{pmatrix} \qquad B = \begin{pmatrix} 0 & 0 & 1 \\ 0 & 0 & 0 \\ gD & 0 & 0 \end{pmatrix}$$

$$W = \begin{pmatrix} \overline{\eta} \\ Q_x \\ Q_y \end{pmatrix} \qquad C = \begin{pmatrix} 0 \\ c_x \\ c_y \end{pmatrix} \qquad M = \begin{pmatrix} 0 \\ m_x \\ m_y \end{pmatrix}$$

where C^T is transposed matrix of C.

Introducing $\beta_x = \frac{A\triangle t}{\triangle x}$, $\beta_y = \frac{B\triangle t}{\triangle y}$ and $\beta_c = C\triangle t$, Eq.(C.7) can be rewritten as

$$(1 + \beta_x + \beta_y + \beta_c)W^{n+1} = W - \triangle tM \tag{C.8}$$

By adding $\beta_x\beta_y(W^{n+1} - W)$ and $\beta_c\beta_y(W^{n+1} - W)$ into above equation, both are high order truncation errors, we have

$$(1 + \beta_x + \beta_c)(1 + \beta_y)W^{n+1} = (1 + \beta_x\beta_y + \beta_c\beta_y)W - \triangle tM \tag{C.9}$$

Eq.(C.9) can be easily split into two parts

$$(1 + \beta_x + \beta_c)W^* = (1 - \beta_y)W - \triangle tM \tag{C.10}$$

$$(1 + \beta_y)W^{n+1} = W^* + \beta_y W \tag{C.11}$$

(C.10) and (C.11) emerge into (C.9) once W^* is eliminated. Writing (C.10) and (C.11) in detail, results in

$$\overline{\eta}^* + \frac{\triangle t}{\triangle x}\delta_x q_x^* = \overline{\eta} - \frac{\triangle t}{\triangle y}\delta_y q_y \tag{C.12}$$

$$(1 + \triangle tc_x)q_x^* + \frac{\triangle t}{\triangle x}gD\delta_x\overline{\eta}^* = q_x - \triangle tm_x \tag{C.13}$$

$$(1 + \triangle tc_y)q_y^* = q_y - \frac{\triangle t}{\triangle y}gD\delta_y\overline{\eta} - \triangle tm_y \tag{C.14}$$

and

$$\overline{\eta}^{n+1} + \frac{\triangle t}{\triangle y}\delta_y q_y^{n+1} = \overline{\eta}^* + \frac{\triangle t}{\triangle y}\delta_y q_y \tag{C.15}$$

$$q_x^{n+1} = q_x^* \tag{C.16}$$

$$q_y^{n+1} + \frac{\triangle t}{\triangle y}gD\delta_y\overline{\eta}^{n+1} = q_y^* + \frac{\triangle t}{\triangle y}gD\delta_y\overline{\eta} \tag{C.17}$$

Substituting (C.16) into (C.12) and (C.13), we obtain x-sweep

$$\begin{cases} \overline{\eta}^* - \overline{\eta} + \frac{\triangle t}{\triangle x}\delta_x q_x^{n+1} + \frac{\triangle t}{\triangle y}\delta_y q_y = 0 \\ (1 + \triangle t c_x) q_x^{n+1} - q_x + \frac{\triangle t}{\triangle x} g D \delta_x \overline{\eta}^* + \triangle t m_x = 0 \end{cases} \tag{C.18}$$

and after combining (C.14) and (C.17), we get y- sweep

$$\begin{cases} \overline{\eta}^{n+1} - \overline{\eta}^* + \frac{\triangle t}{\triangle y}\delta_y q_y^{n+1} - \frac{\triangle t}{\triangle y}\delta_y q_y = 0 \\ (1 + \triangle t c_y) q_y^{n+1} - q_y + \frac{\triangle t}{\triangle y} g D \delta_y \overline{\eta}^{n+1} + \triangle t m_y = 0 \end{cases} \tag{C.19}$$

In the second equation of (C.19) the high order term $\frac{(\triangle t)^2}{\triangle y} g D c_y \delta_y (\overline{\eta}^{n+1} - \overline{\eta})$ has been omitted.

The above two set equations are almost identical to those developed in chapter 3.

APPENDIX D
DOUBLE-SWEEP METHOD IN SOLVING NUMERICAL MODELS

Appendix C will present the details of double-sweep method used in chapter 3.

Continuity-Momentum Equations

(1) X-Sweep

Equation (3.21) in chapter 3 read

$$\overline{\eta}^*_{i,j} + P_{i,j}U^{n+1}_{i+1,j} - P_{i-1,j}U^{n+1}_{i,j} = C_{i,j} \tag{D.1}$$

$$A_{i,j}U^{n+1}_{i,j} + R1\overline{\eta}^{n+1}_{i+1,j} - R1\overline{\eta}^*_{i,j} = B_{i,j} \tag{D.2}$$

where

$$\begin{aligned}
R1 &= \frac{g\triangle t}{\triangle x} \\
P_{i,j} &= \frac{\triangle t}{2\triangle x}(D_{i+1,j} + D_{i,j}) \\
C_{i,j} &= \overline{\eta}_{i,j} - \frac{\triangle t}{2\triangle y}[V_{i,j+1}(D_{i,j+1} + D_{i,j}) - V_{i,j}(D_{i,j} + D_{i,j-1})] \\
A_{i,j} &= 1 + \frac{f\triangle t}{(D_{i,j} + D_{i-1,j})} \mid (u_t)_{i,j} \mid_z \\
B_{i,j} &= U_{i,j} - \frac{\triangle t}{2\triangle x}U_{i,j}(U_{i+1,j} - U_{i-1,j}) - \frac{\triangle t}{8\triangle y}(V_{i,j+1} + V_{i,j} + V_{i-1,j+1} \\
&\quad + V_{i-1,j})(U_{i,j+1} - U_{i,j-1}) - \frac{\triangle t}{\rho(D_{i,j} + D_{i-1,j})}\{\frac{2}{\triangle x}[(S_{xx})_{i,j} - (S_{xx})_{i-1,j}] - \frac{1}{2\triangle y} \\
&\quad [(S_{xy})_{i,j+1} - (S_{xy})_{i,j-1} + (S_{xy})_{i-1,j+1} - (S_{xy})_{i-1,j-1}]\} + (FL_{yy})_{i,j} + (FL_{yz})_{i,j}
\end{aligned}$$

The quantities without superscripts denote the value at time level n. $\mid (u_t)_{i,j} \mid_z$, $(FL_{yy})_{i,j}$ and $(FL_{yz})_{i,j}$ are defined in (3.18) in chapter 3.

The solutions of $\overline{\eta}^*_{i,j}$ and $U^{n+1}_{i,j}$ are assumed with the forms as

$$\overline{\eta}^*_{i,j} = F1_i + E1_i U^{n+1}_{i,j} \tag{D.3}$$

$$U^{n+1}_{i,j} = F2_{i-1} + E2_{i-1}\overline{\eta}^*_{i-1,j} \tag{D.4}$$

Substituting (D.3) and (D.4) into (D.2) and (D.1), respectively, we obtian

$$\begin{cases} \overline{\eta}^*_{i,j} = F1_i + E1_i U^{n+1}_{i,j} \\ U^{n+1}_{i,j} = F2_{i-1} + E2_{i-1}\overline{\eta}^*_{i-1,j} \end{cases} \tag{D.5}$$

which is the same as (3.23) in chapter 3. The definitions of $F1$, $E1$, $F2$ and $E2$ are also given in chapter 3.

(2) Y-Sweep

Equation (3.22) in chapter 3 gave

$$\overline{\eta}^{n+1}_{i,j} + Q_{i,j} V^{n+1}_{i,j+1} - Q_{i,j-1} V^{n+1}_{i,j} = Z_{i,j} \tag{D.6}$$

$$R_{i,j} V^{n+1}_{i,j} + R2\overline{\eta}^{n+1}_{i,j} - R2\overline{\eta}^{n+1}_{i,j-1} = S_{i,j} \tag{D.7}$$

where

$$\begin{aligned}
R2 &= \frac{g\triangle t}{\triangle y} \\
Q_{i,j} &= \frac{\triangle t}{2\triangle y}(D_{i,j+1} + D_{i,j})_* \\
Z_{i,j} &= \overline{\eta}^*_{i,j} - \frac{\triangle t}{2\triangle y}[V_{i,j+1}(D_{i,j+1} + D_{i,j})_* - V_{i,j}(D_{i,j} + D_{i,j-1})_*] \\
R_{i,j} &= 1 + \frac{f\triangle t}{2(D_{i,j} + D_{i,j-1})_*} \mid (u_t)_{i,j} \mid_y \\
S_{i,j} &= V_{i,j} - \frac{\triangle t}{8\triangle x}(U_{i+1,j} + U_{i,j} + U_{i+1,j-1} + U_{i,j-1})^{n+1}(V_{i+1,j} - V_{i-1,j}) \\
&\quad - \frac{\triangle t}{2\triangle y} V_{i,j}(V_{i,j+1} - V_{i,j-1}) - \frac{\triangle t}{\rho(D_{i,j} + D_{i,j-1})_*}\{\frac{1}{2\triangle x}[(S_{zy})_{i+1,j} - (S_{zy})_{i-1,j} \\
&\quad + (S_{zy})_{i+1,j-1} - (S_{zy})_{i-1,j-1}]\} + \frac{2}{\triangle y}(S_{yy})_{i,j} - (S_{yy})_{i,j-1}] + (FL_{zy})_{i,j} + (FL_{yy})_{i,j}
\end{aligned}$$

where $\mid (u_t)_{i,j} \mid_y$, $(FL_{zy})_{i,j}$ and $(FL_{yy})_{i,j}$ are defined in (3.20) in chapter 3. The quantities with the subscripts $*$ are up-date water depth defined as $D_* = h + \overline{\eta}^*$.

As done in x-sweep, finally, we have

$$\begin{cases} \overline{\eta}^{n+1}_{i,j} = F3_j + E3_j V^{n+1}_{i,j} \\ V^{n+1}_{i,j} = F4_{j-1} + E4_{j-1}\overline{\eta}^{n+1}_{i,j-1} \end{cases} \tag{D.8}$$

which is the same as (3.24) in chapter 3.

Wave Equation

Rewriting (3.28) in chapter 3 by the orders of grids, we obtain

$$A_{i+1,j+1}[\frac{\triangle x}{4\triangle y}C0_{i+1,j} - \frac{i\triangle x}{2(\triangle y)^2}C1_{i+1,j}] + A_{i+1,j}[1 + \frac{i\triangle x}{2(\triangle y)^2}C1_{i+1,j} + \frac{B2_{i+1,j}}{2}$$
$$+\frac{\triangle x}{4\triangle y}B3_{i+1,j} + \frac{\triangle x}{2}C4_{i+1,j} + \frac{i\triangle x}{2}C5_{i+1,j}] + A_{i+1,j-1}[-\frac{\triangle x}{4\triangle y}C0_{i+1,j}$$
$$-\frac{\triangle x}{2(\triangle y)^2}C1_{i+1,j}] = Q_{i,j} \tag{D.9}$$

or

$$F1_{i+1,j}A_{i+1,j+1} + F2_{i+1,j}A_{i+1,j} + F3_{i+1,j}A_{i+1,j-1} = Q_{i,j} \tag{D.10}$$

where

$$B2_{i,j} = \frac{C2_{i,j} - C2_{i-1,j}}{C2_{i,j} + C2_{i-1,j}}$$
$$B3_{i,j} = \frac{C3_{i,j+1} - C3_{i,j-1}}{C2_{i,j}}$$
$$F1_{i,j} = \frac{\triangle x}{4\triangle y}C0_{i,j} - i\frac{\triangle x}{2(\triangle y)^2}C1_{i,j}$$
$$F2_{i,j} = 1 + M_{i,j}$$
$$F3_{i,j} = -\frac{\triangle x}{4\triangle y}C0_{i,j} - i\frac{\triangle x}{2(\triangle y)^2}C1_{i,j}$$
$$M_{i,j} = \frac{i\triangle x}{2(\triangle y)^2}C1_{i,j} + \frac{B2_{i,j}}{2} + \frac{\triangle x}{4\triangle y}B3_{i,j} + \frac{i\triangle x}{2}C4_{i,j} + \frac{i\triangle x}{2}C5_{i,j}$$

$Q_{i,j}$ is the all terms at rows below to $i+1$.

$$Q_{i,j} = -F1_{i,j}A_{i,j+1} - F4_{i,j}A_{i,j} - F3_{i,j}A_{i,j-1}$$

in which

$$F4_{i,j} = -1 + M_{i,j}$$

After some manipulations as did in x-sweep continuity-momentum equation, Eq.(D.10) can be rewritten as, in an implicit marching approach

$$A_{i,j+1} = R2_j + R1_jA_{i,j} \tag{D.11}$$

where

$$R1_j = \frac{-F3_{i,j+1}}{F2_{i,j+1} + F1_{i,j+1}R1_{j+1}}$$

$$R2_j = \frac{Q_{i,j+1} - F1_{i,j+1} R2_{j+1}}{F2_{i,j+1} + F1_{i,j+1} R1_{j+1}}$$

The double sweep will start from offshore, i=1, in y direction, and give the results row by row till shoreline, i=idry.

BIBLIOGRAPHY

Arthur,R.S., "Refraction of Shallow Water Waves: the Combimed Effect of Current and under Water Topography," Transactions of America Geophysical Union, Vol.31 (4), 1950, pp549-552.

Arthur,R.S., Munk,W.H., and Isaacs,J.D., "The Direct Construction of Wave Rays," Transactions of the American Geophysical Union, Vol.33 (6), 1952, pp 855-865.

Berkhoff,J.C.W., "Computation of Combined Refraction Diffracton," Proceedings, 13th Conference on Coastal Engineering, Vancouver, 1972.

Birkemier,W.A., and Dalrymple,R.A., "Numerical Model for the Prediction Wave Set-up and near Shore Circulations," ONR Technical Report 1, Ocean Engineering Report 3, Department of Civil Engineering,University of Delaware, Newark, Delaware, 1976.

Booij,N., "Gravity Waves on Water with Non-uniform Depth and Current," Report No. 81-1, Department of Civil Engineering, Delft University of Technology, Delft, 1981.

Booij,N., "A Note on the Accuracy of the Mild-Slope Equation," Coastal Engineering, Vol. 7, 1983, pp 191-203.

Bowen,A.J., Inman,D.L., and Simmons, "Wave Set-down and Set-up," Journal of Geophysical Research, Vol. 73 (8),1968, pp 2596-2577

Butler,H.L., and Sheng,Y.P., "ADI Procedure for Solving the Shallow-Water Equations in Transformed Coordinates," ARO Report 82-3, Proceedings of the 1982 Army Numerical Analysis and Computers Conference, Vicksburg, Mississippi, 1982.

Chen, Y.-H., and Wang,H., "Numerical Model for Nonstationary Shallow Water Wave Spectral Transformation," Journal of Geophysical Research, Vol.88 (C14), 1983, pp 9851-9863.

Chu.,V.H., and Mei.,C.C., "On Slowly-Varying Stokes Waves," Water Resources and Hydrodynamics Laboratory, Report No. 125, Cambridge, Massachusetts, 1970.

Dally,W.R., "A Numerical Model for Beach Profile Evolution," Thesis. Civil Engineering Department, University of Delaware, Newark, Delaware, 1980.

Dally,W.R., Dean,R.G., and Dalrymple,R.A., "Modeling Wave Transformation in the Surf Zone," U.S. Army Coastal Engineering Research Center, Vicksburg, Mississippi. Also in Proceedings, 19th Conference on Coastal Engineering, Houston, Texas, 1984.

Dean,R.G., and Dalrymple,R.A., Water Wave Mechanics for Scientists and Engineers, Prentice-Hall,Inc, Englwood Cliffs, N.J., 1983.

Dobson, R.S., "Some Applications of Digtal Computers to Hydraulic Engineering Problems," TR-80, Ch. 2, Department of Civil Engineering, Stanford University, Palo Alto, Calif., 1967.

Ebersole,B.A., and Dalrymple,R.A., "A Numerical Model for Nearshore Circulation Including Convective Accelerations and Lateral Mixing, " Ocean Engineering Report No. 21, Department of Civil Engineering, University of Delaware, Newark, Delaware, 1979.

Goda,Y., Yoshimura.,J., and Ito,M., "Reflection and Diffraction of Water Waves by an Insular Breakwater," Report of the Port and Harbor Research Institute, Vol. 10 (2), 1971, pp 4-51.

Grant,W.D., and Madsen,O.S., "Combnined Wave and Current Interaction with a Rough Bottom," Journal of Geophysical Research, Vol. 84 (C4), 1979, pp 1979-1808.

Hedge, T.S., "An Emperical Modification to Linear Wave Theory," Proceedings, Institute of Civil Engineering, Vol. 61 (2), 1976, pp 575-579

Ippen,A.T. (Editor), Estuary and Coastaline Hydrodynamics, McGraw-Hill, New York, 1966.

Ismail,N.M., "Effect of Opposing Waves on the Mixing of a Horizontal Surface Momentun Jet," Technical report HEI 27-9, University of California Hydraulic Engineering Laboratory, 1981.

Johnson,J.W., O'Brien,M.P., and Isaacs,J.D.,"Graphical Construction of Wave Refraction Diagrams," HO No. 605, TR-2, U.S. Naval Oceanographic Office, Washington, D.C., 1948.

Jonsson,I.G., "Wave Boundary Layer and Friction Factor," Proceedings, 10th International Conference on Coastal Engineering, Tokyo,1966.

Jonssen,I.G., and Garlsen,N.A., "Experimental and Thoretical Investigations in an Oscillatory Rough Turbulent Boundary Layer," Journal of Hydraulic Research, Vol. 14 (1), 1976, pp 45-60.

Kamphuis,J.W., "Friction factor under Oscillatory Waves," Proceedings, American Society of Civil Engineering, Vol.101 (WW2), 1975, pp135-144.

Keller,J.B., "Surface Waves on Water of Non-uniform Depth," Journalof Fluid Mechanics, Vol. 4, 1958, pp 607-614.

Kirby,J.T., "A Note on Linear Surface Wave-Current Interaction over Slowly Varying Topography," Journal of Geophysical Research, Vol. 89, 1984, pp 745-747.

Kirby,J.T., "Propagation of Weakly-Nonlinear Surface Water Waves in Region with Varying Depth and Current," Technical Report No. 14, University of Delaware, Newark, Delaware, 1983.

Kirby,J.T., and Dalrymple,R.A., "A Parabolic Equation for the Combined Refraction-Diffraction of Stokes Waves by Mildly Varying Topography," Journal of Fluid Mechanics, Vol. 136, 1983a, pp 453-466.

Kirby,J.T., and Dalrymple,R.A., " Numerical Modeling of the Nearshore Region," Technical Report CE-82-24, Department of Civil Engineering, University of Delaware, Newark, Delaware, 1983b.

Kirby,J.T., and Dalrymple,R.A., "An Approximate Model for Nonlinear Dispersion in Monochomatic Wave Propagation Models," Coastal Engineering, Vol. 9, 1986, pp 545-561.

Kirby,J.T., and Dalrymple,R.A., "Verification of a Parabolic Equation for Propagation of Weakly-Nonlinear Waves," Coastal Engineering, Vol. 8, 1984, pp 255-279.

Kirby,J.T., Dalrymple,R.A., and Liu,P.L-F., "Modification of Edge Waves by Barred-Beach Topography," Coastal Engineering, Vol.5, 1981, pp 35-49.

Liu,P.L.-F., "Combined Refraction and Diffraction: Comparison Between Theory and Experiments," Journal of Geophysical Research, Vol. 87 (C8), 1982, pp 5723-5730.

Liu,P.L.-F., "Viscous Effect on the Evolution of Stokes Waves," Journal of Waterway, Port, Coastal and Ocean Engineering, Vol. 112 (1), 1986, pp 55-63.

Liu,P.L.-F., and Lozano,C., "Combined Wave Refraction and Diffraction," Proceeding of the Coastal Structures '79 Conference, Alexandria, Virginia, 1979.

Liu,P.L.-F., Lozano,C.J., and Pantazaras,N., "An Asymptotic Theory of Combined Wave Refraction and Diffraction," Applied Ocean Research, Vol.1, 1979, pp137-146.

Liu,P.L.-F., and Tsay,T.-K., "Refraction-Diffraction Model for Weakly Nonlinear Water Waves," Journal of Fluid Mechanics, Vol.141, 1984, pp265-274.

Liu,P.L.-F., Yoon,S.B., and Kirby,J.T., "Nonlinear Refraction-Diffraction of Waves in Shallow Water," Jounal of Fluid Mechanics, Vol. 153, 1985 pp185-201.

Longuet-Higgins,M.S., "Longshore Current Generated by Obliquely Incident Sea Waves, 1," Journal of Geophysical Research, Vol. 75 (33), 1970a, pp 6778-6789.

Longuet-Higgins,M.S., "Longshore Current Generated by Obliquely Incident Sea Waves, 1," Journal of Geophysical Research, Vol. 75 (33), 1970b, pp 6790-6801.

Longuet-Higgins,M.S., and Stewart,R.W., "The change in Amplitude of Short Gravity Waves on Steady Non-uniform Current," Journal of Fluid Mechanics, Vol.10, 1960a, pp529-549.

Longuet-Higgins,M.S., and Stewart,R.W., "Changes in the Form of Short Gravity Waves on Long Waves and Tidal Current," Journal of Fluid Mechanics, Vol.8, 1960b, pp 565-583.

Longuet-Higgins,M.S., and Stewart,R.W., "Radiation Stress and Mass Transport in Gravity Waves with Application to Surf Beats," Journal of Fluid Mechanics, Vol.33, 1962, pp 481-504.

Longuet-Higgins,M.S., and Stewart,R.W., "Radiation in Water Waves: A Physical Discussion with Applications," Deep-Sea research, Vol.11, 1964, pp529-563.

Lozano,C., and Liu,P.L.-F., "Refraction-Diffraction Model for Linear Surface Water Waves," Journal of Fluid Mechanics, Vol. 101 (4), 1980, pp705-720.

Luke,J.C., "A Variational Principle for a Fluid with a Free Surface," Journal of Fluid Mechanics, Vol. 27, 1967, pp 395-397.

McCowan,J., "On the Highest Wave of Permanent Type," Philosophical Magazine and Journal Science, Vol.38, 1894.

Mei,C.C., The Applied Dynamics of Ocean Surface Waves, Wiley-Interscience, New York, 1982.

Memos,C.D., "Diffraction of Waves Through a Gap Between Two Inclined Breakwaters," Ph.D. Thesis, University of London, London, England, 1976.

Montefusco,L., "The Diffraction of a Plane Wave by an Isolated Breakwater," Meccanica, Vol.3, 1968, pp 156-166.

Noda,E.K., Sonu.C.J., Rupert,V.C., and Collins,J.I., " Nearshore Circulations under sea Breeze Conditions and Wave- Current Interactions in the Surf-Zone," Tetry Technical Report TC-149-4, 1974.

O'Brien,M.P., and Mason, "A Summary of the Theory of Oscillatory Waves," Technical Report 2, Beach Erosion Board, 1940.

Penny,W.G., and Price,A.T., "Diffraction of Sea Waves by a Breakwater," Artificial Harbors, Technical History No. 26, Sec. 3-D, Directorate of Miscellaneous Weapons Development, 1944.

Penny,W.G., and Price,A.T., "The Diffraction Theory of Sea Waves by Breakwater and the Shelter Afforded by Breakwater," Philosophical Transactions of the Royal Society, Series A, Vol. 244, 1952, pp 253-263

Peregrine,D.H., "Wave Jumps and Caustics in the Propagation of Finite-Amplitude Water Waves," Journal of Fluid Mechanics, Vol. 136,1983, pp435-452.

Phillips,O.M., The Dynamics of the Upper Ocean, 2nd Edition,Cambridge University Press, Cambridge, 1977.

Radder,A.C., "On the Parabolic Equation Method for Water Wave Propagation," Journal of Fluid Mechanics, Vol. 95, 1979, pp159-176.

Schlichting,H., Boundary Layer Theory, 7th Edition, McGraw-Hill Book Company, New York, 1979.

Sheng,Y.P., "Modeling the Hydrodynamics and Dispersion of Sediment in the Mississippi Sound," A.R.A.P. Report, No. 455, Princeton, New Jersey, 1981.

Skovgaard,O., Jonsson,I.G., and Bertelsen,J.A., " Computation of Wave Heights due to Refraction and Friction," ASCE, Journal of Waterways, Harbors and Coastal Engineering Division, Vol.101 (WW1), 1975,pp15-32.

Sommerfeld,A., "Mathematische Theorie der Diffraction," Mathematische Annals, Vol.47, 1896, pp 317-374.

Swart,D.H., "Offshore Sediment Transport and Equilibrium Beach Profiles," Publication No. 132, Delft Hydraulic Laboratory, Delft, 1974.

Tsay, T.-K., and Liu,P.L.-F., "Numerical Solution of Water-Wave Refraction and Diffraction Problems in the parabolic Approximation," Journal of Geophysical Research, Vol. 82 (C10), 1982, pp 7932-7940.

Vemulakonda,S.R., "Erosion Control os Scour During Construction," Technical Report HL-80-3, U. S. Army Waterways Experiment Station, Vicksburg, Mississippi, 1984.

Wang,H., and Yang,W.-C., "Wave Spectral Transformation Measurements at Sylt, North Sea," Coastal Engineering, Vol.5, 1981, pp 1-34.

Whitham,G.B., "Mass, Momentum and Energy Flux in Water Waves," Journal of Fluid Mechanics, Vol.12, 1962, pp135-147.

Whitham,G.B., "Non-linear Dispersion of Water Waves," Journal of Fluid Mechanics, Vol. 27 (2), 1967, pp 399-412.

Wiegel,R.L., "Diffraction of Waves by a Semi-infinite Breakwater," Journal of the Hydraulic Division, ASCE Vol.88 (HY1), 1962, pp27-44.

BIOGRAPHICAL SKETCH

Yixin Yan was born January 31, 1949, in Shanghai, China. He received his Bachelor of Engineering degree in harbor and navigation engineering from Hehai University, Nanjing, China, in 1978. He then enrolled as a graduate student in the Hehai University. In 1981, he graduated with Master of Engineering in coastal engineering. In August, 1982, he entered the graduate school at the University of Florida in the Department of Coastal and Oceanographic Engineering. He has worked as a research assistant while earning the Doctor of Philosophy degree.

I certify that I have read this study and that in my opinion it conforms to acceptable standards of scholarly presentation and is fully adequate, in scope and quality, as a dissertation for the degree of Doctor of Philosophy.

Hsiang Wang, Chairman
Professor of Engineering Science and Coastal and Oceanographic Engineering

I certify that I have read this study and that in my opinion it conforms to acceptable standards of scholarly presentation and is fully adequate, in scope and quality, as a dissertation for the degree of Doctor of Philosophy.

Robert G. Dean
Graduate Research Professor of Coastal and Oceanographic Engineering

I certify that I have read this study and that in my opinion it conforms to acceptable standards of scholarly presentation and is fully adequate, in scope and quality, as a dissertation for the degree of Doctor of Philosophy.

James E. Keesling
Professor of Mathematics

I certify that I have read this study and that in my opinion it conforms to acceptable standards of scholarly presentation and is fully adequate, in scope and quality, as a dissertation for the degree of Doctor of Philosophy.

James T. Kirby
Assistant Professor of Coastal and Oceanographic Engineering

I certify that I have read this study and that in my opinion it conforms to acceptable standards of scholarly presentation and is fully adequate, in scope and quality, as a dissertation for the degree of Doctor of Philosophy.

Ulrich H. Kurzweg
Professor of Engineering Science

I certify that I have read this study and that in my opinion it conforms to acceptable standards of scholarly presentation and is fully adequate, in scope and quality, as a dissertation for the degree of Doctor of Philosophy.

D. Max Sheppard
Professor of Coastal and Oceanographic Engineering

This dissertation was submitted to the Graduate Faculty of the College of Engineering and to the Graduate School and was accepted as partial fulfillment of the requirements for the degree of Doctor of Philosophy.

August 1987

Dean, College of Engineering

Dean, Graduate School